ABSTRACT

Title of Document: EVALUATING RISKS OF DAM-RESERVIOR SYSTEMS USING EFFICIENT IMPORTANCE SAMPLING

Qianli Deng (Shally), Doctor of Philosophy, 2016

Directed By: Professor, Dr. Gregory B. Baecher
Department of Civil and Environmental Engineering

The occurrence frequency of failure events serve as critical indexes representing the safety status of dam-reservoir systems. Although overtopping is the most common failure mode with significant consequences, this type of event, in most cases, has a small probability. Estimation of such rare event risks for dam-reservoir systems with crude Monte Carlo (CMC) simulation techniques requires a prohibitively large number of trials, where significant computational resources are required to reach the satisfied estimation results. Otherwise, estimation of the disturbances would not be accurate enough.

In order to reduce the computation expenses and improve the risk estimation efficiency, an importance sampling (IS) based simulation approach is proposed in this dissertation to address the overtopping risks of dam-reservoir systems. Deliverables of this study mainly include the following five aspects: 1) the reservoir inflow hydrograph model; 2) the dam-reservoir system operation model; 3) the CMC

simulation framework; 4) the IS-based Monte Carlo (ISMC) simulation framework; and 5) the overtopping risk estimation comparison of both CMC and ISMC simulation. In a broader sense, this study meets the following three expectations: 1) to address the natural stochastic characteristics of the dam-reservoir system, such as the reservoir inflow rate; 2) to build up the fundamental CMC and ISMC simulation frameworks of the dam-reservoir system in order to estimate the overtopping risks; and 3) to compare the simulation results and the computational performance in order to demonstrate the ISMC simulation advantages.

The estimation results of overtopping probability could be used to guide the future dam safety investigations and studies, and to supplement the conventional analyses in decision making on the dam-reservoir system improvements. At the same time, the proposed methodology of ISMC simulation is reasonably robust and proved to improve the overtopping risk estimation. The more accurate estimation, the smaller variance, and the reduced CPU time, expand the application of Monte Carlo (MC) technique on evaluating rare event risks for infrastructures.

EVALUATING RISKS OF DAM-RESERVIOR SYSTEMS USING EFFICIENT IMPORTANCE SAMPLING

By

Qianli Deng

Dissertation submitted to the Faculty of the Graduate School of the
University of Maryland, College Park, in partial fulfillment
of the requirements for the degree of
Doctor of Philosophy
2016

Advisory Committee:
Dr. Gregory B. Baecher, Chair/Advisor
Dr. Mark Austin
Dr. Kaye L. Brubaker
Dr. David J. Lovell
Dr. Guangming Zhang, Dean's representative

Acknowledgements

I would like to acknowledge and thank the many individuals and groups who have contributed directly or indirectly to the completion of this research. First, I would like to express my deepest thankfulness to my Ph.D adviser Dr. Gregory B. Baecher, for his continuous guidance and mentorship throughout my studies at Maryland. His wisdom, knowledge, and commitment to the highest standards inspire and motivate me. I feel so honored to have the chance to work with him.

I am also truly grateful to the remaining committee members. Thanks to Dr. Mark Austin, who is also my M.S advisor of Applied Statistics and Scientific Computing. His invaluable advice and inspiration helped me overcome many difficulties in my research. Thanks to Dr. David J. Lovell, who is also the professor whom I worked with as a TA. Without his introduction and encouragement, I would not have had the courage to pursue my Ph.D. Thanks to Dr. Kaye L. Brubaker and Dr. Guangming Zhang for kindly accepting to be on my committee and providing constructive advice and suggestions.

I would also like to thank Ontario Power Generation for providing case information. Thanks to my colleagues Adiel Komey and Dr. Farshad Abedinisohi for offering critical suggestions on the model formulation. Thanks to all my friends for encouraging and helping with my research. I will never forget the great times studying and discussing with such an intelligent group of people who are passionate about knowledge and science.

Finally, special thanks go to my beloved family. I would not have accomplished this work without their love, understanding, and unconditional support through these years. I appreciate them for always being there for me and making me happy. This dissertation is dedicated to them.

Table of Contents

List of Tables

List of Figures

Chapter 1: Introduction

1.1 Research Motivation

Dam-reservoir systems are a critical component of water infrastructure, providing services such as water, power, flood control, recreation, and many economic possibilities (Vedachalam and Riha 2014). The successful performance of a dam-reservoir system depends on the aggregate satisfactory performance that prevents a failure and uncontrolled release of the reservoir. However, hundreds of dam failures have occurred throughout U.S. history that have caused immense property and environmental damage and have taken thousands of lives. Take the Lawn Lake Dam failure of 1982, for instance. The sudden release of 849,000 m^3 of water resulted in a flash flood that killed three people and caused $31 million of damage. In 1996, the Meadow Pond Dam also failed with big loss. About 350,000 m^3 of water was released, and resulted in one fatality, two injuries, and damage to multiple homes. In 2006, the Ka Loko Dam burst, resulting in a flood that caused seven fatalities and destroyed several homes. According to the Association of State Dam Safety Officials (2015), 173 dam failures and 587 incidents were reported from January 2005 through June 2013 by the state dam safety programs. Dam failures are not particularly common, but continue to occur (Baecher et al., 2011). The number of dams identified as unsafe is also increasing at a faster rate than those being repaired, as dam age and population increase. In the future, the potential for deadly dam failures will continue to grow.

Potential failure modes for dam-reservoir systems were explored by researchers. Overtopping is one of the most common failure modes for the dam-reservoir systems with significant consequences. According to national statistics, overtopping due to inadequate spillway design, debris blockage of spillways, or settlement of the dam crest accounts for approximately 34% of all U.S. dam failures (Association of State Dam Safety Officials 2015). Other causes include piping, seepage, internal erosion (Curt et al. 2010), and inadequate maintenance. A similar proportion has also been concluded by Kuo et al. (2008) and Zhang et al. (2009). In general, overtopping is the most common failure cause of dam-reservoir systems, particularly for the homogeneous earth-fill dams and zoned earth-fill dams. Spillways, foundations, and downstream slopes are the potential locations of the risks. Overtopping flows can erode down through an embankment dam, releasing the stored waters, potentially in a manner that can cause catastrophic flooding downstream as well as a total loss of the reservoir.

Although overtopping results in significant consequences, in reality, such events have a very low probability of occurrence for a specific dam-reservoir system. Those events are defined as rare events. Estimation of the rare-event probabilities with crude Monte Carlo (CMC) simulation requires a prohibitively large number of trials, where significant computational resources are required to reach the satisfied estimation results. Otherwise, estimation of the disturbances would not be accurate enough.

Accordingly, computational expense served as one of the prohibitive reasons that the simulation technique has not been widely applied to the reservoir operation.

In view of the very large number of options of configuration, capacity and operating policy, simulation without preliminary screening or adjustment would be very time consuming. Understanding the sources of simulation-based estimation errors and minimizing error rates at a reasonable cost are consequently important aspects of these practical problems. In order to fill in the research gap, the rare-event simulation technique is needed and plays a critical role in evaluating the overtopping risks of dam-reservoir systems.

1.2 Research Objectives and Scope

The overtopping frequencies of dam-reservoir systems serve as critical indexes representing dam safety statuses. In order to reduce the computation expenses and improve the risk estimation efficiency, an importance sampling (IS) based simulation approach is proposed in this study. The overtopping probability calculation process are addressed specifically for dam-reservoir systems. Deliverables of this study mainly include the following five aspects:

- The reservoir inflow hydrograph model;
- The dam-reservoir system operation model;
- The CMC simulation framework;
- The importance sampling based Monte Carlo (ISMC) simulation framework;
- The overtopping risk estimation comparison of both the CMC and the ISMC simulation.

These results that this study is intended to reach would explore a new supplement for the dam safety design. In a broader sense, this study would also meet the following three expectations:

- To address the natural stochastic characteristics of the dam-reservoir system, such as the reservoir inflow rate;
- To build up the fundamental CMC and ISMC simulation frameworks of the dam-reservoir system in order to estimate the overtopping risks; and
- To compare the simulation results and the computational performance, in order to demonstrate the advantage of ISMC simulation.

Overall, there are two major contributions that this study would make. From one perspective, the estimation results of overtopping probability could be used to guide the future dam safety investigations and studies, and to supplement the conventional analyses in making decisions on the dam-reservoir system improvements. From the other perspective, the proposed methodology of ISMC simulation would improve the overtopping estimation results. The more accurate estimation of probability, the smaller variance of simulation results, and the significantly reduced CPU time, expand the application of MC technique on evaluating the overtopping risks of dam-reservoir systems.

1.3 Organization of Dissertation

Based on the proposed research objectives and scope, this dissertation consists of six chapters. Details of Chapters 2-6 are summarized as follows:

Chapter 2 sets up the fundamental dam-reservoir system model for simulation modeling and analysis. Both the inflow hydrograph model and the dam-reservoir system operation model are built in this chapter, which are also connected internally.

Chapter 3 conducts detailed simulations to estimate the overtopping risks of the dam-reservoir system with the randomness. Both the CMC simulation and the ISMC simulation frameworks are developed with methodology and application comparison.

Chapter 4 applies the proposed simulation models to Little Long dam-reservoir system. The results from the inflow hydrograph model play as the prerequisites for future inflow simulation, and the simulated inflow results serve as the input variables for the reservoir operations model. Final outputs would be the reservoir water elevation through the specified time period.

Chapter 5 starts with the introduction of simulation implementation, including two perspectives: 1) the simulation platform; and 2) the importance sampling density selection. The simulation results are presented including both the overtopping probability estimation and the computational performance measurement.

Chapter 6 concludes the work. Contributions and limitations are summarized with future directions listed.

The following Figure 1-1 demonstrates the structure in terms of the chapter contents, which displays the composition of dam-reservoir system overtopping risks.

1.4 Overview of Research Outcome

In general, the dissertation could be divided into two parts: theoretical bases and case study. In both parts, the performance modeling and simulation are discussed as a sequence. In order to show the general logic of the dissertation in a more organized way, Table 1-1 below presents the overviews and the outcomes with the corresponding sections. Discussions of each topic are involved throughout the dissertation.

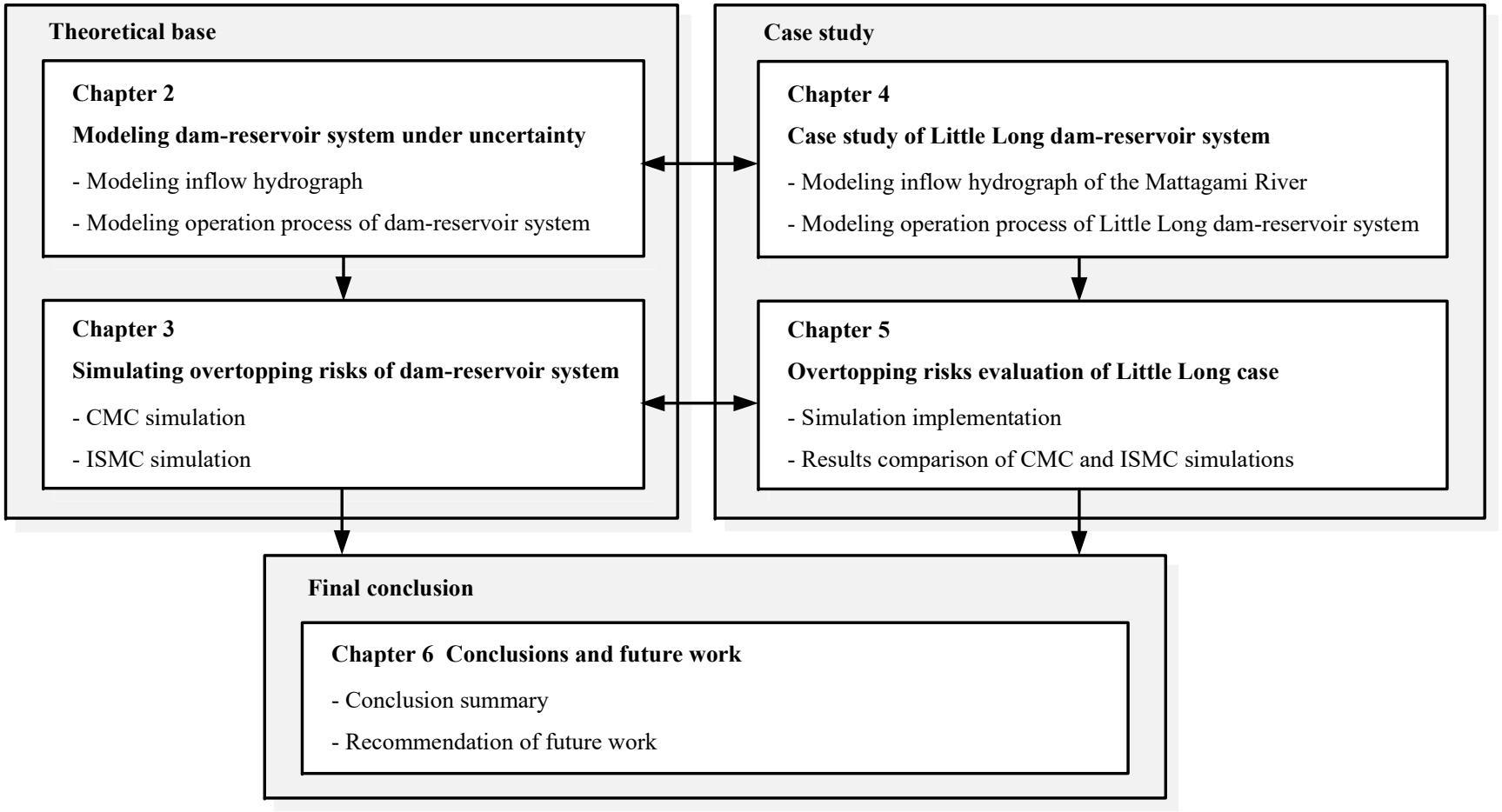

Figure 1-1 Dissertation structure in terms of chapter contents

Table 1-1 Research outcomes and relevant sections

Research outcome			Theoretical base	Case study
Modeling	Modeling inflow hydrograph		Section 2.3	Section 4.2
	Modeling operation of dam-reservoir system		Section 2.4	Section 4.3
Simulation	CMC	Simulation of inflow hydrograph	Section 3.3	Sections 5.2, 5.3
		Simulating dam-reservoir operation		
	ISMC	Simulation of inflow hydrograph	Section 3.4	
		Simulating dam-reservoir operation		

Chapter 2: Modeling Performance of Dam-Reservoir System under Uncertainty

2.1 Introduction

In order to address the overtopping risks of dam-reservoir system effectively, a valid dam-reservoir model is needed to identify the system performance with sequential correlations. The goal of this chapter is to propose a theoretical model to address the dam-reservoir system dynamics, which also serves as the prerequisites for the simulation model in Chapter 3. Both the inflow hydrograph model and the general dam-reservoir system operation model are involved in this chapter, which are connected to each other internally. In the inflow hydrograph modeling part, transformation, statistical pattern testing, and seasonal time series modeling are applied. Uncertainties that play as one of the critical roles resulting in the system failure have also been taken into consideration. In the dam-reservoir system operation modeling part, the reservoir routing that incorporates the operation rules is also involved to evaluate the dam overtopping probability. Outflow controls are thus considered as the critical factors with both the outflow releasing rate and the corresponding reservoir water elevations as the outputs.

2.2 Literature Review on Critical Factors Leading to Overtopping Risks

Dam-reservoir system reliability is the ability of a dam-reservoir system to perform its required functions under the stated conditions for a specified period of time. In recent years, there has been a growing tendency to assess dam safety by statistical and

simulation methods in hydro-system engineering. In practice, Xu and Zhang (2009) analyzed the breaching parameters for earth and rockfill dams through a multi-parameter nonlinear regression model, including breach depth, breach top width, average breach width, peak outflow rate, and failure time. The dam erodibility was found to be the most important influencing factor for the five parameters. A similar research has also been done by Gee (2009). Analytical techniques for the estimation of dam breach parameters were evaluated and compared. Relationships among the above key parameters were also fitted, such as water depth behind the dam and historic observations. Froehlich (2008) also analyzed the embankment dam breach parameters and their uncertainties. Predicted peak flows and water elevations downstream from breached embankment dams were estimated through statistical analysis and MC simulation. For works that are complex and unique, an expert's elicitation is necessary when the data is imprecise or insufficient. To support expert diagnosis and risk analysis of dam performances, a method was thus proposed by Pevras et al. (2006). Tools were developed to the dam safety policy level to aid emergency managers and communities in appraising private dam safety. Analysis of the social and environmental costs and threats associated with dam safety issues were also provided (Pisaniello et al. 2011; Pisaniello and McKay 2007).

In order to address the characteristics of dam-reservoir system performance effectively, this section reviews the past research on the critical factors leading to the overtopping risks. Uncertainties underlying in both the inflows and outflows have been taken into consideration.

2.2.1 Inflow Hydrograph and Time Integration

Hydrologic risk analysis for the dam safety relies on a series of probabilistic analyses of rainfall-runoff and flow routing models. To the overtopping risks specifically, underlying uncertainties in the inflow variations serve as one of the major factors leading to the system failure. According to Kwon and Moon (2006), estimation of the overtopping risks applied to the Soyang Dam in South Korea illustrates that the traditional parametric approach can lead to potentially unrealistic estimates of dam safety. They proposed that the simulation-based approaches could provide rather reasonable estimates and an assessment of sensitivity to key parameters. Hsu et al. (2010) also developed a probability-based methodology to evaluate dam overtopping probability that accounts for uncertainties arising from wind speed and peak flood. A wind speed frequency model and flood frequency analysis including various distribution types and uncertainties were presented. The IS and Latin Hypercube sampling methods were also proposed to generate the samples of peak flow rate and wind speed especially for rare events. Similar research was also done by Sun et al. (2012). These works provide varied methodologies to analyze the peak inflow rates based on historical data, which set up the theoretical foundation for overtopping risk analysis.

Due to the integration effect of reservoir, the peak inflow rates are not the unique factor within the inflow that decide the reservoir water elevation. Several past research studies also took the high inflow period and the total inflow volume into consideration. According to Poulin (2007), the bivariate return period and the conditional density of the volume given that the flow exceeds a given threshold were

computed. The results showed that out of the seven copula families tested, five overestimated the return periods of correlated extreme events. These results brought to the forefront the importance of the tail dependence in order to estimate the risk adequately. As a new risk assessment methodology for dam safety, copulas was also used in Klein et al. (2011)'s research. Characteristics of flood events including peak, volume and shape were taken into the multivariate probabilistic evaluation. Then, a methodology for flood risk assessment was presented which was applied in two case studies in Germany. Goodarzi et al. (2012) also presented the application of risk and uncertainty analysis to dam overtopping based on the univariate and bivariate flood frequency analyses. The overtopping risk of the Doroudzan Dam was evaluated for all six inflow hydrographs by considering quantile of flood peak discharge, initial depth of water in the reservoir, and discharge coefficient of spillway as uncertain variables and using two uncertainty analysis methods.

The peak annual inflow rates and the high inflow period usually simplify the actual situations, which might result in underestimating the extreme risks. In order to involve more information from the inflow data, time series modeling is considered as an efficient statistical tool. Time-series modeling in hydrology has a long tradition. Assumptions have been made that it is possible to develop a general type of model capable of representing most relevant statistical characteristics of historic stream flow series. The origins of the concept can be traced back as far as Hazen (1914) and in more recent times to Lohani et al. (2012) and Valipour (2013). Seasonal patterns for both the general trend and uncertain fluctuation could be effectively addressed through the time series modeling. Beyond the seasonal cycle and mean trend, time

series approach was also used to generate synthetic hydrologic records, to forecast hydrologic events, to detect trends and shifts in hydrologic records, and to fill in missing data and extend records (Chiew et al. 1993; Kuo and Sun 1993). According to Box and Jenkins (1976), the Auto Regressive Integrated Moving Average (ARIMA) model or Box-Jenkins model became one of the general time series models used for hydrological forecasting. Valipour (2013) also resulted that the ARIMA model was an appropriate tool to forecast annual rainfall. Expanding to the nature of flood risks, related research could also be traced to Apel et al. (2006). In the study, a probabilistic modelling system for assessing flood risks was developed representing the relevant meteorological, hydrological, hydraulic, geo-technical, and socio-economic processes. Kang et al. (2007) also conducted a sensitivity analysis of the flood safety of Yongdam Dam using a regional climate change simulation. The result indicated that the number of floods remained almost the same, but the magnitude of a single flood event and the recovery from it became worse.

2.2.2 Outflow Controls and Disturbances

Besides the inflow hydrograph and time integration, the outflow control is another critical factor that decides the dam-reservoir overtopping risks. In the classical method of reservoir system reliability analysis, the operation policy is used as a number of physical bounds on a reservoir system. From the outflow perspective, optimizing the dam-reservoir system operation has been a major area of study in water resources management. According to Li et al (2010), the field of data mining techniques was developed as an alternative approach for reservoir system

optimization. Data mining techniques such as genetic algorithms, neural networks, decision tree, and particle swarm optimization were described in detail. Karamouz et al (2005) also presented a decision support system for multipurpose reservoir operation. The key components of the system were four main modules: database management, inflow modeling and forecasting, operation management, and real-time operation. In the research of Ganji and Jowkarshorijeh (2011), inflow and reservoir storage were considered uncertain variables. The algorithm of advance first order second moment method (AFOSM) was implemented, in order to determine the monthly probability of failure in water allocation without the aid of simulation. The final results showed that the outputs from the AFOSM method were similar to those from the MC simulation method. Xu et al. (2014) also proposed rules for multistage optimal hedging operations that incorporate uncertain inflow predictions for large reservoirs with multiyear flow regulation capacities. Three specific rules for determining the optimal outflow releasing were derived, and a solution algorithm was then developed based on the optimality conditions and the three rules.

Disturbance is another important factor affecting the dam-reservoir system safety. Without considering disturbances, overtopping risks would be potentially underestimated. According to Osti et al. (2011), the breach mechanism of the Tam Pokhari moraine dam failure in the Mt. Everest region had many reasons. The dam's internal structure played a crucial role in forming a landslide that triggered the excess overflow and finally the breach of the dam. The rainfall and seismological activities of that particular day, which hit the record high, were also important in triggering the failure. A similar concept was also explained in the failure of Teton Dam, an earthen

dam on the Teton River in Idaho of United States. The failure occurred not because of some unforeseeable fatal combination, but because the many combinations of unfavorable circumstances inherent in the situation were not visualized, and because adequate defenses against these circumstances were not included in the design (Delatte 2008).

To expand the research perspective, several studies were designed to add in the exterior disturbance factors that may lead to the overtopping risks. Incorporating the uncertainties of gate availability, Kuo et al. (2007) determined the optimal dam inspection interval under the consideration of overtopping risks. Considerations were also given to the inspection cost and the dam break cost. Following this research, Kuo et al. (2008) proposed an innovative concept to evaluate dam overtopping by taking into account spillway gate availability. The framework consisted of three parts: 1) evaluation of conditional overtopping risk for different numbers of malfunctioning spillway gates, 2) evaluation of spillway gate availability, and 3) dam inspection scheduling. Results showed that the overtopping risk considering the availability of the spillway gates was higher than the one without considering availability of the spillway gates.

In order to incorporate all the critical factors discussed above which lead to the overtopping risks of dam-reservoir systems, the inflow hydrograph modeling and dam-reservoir system operation modeling are developed. Detailed information is presented in the following two sections.

2.3 Modeling Inflow Hydrograph under Uncertainty

In order to address the characteristics of dam-reservoir system, the inflow hydrograph modeling plays as the first and most critical role connecting different modules with uncertainty. From the stochastic inflows perspective, the following four measures need to be conducted in order to identify the underlying patterns within the inflow hydrograph: 1) logarithmic transformation; 2) Fourier decomposition; 3) differencing and seasonal differencing; and 4) fitting to the ARIMA and seasonal ARIMA model. The final output from the inflow hydrograph model would be a white noise series, which could be generated independently through a standard Gaussian distribution. The model built in this chapter serves as the fundamental basis for the future inflow simulation.

2.3.1 Logarithmic Transformation and Fourier Decomposition

Inflow time series is usually considered as a combination of quasi-periodic signals contaminated by noise, so prediction accuracy can be improved by data preprocessing. The logarithmic transformation is a nonlinear transformation, which reduces positive skewness and compresses the upper end of the distribution, while stretching out the lower end. There are three common reasons why the logarithms are applied: 1) the following statistical techniques work best with data that are single-peaked and symmetric (symmetry); 2) the following techniques work best when the variability is roughly the same (homoscedasticity); 3) it is easier to describe the relationship between variables when it's approximately linear (linearity). Tailoring to

the nature of reservoir inflow hydrograph, logarithmic transformation is adopted in order to organize the datasets and demonstrate the patterns more visible.

Seasonality is one of the major factors that affects the reservoir inflows. In general, reservoir inflows follow seasonal fluctuations, caused mainly by climate conditions. As a result, the Fourier decomposition could be conducted in order to discern seasonal components, following logarithmic transformation of reservoir inflow data series. The Fourier series is a sum of sine and cosine functions that describes a periodic signal. With different amplitudes and frequencies, the Fourier decomposition explains the series entirely as a composition of sinusoidal functions. The generic element of the inflow sample $I_1, I_2, ..., I_n$ is expressed as the *n*th partial sum of the Fourier series showing in Equation (2-1).

$$I(t) = \frac{a_0}{2} + \sum_{j=1}^{n} \left\{ a_j \cos(\omega_j t) + b_j \sin(\omega_j t) \right\}, \qquad j \in \{1, 2, ..., n\} \text{ and } t \in \{0, 1, ..., n_{pt}\} \tag{2-1}$$

where $I(t)$ stands for the stochastic inflow rate at time t, where t is discrete and $t \in \{0, 1, ..., n_{pt}\}$; n stands for the number of Fourier series frequencies; ω_j stands for the angular velocity that accomplish j cycles in the T periods spanned by the data; and n_{pt} stands for the length of series for time series modeling.

Detailed calculation of ω_j is shown in Equation (2-2). a_j, where $j = 0, 1, ..., n$ and b_j, where $j = 1, 2, ..., n$ stands for the Fourier coefficients with detailed calculation process shown in Equations (2-3), (2-4), and (2-5).

$$\omega_j = \frac{2\pi j}{T}, \quad j \in \{1,2,...,n\} \tag{2-2}$$

where T stands for the total number of coefficients from data points. Assuming that $T = 2n$ is even, this sum comprises T functions at frequencies that are equally spaced points in the interval [0, π].

In order to represent all the cyclic patterns in the time series, the sinusoidal components need to be fitted into the time series and leave the residuals as random. Parametric fitting involves finding coefficients for one or more models that fit to data.

$$a_0 = \frac{2}{T}\int_{-T/2}^{T/2} I(t)dt \tag{2-3}$$

$$a_j = \frac{2}{T}\int_{-T/2}^{T/2} I(t)\cos(\omega_j t)dt \tag{2-4}$$

$$b_j = \frac{2}{T}\int_{-T/2}^{T/2} I(t)\sin(\omega_j t)dt \tag{2-5}$$

where a_j, $j \in \{0,1,...,n\}$ and b_j, $j \in \{1,2,...,n\}$ stands for the Fourier coefficients; T stands for the designed periods of data points; ω_j stands for the angular velocity that accomplish j cycles in the T periods spanned by the data; and $I(t)$ stands for the stochastic inflow rate at time t.

Based on the Fourier decomposition, the seasonal pattern existing in the logarithm of inflow hydrograph has been identified, which could be applied as a fixed cycle pattern in further simulation. Thus after Fourier decomposition, the seasonal trends have been removed from the original data series.

2.3.2 Pattern Testing for Time-Series Data

There are five different tests (Augmented Dickey–Fuller Test, Kwiatkowski-Phillips-Schmidt-Shin Test, Box-Pierce and Ljung-Box Test, autocorrelation function, and partial autocorrelation function) proposed in the inflow hydrograph model as a sequence, in order to check the stationarity and pattern existence of inflow time series data. The necessity of differencing and seasonal differencing is decided based on the test results. Detailed test information is explained one by one as follows.

A unit root is a feature of processes that evolve through time that can cause problems in statistical inference involving time series models. In statistics and econometrics, an Augmented Dickey–Fuller test (ADF) is a test for a unit root in a time series sample. It is an augmented version of the Dickey-Fuller test for a larger and more complicated set of time series models. The ADF test for a unit root assesses the null hypothesis of a unit root using the model in Equation (2-6).

$$y_t = c + \delta t + \phi y_{t-1} + \beta_1 \Delta y_{t-1} + \beta_2 \Delta y_{t-2} + ... + \beta_p \Delta y_{t-p} + \varepsilon_t ,$$
$$t \in \{0,1,...,n_{pt}\} \tag{2-6}$$

where y_t stands the tth item of tested time series $\{y_t : t = 0,1,...,n_{pt}\}$; c stands for the drift coefficient; δ stands for the deterministic trend coefficient; and ϕ stands for the AR(1) coefficient. Δ is the differencing operator that $\Delta y_t = y_t - y_{t-1}$. The number of lagged difference term p, is user specified. ε_t stands for a mean zero innovation process; and n_{pt} stands for the length of time series for pattern testing.

The null hypothesis of a unit root, H0: $\phi = 1$. And the alternative hypothesis, H1: $\phi < 1$. Variants of the model allow for different growth characteristics. The model with $\delta = 0$ has no trend component, and the model with $c = 0$ and $\delta = 0$ has no drift or trend. Ordinary least squares (OLS) regression is performed to estimate the coefficients in the alternative model. If the test statistic is less than the critical value, then the null hypothesis of $\phi = 1$ is rejected and no unit root is present. The test that fails to reject the null hypothesis, fails to reject the possibility of a unit root.

In mathematics and statistics, a stationary process is a stochastic process whose joint probability distribution does not change when shifted in time. ARIMA and seasonal ARIMA models are only applied to the stationary time series. As a result, Kwiatkowski-Phillips-Schmidt-Shin (KPSS) test is applied there, which is a stationarity test that is more straightforward of the null hypothesis of trend stationarity against the alternative of a unit root. The test uses the structural model showing in Equations (2-7) and (2-8).

$$y_t = c_t + \delta t + u_{1t}, \quad t \in \{0,1,...,n_{pt}\} \tag{2-7}$$

$$c_t = c_{t-1} + u_{2t}, \quad t \in \{0,1,...,n_{pt}\} \tag{2-8}$$

where c_t stands for the random walk; δ stands for the deterministic trend coefficient; t stands for the time index, where $t \in \{0,1,...,n_{pt}\}$; $\{u_{1t}; t = 0,1,...,n_{pt}\}$ stands for a stationary process; u_{2t} stands for an independent and identically

distributed process with mean 0 and variance σ^2; and n_{pt} stands for the length of time series for pattern testing.

Accordingly, the null hypothesis of the KPSS test H0: $\sigma^2 = 0$, which implies the random walk term, c_t, is constant and acts as the model intercept. The alternative hypothesis H1: $\sigma^2 > 0$, which introduces the unit root in the random walk. The test statistic is shown in Equation (2-9).

$$Q_{pt} = \sum_{t=1}^{n_{pt}} S_t^2 / (s^2 n_{pt}^2) \tag{2-9}$$

where Q_{pt} stands for the test statistic; n_{pt} stands for the length of time series for pattern testing; s^2 is the Newey-West estimate of the long-run variance; S_t stands for the partial sum of residuals $S_t = \sum_{t=1}^{n_{pt}} \hat{u}_{2t}$ based on the least squares estimation. KPSS test also performs a regression to find the OLS fits between the data and the null model.

The Box-Pierce (BP) and Ljung-Box (LB) Tests compute the BP and LB test statistic for examining the null hypothesis of independence in a given time series. The LB test is a type of statistical test determining whether autocorrelations of a time series are different from zero. Instead of testing randomness at each distinct lag, it tests the overall randomness based on a number of lags. The LB test is also closely connected to the BP Test, which is a simplified version.

The null hypothesis of H0: correlation coefficients $\rho_1 = \rho_2 = ... = \rho_m = 0$ that the data are distributed independently. The alternative hypothesis is: H1: the data are not distributed independently. For the LB test, statistic is shown in Equation (2-10).

$$Q_{pt} = n_{pt}(n_{pt}+2)\sum_{h=1}^{m}\frac{\hat{\rho}_h^2}{n_{pt}-h} \tag{2-10}$$

where m stands for the total number of lags being tested; Q_{pt} stands for the test statistic that follows a χ_m^2 distribution (the chi-squared distribution with m degrees of freedom); n_{pt} stands for the length of time series for pattern testing; and $\hat{\rho}_h$ stands for the sample autocorrelation at lag h. For the BP test, the test statistic is shown in Equation (2-11).

$$Q_{pt} = n_{pt}\sum_{h=1}^{m}\hat{\rho}_h^2 \tag{2-11}$$

where m stands for the total number of lags being tested; Q_{pt} stands for the test statistic that follows a χ_m^2 distribution (the chi-squared distribution with m degrees of freedom); n_{pt} stands for the length of time series for pattern testing; and $\hat{\rho}_h$ stands for the sample autocorrelation at lag h. Simulation studies have shown that the LB statistic is suitable for all sample sizes, including the smaller ones.

Followed by the previous tests, autocorrelation function (ACF) and partial autocorrelation function (PACF) also serve as a good supplement to build the ARIMA and seasonal ARIMA model. The ACF is a set of correlation coefficients between the series and lags of itself over time. And the PACF is the partial correlation coefficients between the series and lags of itself. Both the ACF and PACF plots help

to identify the numbers of autoregressive (AR) or moving average (MA) terms in an ARIMA model.

2.3.3 Fitting ARIMA and Seasonal ARIMA Model

Differencing and seasonal differencing have been widely used particularly by analysts who are fitting ARIMA models to time series data. In general, the residuals from Fourier decomposition might be autocorrelated at many lags. A model with no orders of differencing assumes that the original series is stationary. A model with one order of differencing assumes that the original series has a constant average trend. A model with two orders of total differencing assumes that the original series has a time-varying trend. Based on the testing results, differencing and seasonal differencing would be conducted in order to remove the nonstationarity. As shown in Equation (2-12), differencing a time series stands for computing the differences between adjacent values.

$$\Delta Y_t = Y_t - Y_{t-1}, \quad t \in \{1, \ldots, n_{pt}\} \tag{2-12}$$

where $\{Y_t : t = 0, 1, \ldots, n_{pt}\}$ stands for the residual time series; ΔY_t stands for the difference of residual time series; and n_{pt} stands for the length of time series for pattern testing. Seasonal differencing of a time series computes the differences at certain seasonal time lags. Seasonal differencing removes seasonal trend and can also get rid of a seasonal random walk type of nonstationarity. As defined in Equation (2-13), the seasonal difference of period s for the series is shown below.

$$\Delta_s Y_t = Y_t - Y_{t-s}, \quad t \in \{s+1, ..., n_{pt}\} \tag{2-13}$$

where $\{Y_t : t = 0,1,...,n_{pt}\}$ stands for the residual time series; s stands for time span of repeating seasonal pattern, where $s < n_{pt}$; and $\Delta_s Y_t$ stands for the seasonal difference of residual time series; and n_{pt} stands for the length of time series for pattern testing. The optimal order of differencing is often the order of differencing at which the standard deviation is lowest.

After stationization by differencing, the next step is to fit the series into an ARIMA model. The AR or MA terms are determined in order to correct autocorrelations that remain in the differenced series. The seasonal ARIMA model incorporates both non-seasonal and seasonal factors in a multiplicative model. One shorthand notation for the model is ARIMA $(p,d,q) \times (P,D,Q)_s$, with (p,d,q) standing for the non-seasonal part, and $(P,D,Q)_s$ standing for the seasonal part. In more details, p stands for the non-seasonal AR order. d stands for the non-seasonal differencing. q stands for the non-seasonal MA order. P stands for seasonal AR order. D stands for the seasonal differencing. Q stands for the seasonal MA order, and s stands for the time span of repeating seasonal pattern. The model could be formally expressed as Equation (2-14) shown below. On the left side, the seasonal and non-seasonal AR components multiply each other, and on the right side, the seasonal and non-seasonal MA components multiply each other.

$$\Phi(B^s)\varphi(B)y_t = \Theta(B^s)\theta(B)e_t \tag{2-14}$$

where B stands for the backward shift operator, as $By_t = y_{t-1}$; s stands for the time span of repeating seasonal pattern; Φ stands for the function of seasonal AR process; and φ stands for the function of AR process. On the right hand side, Θ stands for the function of seasonal MA process; θ stands for the function of MA process; and e_t stands for the error term, which is an independent, identically distributed (i.i.d) variable sampled from a normal distribution with zero mean, named white noise.

To be more in specific, the non-seasonal components selected are shown below. The AR process is shown in Equation (2-15), and the MA process is shown in Equation (2-16).

$$\varphi(B) = 1 - \varphi_1 B - ... - \varphi_p B^p \tag{2-15}$$

$$\theta(B) = 1 + \theta_1 B + ... + \theta_q B^q \tag{2-16}$$

where φ stands for the function of AR process; θ stands for the function of MA process; φ_i, $i = 1, 2, ..., p$, stands for the parameters of the autoregressive part of the model; p stands for the non-seasonal AR order; θ_i, $i = 1, 2, ..., q$, stands for the parameters of the moving average part; and q stands for the non-seasonal MA order.

The seasonal components are also selected separately and are shown below. The seasonal AR process is shown in Equation (2-17), and the seasonal MA process is shown in Equation (2-18).

$$\Phi(B^s) = 1 - \Phi_1 B - ... - \Phi_P B^{Ps} \tag{2-17}$$

$$\Theta(B^s) = 1 + \Theta_1 B^s + ... + \Theta_Q B^{Qs} \quad (2\text{-}18)$$

where Φ stands for the function of seasonal AR process; Θ stands for the function of seasonal MA process; s stands for the time span of repeating seasonal pattern; Φ_i, $i = 1, 2, ..., P$, stands for the parameters of the seasonal autoregressive part of the model; P stands for the seasonal AR order; Θ_i, $i = 1, 2, ..., Q$, stands for the parameters of the seasonal moving average part; and Q stands for the seasonal MA order.

Innovations of the ARIMA model are i.i.d. as the white noise. Since the density function is usually a bell-shaped curve symmetrically around the mean, the normal distribution and the student's t distribution are selected as the two most common symmetric distributions used for innovation fitting.

2.4 Modeling Operation Process of Dam-Reservoir System

In functional terms, the purpose of the dam, reservoir and hydraulic structures together is to intercept uncontrolled stream flows and transform them into controlled outflows. According to Afzali et al. (2008), the objective of reservoir outflow releasing philosophy is to minimize the sum of reservoir releases, and in the meanwhile, maximize the sum of reservoir storages in each of the time periods, subject to a reliability constraint on the hydropower system's energy yield. As a result, a tradeoff exists in the outflow control process. On the one hand, water releasing through the spillway is a loss of power generation potentials. Also, release from the system over and above the normal discharges through the system represents

a potentially dangerous and damaging disturbance in the downstream flows. On the other hand, the structure of the dam must be safe against unexpected changes in the reservoir water elevation. When the water elevation changes suddenly, the released outflow rates of the reservoir water must be arranged correspondingly. Otherwise, extreme water elevation would thus occur.

This section intends to model the general operation process of dam-reservoir system, including the reservoir hydrologic routing and outflow control. Model inputs of this section are the inflow hydrograph derived from the previous Section 2.3, and the model outputs of this section are the outflow discharge and reservoir water elevation. Compared to the dam-reservoir system in the real world, the model proposed is a simplified version to show how functionally each of the system modules are arranged. Evaporation has not been taken into consideration at this moment. The model built in this chapter serves as the fundamental basis of future reservoir operation simulation, and overtopping risk estimation.

2.4.1 Reservoir Hydrologic Routing

In hydrology, routing is a technique used to predict the changes in shape of a hydrograph as water moves through a river channel or a reservoir. From the perspective of outflow control, hydrologic routing is the major logic describing the storage-discharge-stage relationships for the dam-reservoir system. Hydrologic methods are based on the concept that inflow, outflow, and storage must adhere to the conservation of mass principle. Reservoir hydrologic routing also involves the application of the continuity equation to a storage facility in which outflow is an

invertible function of the storage volume for a particular geometry. Simply speaking, the inflow to the river reach is equal to the outflow of the river reach plus the change of storage. Thus, the water storage in reservoir changes within a time interval that can be determined from the continuity equation, Equations (2-19) and (2-20).

$$\frac{dS(t)}{dt}=I(t)\text{-}O(t) \tag{2-19}$$

$$S(t)=\int_{0}^{\infty} I(t)\text{-}O(t)dt \tag{2-20}$$

where $S(t)$ stands for the stochastic storage volume at time t; $I(t)$ stands for the stochastic inflow rate at time t; and $O(t)$ stands for the outflow rate at time t. In a discrete form, the simulation modeling is considered, a rough discrete approximation of Equation (2-19) is demonstrated as Equation (2-21) shown below.

$$\frac{S(t+\Delta t)-S(t)}{\Delta t}=I(t)\text{-}O(t) \tag{2-21}$$

where Δt stands for the slight time increase from time t; $S(t)$ stands for the stochastic storage volume at time t; $S(t+\Delta t)$ stands for the storage volume at time $t+\Delta t$; $I(t)$ stands for the stochastic inflow rate at time t; and $O(t)$ stands for the outflow rate at time t. If the time increase is set as $\Delta t=1$, Equation (2-21) could be simplified as Equation (2-22).

$$S(t+1)-S(t)=I(t)\text{-}O(t), \qquad t\in T=\{1,2,...,n_{md}\} \tag{2-22}$$

where t becomes an integer standing for certain time period t; $S(t)$ stands for the stochastic storage volume at time t; $I(t)$ stands for the stochastic inflow rate at time t;

$O(t)$ stands for the outflow rate at time t; ; and n_{md} stands for the length of time series for dam-reservoir system modeling.

The depth of water and reservoir geometry combines to define the reservoir cross-sectional area. Thus when the reservoir geometry is known, the change in the reservoir water storage could be directly calculated from the change of water elevations, which is much easier to estimate in real practice. In a simplified situation, the following Equation (2-23) could demonstrate the relation.

$$S(t+1) - S(t) = \eta\left[H(t+1) - H(t)\right], \qquad t \in T = \{1, 2, ..., n_{md}\} \tag{2-23}$$

where $\eta[\cdot]$ stands for the function of estimating the reservoir water storage based on the change of water elevations; $S(t)$ stands for the stochastic storage volume at time t; $H(t)$ stands for the stochastic reservoir water elevation at time t; and n_{md} stands for the length of time series for dam-reservoir system modeling.

Spillway gates give the operator a greater control of the outflow rate. In most situations, the reservoir operators rely on the rule curves and other agreed upon operating rules, as well as their own judgment and experience in making reservoir release decisions. The water elevation is normally within the operating headwater level range. The limit of the headwater level is the absolute maximum operating level. The difference between the absolute maximum and maximum operating levels is the flood allowance, which is used to hold water in extreme conditions to reduce downstream flooding. The storage between the absolute minimum and minimum operating levels is used if a system energy emergency occurs. Under normal

operating conditions with equivalent discharges at each station, the full operating range would rarely be utilized.

Overtopping failures occur when the pressure set on the body of the dam exceeds the stable state. When the reservoir storage has reached an appropriate limit, spillways are designed to pass the excess flood-waters, initially through a primary spillway. If large floods exceed the capacity of the primary spillway, emergency spillway would pass the extra water. However, when an extreme flood event occurs, the flows can exceed the combined spillway capacity, spilling over the top of the dam, causing overtopping. In mathematical expression, the overtopping would occur when the reservoir water elevation $H(t) > h_{failure}$ for any t in the evaluation period.

2.4.2 Markov Decision Process of Dam-Reservoir System Operation

In probability theory and statistics, a Markov process, named after the Russian mathematician Andrey Markov, is a stochastic process that satisfies the Markov property, which can be thought as memoryless. One can make predictions for the future of the process based solely on its present state, which has no dependence on knowing the process's full history. Based on the Markov process, a Markov decision process (MDP) is a Markov reward process with decisions, in which all states are Markov. MDP has been used since the early fifties for the planning and operation of dam-reservoir systems (Feinberg and Shwartz 2012). The transition equations of mass conservation for the reservoir storages are akin to those found in inventory theory.

Interpreting Equations (2-22) and (2-23) from a different perspective, the following Equations (2-24) and (2-25) construct a rather simplified version to show how functional the dam-reservoir systems are arranged.

$$O(t) = \varsigma[I(t), H(t)], \qquad t \in \{0,1,...,n_{md}\} \tag{2-24}$$

where $\varsigma[\cdot]$ stands for the decision rule function of outflows based on the current inflow rate and the reservoir water elevation. $O(t)$ stands for the outflow rate at time t; $I(t)$ stands for the stochastic inflow rate at time t; and $H(t)$ stands for the stochastic reservoir water elevation at time t; and n_{md} stands for the length of time series for the dam-reservoir system modeling.

This means the first relationship among the inflow rate $I(t)$, water elevation $H(t)$, and the outflow rate $O(t)$ has successfully been built. Meanwhile, based on Equations (2-22) and (2-23), Equation (2-25) shown below, could also be derived as another relation among the inflow rate $I(t)$, the water elevation $H(t)$, and the outflow rate $O(t)$.

$$\begin{aligned} H(t+1) &= \eta^{-1}[I(t) - O(t)] + H(t) \\ &= \zeta[I(t), O(t), H(t)] \end{aligned}, \qquad t \in \{0,1,...,n_{md}\} \tag{2-25}$$

where $\eta[\cdot]$ stands for the function of estimating the reservoir water storage based on the change of water elevations; $\zeta[\cdot]$ stands for the general function demonstrating the relations among the inflow rate, the water elevation, and the outflow rate; $I(t)$ stands for the stochastic inflow rate at time t; $O(t)$ stands for the outflow rate at time t; $H(t)$ stands for the stochastic reservoir water elevation at time t; and n_{md} stands for the length of time series for dam-reservoir system modeling.

Combining Equations (2-24) and (2-25), Equation (2-26) can be reached as below. For any time period *t*, the reservoir water elevation could be estimated tracing back to the initial reservoir water elevation, and the incoming historical inflows.

$$\begin{aligned} H(t) &= \zeta[I(t), f[I(t-1), H(t-1)], H(t-1)] \\ &= \xi[I(t), I(t-1), ..., I(1), H_0] \\ t &\in \{0, 1, ..., n_{md}\} \end{aligned}, \quad (2\text{-}26)$$

where $\xi[\cdot]$ stands for the function of reservoir water elevation based on the initial elevation plus the inflows through certain time span; $\zeta[\cdot]$ stands for the general function demonstrating the relations among the inflow rate, the water elevation, and the outflow rate; $H(t)$ stands for the stochastic reservoir water elevation at time t; $I(t)$ stands for the stochastic inflow rate at time t; H_0 stands for the initial water elevation of the reservoir; and n_{md} stands for the length of time series for dam-reservoir system modeling. For the time period t that $t \in \{0, 1, ..., n_{md}\}$, overtopping would occur if $\max[H(t)] > h_{failure}$. Here $h_{failure}$ is the top of dam that could not be exceeded.

The most basic type of MDP is the discrete time MDP, as a tuple of {States, Actions, Transition, Reward, Discount factor}. The state variable stands for the finite set of domain states, which could be observed at discrete time period $t \in \{0, 1, ..., n_{md}\}$. The action variable stands for a finite set of actions. When the system is observed to be at certain state, an action from the action variable should be chosen. Then, two things will happen: 1) the system will receive a reward, and 2) the system will transfer to state at the next period with state transition probability. Thus, the transition stands for the state transition function, which is usually associated with a probability

matrix. The reward variable stands for a reward function, and the discount factor is a number between 0 and 1. Deeming the dam-reservoir system operation as a Markov decision process, Figure 2-1 demonstrates the inner relationship among inflows, outflows, and reservoir water elevations.

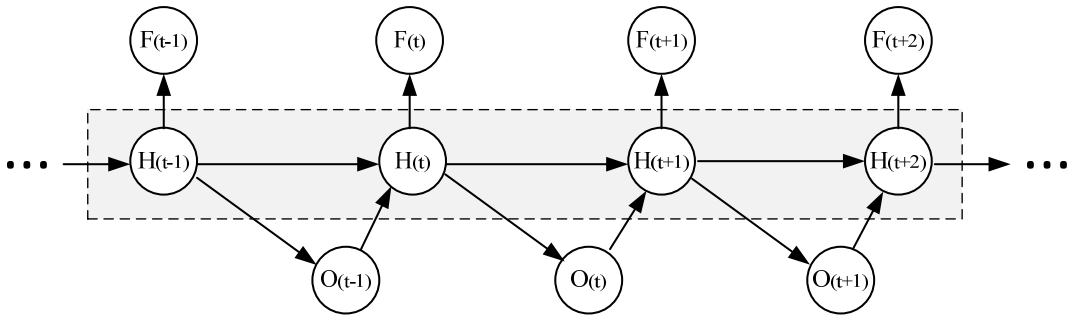

Figure 2-1 Markov decision process of dam-reservoir system operation

The state variables are the reservoir water elevation $\{H(t):t=0,1,...,n_{md}\}$, which represents the volume of water in storage in the reservoir at a certain time period *t*. The decision to be made in period *t* is the quantity of water to release through the turbines and the quantity of water to evacuate through the spillways. As a result, the decision variables are the outflow rates $\{O(t):t=0,1,...,n_{md}\}$. $\{F(t):t=0,1,...,n_{md}\}$ stands for the reward functions which are used for deciding whether overtopping occurs at time period *t*. For the transition rate function, additional hydrologic state variables could be taken into consideration. Hydrologic variables in the state vector also allow consideration of the serial correlation of natural inflows. Differing from the traditional MDP problems, which are expected to find the optimal policy or control to give the optimal expected integrated reward, the reward variables in this situation specifically used for checking whether overtopping

occurs or not are shown as binary variables. In general, this process models the operation process of the dam-reservoir system.

2.5 Summary

In summary, this chapter sets up the fundamental dam-reservoir system model for further simulation modeling and analysis. Both the inflow hydrograph model and the dam-reservoir system operation model are built, which are also connected as a sequence internally. Literature reviews of the critical factors leading to dam-reservoir overtopping risks serves as the basis for the proposed model. Both the inflow hydrograph and the outflow controls are involved. Then, two major parts are included in modeling dam-reservoir system performance under uncertainty: 1) modeling inflow hydrograph; and 2) modeling operation process of the dam-reservoir system. Synchronizing these two parts together in this chapter, performance of the dam-reservoir system is modeled with potential overtopping risks. Uncertainties within the inflow hydrograph and the system operation process are also taken into consideration.

Chapter 3: Simulating Overtopping Risks of Dam-Reservoir System

3.1 Introduction

Following by the model developed from Chapter 2, simulation of the reservoir inflow rate is needed, and could start with multiple independent and identical distributed random variables. The detailed simulation procedures have been presented in this chapter in order to estimate the overtopping risks of the dam-reservoir system under uncertainties. The literature review part firstly focuses on the rare event simulation applied in complex engineering systems. Definitions of the rare events, the advantages of rare event simulation, and the engineering-case applications are introduced within this part. Then, frameworks of both CMC and ISMC simulation are developed with methodology foundations and application comparison. This chapter also serves as the theoretical basis of Chapter 5. The CMC and ISMC simulation methods proposed in this chapter would also apply to the similar engineering cases.

3.2 Literature Review on IS and Rare Event Simulation

3.2.1 Rare Event Simulation and IS

MC methods are a broad class of computational algorithms that rely on repeated random sampling to obtain numerical results (Kalos and Whitlock 2008; Liu 2008). The modern version of the MC method was invented in the late 1940s by Stanislaw Ulam on the nuclear weapons projects at the Los Alamos National Laboratory (Cooper et al. 1989). Immediately after Ulam's breakthrough, John von Neumann

understood its importance and programmed the Electronic Numerical Integrator And Computer (ENIAC) to carry out MC calculations (Neumann 2005). In engineering, MC methods are widely used for sensitivity analysis and quantitative probabilistic analysis in process design. The need of such application arises from the interactive, co-linear and non-linear behaviors of typical process simulations (Roebuck 2012). However, significant computational resources are usually required in the simulation to reach the satisfied results (Bucklew 2004). Otherwise, long wait times or buffer overflows might occur. For a discrete system of moderate complexity, there are a combinatorial large number of possible system states. As is often the case, estimation of the probability of failure and consequences of any given system state involves computationally expensive simulation. It is commonly infeasible to analyze all possible states due to the resources required (Dawson and Hall 2006).

Rare event simulation and quantification come from the need to ensure that undesirable events will not appear. Typically, such an event is the failure of industrial critical systems, for which failure is regarded as a massive catastrophic situation. Usually the system is a "black box" whose output determines safety or failure domains (Walter and Defaux 2015). A great deal of attention has been focused on the development of MC techniques. Today, the rare event simulation applications range from lightwave and optical communication systems (Smith et al. 1997), to industrial routing problems (Chepuri and Homem-de-Mello 2005), and to financial asset pricing (Chan and Wong 2015). According to Bucklew (2004) and Rubino and Tuffin (2009), a rare event means an event that occurs infrequently with a very small probability, but important enough to justify their study. Rare event simulation is thus an umbrella

term for a group of computer simulation methods intended to selectively sample 'special' regions of the dynamic space of systems that are unlikely to visit those special regions through brute-force simulation (Juneja and Shahabuddin 2002). Based on the hazard-rate twisting method, Huang and Shahabuddin (2004) discussed a general approach to estimate rare-event probabilities in static problems.

IS has been extensively investigated by the simulation community in the last decade, which serves as one of the general approaches for speeding up simulations and to accelerate the occurrence of rare events. The basic ideas behind IS were outlined by Kahn and Marshall (1953). Certain values of the input random variables in a simulation have more impact on the parameter being estimated than on others. If these values are emphasized by sampling more frequently, then the estimator variance can be reduced to a better accepted level. Hence, the basic methodology in IS is to choose a distribution that encourages the important values, and to estimate the probability of interest via a corresponding likelihood ratio (LR) estimator. Illustration of ISMC simulation is shown in Figure 3-1. The simulation outputs are weighted to correct for the use of the biased distribution, and this ensures that the new IS estimator is unbiased. The weight is given by the likelihood ratio, that is, the Radon–Nikodym derivative of the true underlying distribution with respect to the biased simulation distribution.

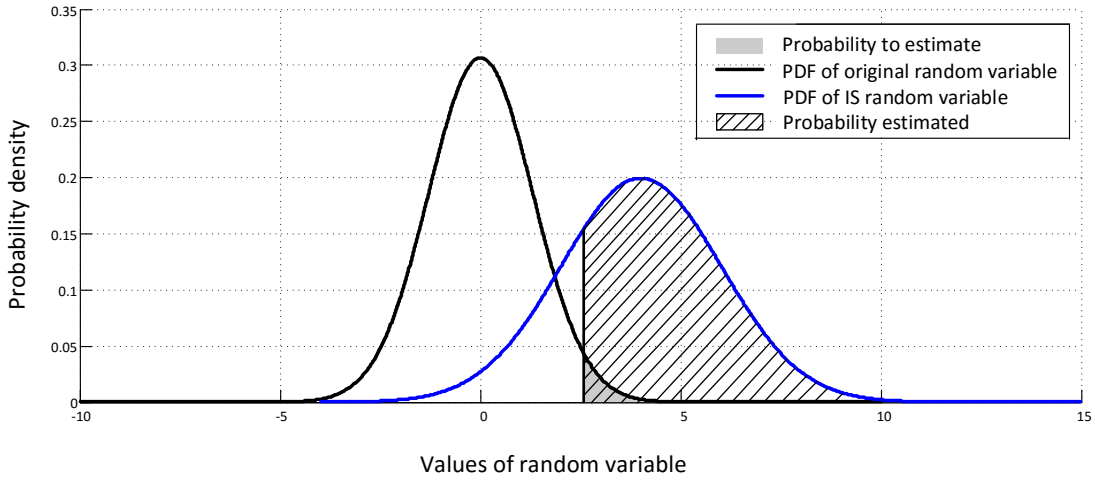

Figure 3-1 Graphical illustration of ISMC simulation

A considerable amount of past research has been devoted to the study of IS techniques in simulation, in particular for rare-event simulation. Based on Glynn and Iglehart (1989)'s research, the IS idea was extended to the problems arising in the simulation of stochastic systems. Discrete-time Markov chains, continuous-time Markov chains, and generalized semi-Markov processes were covered. Shahabuddin (1995) also reviewed fast simulation techniques used for estimating probabilities of rare events and related quantities in different types of stochastic models. Based on the IS technique, multiple variance reduction tools for solving rare event problems could also be found in varied areas (Ding and Chen 2013; Jacquemart and Morio 2013; Morio et al. 2010, 2013).

3.2.2 Applications in Engineering Related Fields

Applications of rare event simulation and IS techniques could frequently be found in the reliability engineering field in the past research, in order to reduce simulation expenses and increase estimation accuracy. According to Alexopoulos and Shultes

(2001), IS in conjunction with regenerative simulation were presented as a promising method for estimating reliability measures in highly dependable Markov systems. L'Ecuyer and Tuffin (2009) and Dai et al. (2012) also considered the Markov chain models and simulation to represent the evolution of multicomponent systems in reliability settings. This is based on dynamic IS and the probability that a given set of nodes was connected in a graph where each link was failed with a given probability. According to Au and Beck (1999), an adaptive IS methodology was proposed to compute the multidimensional integrals encountered in reliability analysis. In the proposed methodology, samples were simulated as the states of a Markov chain and they were distributed asymptotically according to the optimal IS density. IS was also adopted in structural reliability analysis (Dawson and Hall 2006; Grooteman 2008). The case studies proposed demonstrated that the risk could be a complex function of loadings, the resistance and interactions of system components and the spatially variable damage associated with different modes of system failure.

Severe blackouts due to cascading failures in the electric grid are rare but catastrophic. Consequently, the power system becomes another application focus that rare event simulation and IS concentrated on. Belmudes et al. (2008) proposed an approach for identifying rare events that may endanger power system integrity. The approach was also illustrated on the IEEE 30 bus test system when instability mechanisms related to static voltage security were considered. Wang et al. (2011) also presented an effective rare-event simulation technique to estimate the blackout probability. An IEEE-bus electric network was chosen as the application case, and the most vulnerable link in the electric grid was detected, which has the highest

probability of leading to a blackout event. Besides, power system security analysis is often strongly tied with contingency analysis. With variable generation sources such as wind power and due to fast changing loads, power system security analysis has to incorporate sudden changes in injected powers that are not due to generation outages. Perninge et al. (2012) used IS for injected-power simulation to estimate the probability of system failure, given a power system grid state. A comparison to standard CMC simulation was also performed in a numerical example and it indicated a major increase in simulation efficiency.

MC techniques and rare event simulation are also widely used in many other fields. In financial engineering, the accurate measurement of credit risk is often a rare-event simulation problem because default probabilities are low for highly rated obligors and because risk management is particularly concerned with rare but significant losses resulting from a large number of defaults. To solve these problems, Bassamboo et al. (2008) derived sharp asymptotic for portfolio credit risk that illustrated the implications of extremal dependence among obligors. Importance-sampling algorithms were then developed to efficiently compute portfolio credit risk via MC simulation. Glasserman and Li (2005) also provided an IS procedure for the widely used normal copula model of portfolio credit risk. The procedure had two parts: one that applies the IS conditional on a set of common factors affecting multiple obligors, and the other that applies IS to the factors themselves. The relative importance of the two parts of the procedure was determined by the strength of the dependence between obligors. Besides, in the queueing system, Blanchet and Lam (2014) developed rare-event simulation methodology for the analysis of loss events in

a many-server loss system under the quality-driven regime. Heidelberger (1995) also surveyed efficient techniques via simulation for estimating the probabilities of certain rare events. In operational systems, Bee (2009) used IS to estimate tail probabilities for a finite sum of lognormal distributions. And, in public health, Clemencon et al. (2013) focused, in the context of epidemic models, on rare events that might possibly correspond to crisis situations. In biochemical systems, Kuwahara and Mura (2008) proposed an efficient stochastic simulation method to analyze deviations from highly controlled normal behavior in biochemical systems.

3.2.3 Research Gap on Rare Event Simulation Application in Dam-Reservoir System

MC methods are widely used because of their flexibility and robustness. Analytical solutions or accurate approximations are only available for a very restricted class of simple systems. In most cases, engineering systems need to resort to simulation in order to conduct probabilistic estimation and sensitivity analysis. Due to the stochastic nature of a dam-reservoir system, the dynamics of system operations and corresponding overtopping risks could be modeled through MC simulation. According to Wang and Bowles (2006), a simulation-based model was developed on the breach process at multiple breach locations for a dam with an uneven crest under wind and wave action. Dewals et al. (2010) also applied the simulation of flows induced by several failure scenarios on a real complex of dams, involving collapse and breaching of dams in cascade. As an output, the simulation provided emergency planning and risk analysis, including the sequence of successive overtopping and failures of dams, the time evolution of the flow characteristics at all points of the

reservoirs, hazard maps in the downstream valley as well as hydrographs and limnigraphs at strategic locations in the valley. Besides, Tsakiris and Spiliotis (2012) also developed an approach that combined both the simulation and semi-analytical solution, in order to address the dam breach formation caused by overtopping and the resulting outflow hydrograph. Generalized reservoir system operation models include HEC-5, which is the most widely used reservoir operation simulation model, IRIS and IRAS, the SWD SUPER Modeling System, and the WRAP Modeling System.

Although applications of MC methods range widely from estimating integrals, minimizing difficult functions, to simulating complex systems, they are generally expensive and are only applied to problems that are too difficult to handle by deterministic methods. The overtopping events, in most cases, have very small occurrence probabilities. The standard MC method is not always the most appropriate tool especially when we deal with those rare events. According to Rani and Moreira (2010), simulation without preliminary screening would be very time consuming, in view of the very large number of options of configuration, capacity and operating policy. Dawson and Hall (2006) also pointed out that the computational expense serves as one of the prohibitive reasons that the simulation technique has not been widely applied to reservoir operations. Minimizing simulation based estimation error rates at a reasonable cost is consequently an important aspect of these practical problems. In order to save the computational expenses and increase estimation accuracy, rare event simulation has been adopted for efficient estimation, especially on small probability events. As one of the most common rare event simulation

techniques, IS is involved in many engineering applications in order to achieve variance reduction.

As an extension of CMC simulation, the rare event simulation techniques have been adopted in the dam-reservoir system operation. These researches mostly focus on the critical factors such as peak inflow rate, that might lead to the overtopping events (Hsu et al. 2010; 2012). However, overtopping is a complete process. Generally speaking, the water surface elevation in a reservoir is directly tied to the whole storage volume, with either a linear or a nonlinear relationship based on the reservoir shape. As a result, the stochastic inflow rate integrated within a certain period of time would change the reservoir storage, assuming there is no outflow releasing to the system. Overtopping would potentially occur due to the continuous high inflow volumes, even when the annual peak inflow rate is not extreme. Modeling and simulating a whole system is thus beneficial to the final overtopping estimation. Positive correlations between the peak inflow rate and the inflow volume within a specified time period are proven to exist (Goodarzi et al. 2012; Poulin 2007).

3.3 CMC Simulation of Overtopping Risks

3.3.1 Framework of CMC

For both the CMC and the ISMC simulations, the final objective is to assess the overtopping risk probability of the dam-reservoir system within a specified time scale, which is rather hard by analytical solutions in real practice. MC simulation is implemented to model the operation of the dynamic dam-reservoir systems. In order

to estimate the probability of overtopping events within a certain time scale, the following simulation framework is proposed in this section as a dynamic process shown in Figure 3-2.

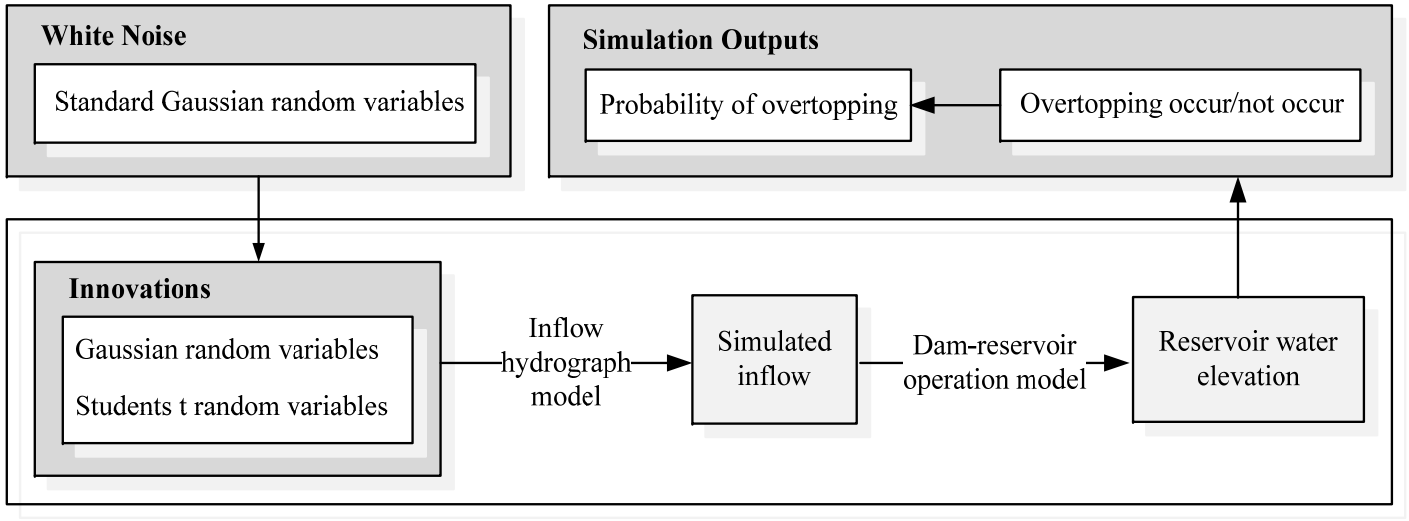

Figure 3-2 Framework of CMC simulation for overtopping risks estimation

For the one-time simulation, a standard Gaussian random series is generated with the same length of given simulation period first. Each element within the series is generated i.i.d. Based on the initial white noise, a series of Gaussian random variables or a series of Student's t random variables are generated with the adjustment parameters coming from existing inflow hydrograph model.

These variables serve as the simulated residuals for the constructed ARIMA and seasonal ARIMA models. The simulated future inflows are reconstructed by adding the seasonal cycle back, which are derived from Fourier decomposition and logarithmic transformation. Then, the reservoir water elevations are simulated based on the dam-reservoir operation model. According to the reservoir water elevation series, the overtopping occurrence would finally be counted as a binary variable. Thus, for multiple simulations, the frequencies of overtopping occurrence are counted and the probability is calculated as the final simulation outputs.

3.3.2 CMC Based Overtopping Probability Estimation

In more detail, two parts are addressed in this section: 1) the transformation of white noise to the ARIMA innovation (the arrow from "White Noise to Innovations" in Figure 3-1); and 2) the CMC simulation algorithm of overtopping probability estimation (the arrow from reservoir water elevation to probability of overtopping).

3.3.2.1 Transformation from white noise to ARIMA innovation

In discrete time, a white noise series is a discrete signal whose samples are regarded as a sequence of serially uncorrelated random variables with zero mean and finite variance. In other words, a single realization of white noise is a random shock, and i.i.d is the simplest representative of white noise. For instance, if each sample within a signal has a normal distribution with zero mean, the signal is said to be a Gaussian white noise. To the specific CMC simulation, transformations from the white noise to the ARIMA innovation are discussed. Since the density function is usually a bell-shaped curve that is symmetric around the mean, the normal distribution and the

Student's t distribution are selected as the two most common symmetric distributions used for innovation fitting. The transformation from the normal distributed white noise to the normal random innovation does not change the distribution nature. The probability density function of the Gaussian distribution is shown in Equation (3-1).

$$f(x) = \frac{1}{\sqrt{2\pi}\sigma_f} \exp\left[\frac{-(x-\mu_f)^2}{2\sigma_f^2}\right], \qquad -\infty < x < \infty \tag{3-1}$$

where $f(\cdot)$ stands for the probability density function of the original random variables; μ_f stands for the mean of the original random variables; and σ_f stands for the standard deviation of the original random variables. Accordingly, the transformation process is developed as shown in Equation (3-2) below.

$$X(t) = \mu_f + \sigma_f Z(t), \qquad t \in \{1, 2, ..., n_C\} \tag{3-2}$$

where $X(t)$ stands for the normal random innovation at time *t*; μ_f stands for the mean of the original random variables; σ_f stands for the standard deviation of the original random variables; $Z(t)$ stands for the normal distributed white noise at time *t*; and n_C stands for the length of time series for the CMC simulation.

To prove Equation (3-2), suppose $\sigma_f > 0$ and note that the cumulative distribution function (cdf) of the random variable *X* is given by the following Equation (3-3). Transformation could be performed from the normal distributed white noise Z to the normal random innovation *X*.

$$F_X(a_{cut}) = P\{X \le a_{cut}\} = P\{\mu_f + \sigma_f Z \le a_{cut}\}$$
$$= P\left\{Z \le \frac{a_{cut} - \mu_f}{\sigma_f}\right\} = F_Z\left(\frac{a_{cut} - \mu_f}{\sigma_f}\right) \tag{3-3}$$

where $F_X(\cdot)$ stands for the cdf of the normal random innovation; Z stands for the normal distributed white noise; μ_f stands for the mean of the original random variables; σ_f stands for the standard deviation of the original random variables; and a_{cut} stands for the cutoff value of rare event probability estimation. In the dam-reservoir case, a_{cut} is the dam crust height that could not exceed. Otherwise, the overtopping would occur.

The following Equations (3-4) and (3-5) are thus developed correspondingly in order to demonstrate the transformation from the normal distributed white noise Z to the normal random innovation *X*.

$$F_X(a_{cut}) = \int_{-\infty}^{(a_{cut}-\mu_f)/\sigma_f} \frac{1}{\sqrt{2\pi}} \exp\left(-\frac{z^2}{2}\right) dz$$
$$= \int_{-\infty}^{a_{cut}} \frac{1}{\sqrt{2\pi}\sigma_f} \exp\left\{-\frac{(x-\mu_f)^2}{2\sigma_f^2}\right\} dx \tag{3-4}$$

$$f_X(a_{cut}) = \frac{1}{\sqrt{2\pi}\sigma_f} \exp\left\{-\frac{(x-\mu_f)^2}{2\sigma_f^2}\right\}, \qquad -\infty < x < \infty \tag{3-5}$$

where $F_X(\cdot)$ stands for the cdf of the normal random innovation; $f_X(\cdot)$ stands for the pdf of the normal random innovation; a_{cut} stands for the cutoff value of rare event

probability estimation; μ_f stands for the mean of the original random variables; and σ_f stands for the standard deviation of the original random variables.

The transformation process from the normal distributed white noise to the Student's t random innovation starts with the transformation from the normal random innovation to the Student's t random innovation. As a sequence, the normal distributed white noise could be transferred to the normal random innovation, and then to the Student's t random innovation. Given a generator of i.i.d. standard Gaussian random variates, t_k distributed random variates with any positive integer degree of freedom *k* could be generated by using the relation as Equation (3-6) shown below.

$$X_{st}(t) = Z_{k+1}(t) / \sqrt{k^{-1} \sum_{i=1}^{k} Z_i(t)^2} , \qquad t \in \{1, 2, ..., n_C\} \tag{3-6}$$

where $X_{st}(t)$ stands for the Student's t random innovation at time *t* ; $Z_{(\cdot)}(t)$ stands for the normal distributed white noise at time *t*; *k* stands for the degree of freedom for the student's t distribution, which could be approximated by the Maximum Likelihood Estimation (MLE); and n_C stands for the length of time series for CMC simulation.

3.3.2.2 CMC simulation-based probability estimation

Specifically for our case, estimating the probability of overtopping events serves as our main focus, which is also relatively small for most dam-reservoir systems. As showing below, Equation (3-7) represents the mathematical expression of overtopping probability.

$$l = P\left(\max[H(t)] \geq h_f\right) = E\left(I_{\{\max[H(t)] \geq h_f\}}\right), \quad t \in \{1, 2, ..., n_C\} \tag{3-7}$$

where l stands for the overtopping probability of the dam-reservoir system; $P(\cdot)$ stands for the function of probability value; $H(t)$ stands for the stochastic reservoir water elevation at time *t*; h_f stands for the top of dam that could not be exceeded; $E(\cdot)$ stands for the function of expectation value; $I_{(\cdot)}$ stands for the indicator function with binary values in [0, 1]; and n_C stands for the length-of-time series for the CMC simulation.

Comparing with the ISMC simulation, the algorithm for the CMC simulation is relatively simple and straightforward. The direct simulation method to estimate *l* would be to generate several sequences of simulated reservoir water elevation independently. Then, comparing the maximum value of reservoir water elevation in each sequence with the top of dam, a judgment on whether or not overtopping occurred could be reached. As shown below, Equation (3-8) is adopted as the mathematical expression for the CMC simulation.

$$\hat{l}_C = \frac{1}{N_C} \sum_{j=1}^{N_C} I_{j\{\max[H(t)] \geq h_f\}}, \quad t \in \{1, 2, ..., n_C\} \tag{3-8}$$

where $\hat{l}_C$ stands for the CMC simulation estimator of the overtopping probability for the dam-reservoir system; $H(t)$ stands for the stochastic reservoir water elevation at time *t*; n_C stands for the length of time series for CMC simulation; h_f stands for the top of the dam that could not exceed; $I_{(\cdot)}$ stands for the indicator function with binary

values in [0, 1]; and N_C stands for the iteration of CMC simulation. So, of N_C times simulations, $\sum_{j=1}^{N_C} I_{j\{\max[H(t)]\geq h_f\}}$ times overtopping would occur.

3.3.3 Procedures for CMC Simulation Application

The general procedures for the CMC simulation application in the dam-reservoir system performance modeling is shown in this section. As presented before, the normal distribution and the Student's t distribution are selected as the two most common symmetric distributions used for time series innovation fitting. Thus, the simulation procedures based on the normal random innovation and the Student's t random innovation are included in the discussion. Overlapping exists in multiple procedures and the major differences are the initial random variable generations.

For the CMC simulation with normal distributed innovation, the following steps are listed as the major procedures:

Step 1. Set N_t equal to 0;

Step 2. Set $N_t = N_t + 1$, and N_C as the maximum simulation iterations. If $N_t \geq N_C$, iteration stops and jump to Step 9;

Step 3. Generate $\{Z_1, Z_2, ..., Z_{n_C}\}$, which are i.i.d. as the standard white noise from the distribution of $N(0,1)$ with the time length of n_C. Usually the time is tracking on a daily bases;

Step 4. Transform from the standard white noise series to the normal distributed innovation $\{X_1, X_2, ..., X_{n_C}\}$, which are i.i.d. with the time scale length of n_C;

Step 5. Transform from the normal distributed innovation $\{X_1, X_2, ..., X_{n_C}\}$ to the simulated inflow rate series $\{I(t): t = 1, 2, ..., n_C\}$ with all identified patterns added in;

Step 6. Transform from the simulated inflow rate series $\{I(t): t = 1, 2, ..., n_C\}$ to the reservoir water elevation $\{H(t): t = 1, 2, ..., n_C\}$ based on the developed dam-reservoir operation model;

Step 7. Compare with the height of dam top and justify whether the overtopping occurs or not;

Step 8. Return to Step 2;

Step 9. Count the frequency of overtopping, and estimate the simulated overtopping probability.

3.3.4 Challenges of CMC Simulation

Consider the estimation of the tail probability $l = P\left(\max[H(t)] \geq h_f\right)$ of stochastic random variable $H(t)$ shown in previous Equation (3-4), for a large number h_f. If l is very small, the event $\left\{\max[H(t)] \geq h_f\right\}$ could be called the rare event, and the probability $P\left(\max[H(t)] \geq h_f\right)$ could be called the rare-event probability. Estimation of l via MC simulation is usually followed by the algorithm shown in previous Equation (3-5). The estimator $\hat{l}_C$ is thus defined as the CMC simulation estimator. The accuracy measure for the estimator $\hat{l}_C$ converges to the relative error (RE) of $\hat{l}_C$, defined as Equation (3-9).

$$\kappa = \frac{\sqrt{Var(\hat{l}_C)}}{E(\hat{l}_C)} = \frac{\sqrt{Var(I_{\{\max[H(t)]\geq h_f\}}) / N_C}}{l}, \tag{3-9}$$

where κ stands for the RE of $\hat{l}_C$; $Var(\cdot)$ stands for the variance function; $E(\cdot)$ stands for the function of expectation value; l stands for the overtopping probability for dam-reservoir system; $\hat{l}_C$ stands for the CMC simulation estimator of overtopping probability for the dam-reservoir system; and N_C stands for the iteration of CMC simulation.

As a follow-up of Equation (3-6), the RE of CMC estimator $\hat{l}_C$ is shown in Equation (3-10). Approximation is made due to the extreme small l and large N_C.

$$\kappa = \frac{\sqrt{l(1-l) / N_C}}{l} = \sqrt{\frac{1-l}{N_C l}} \approx \sqrt{\frac{1}{N_C l}}, \tag{3-10}$$

where κ stands for the RE of $\hat{l}$; l stands for the overtopping probability of the dam-reservoir system; and N_C stands for the length of time series for CMC simulation.

As a numerical example, suppose $l = 10^{-6}$ is the tail probability to be estimated through CMC simulation. In order to estimate l accurately with the required RE, the sample size would be reached as Equation (3-11) shown below.

$$N_C \approx \frac{1}{\kappa^2 l}, \tag{3-11}$$

where N_C stands for the iteration of CMC simulation; κ stands for the RE of $\hat{l}_C$; l stands for the overtopping probability of the dam-reservoir system. If the RE

$\kappa = 0.01$, the sample size N_C would reach 10^{10}. As a result, we could reasonably conclude that when the probability l is very small, a very large simulation effort would be required to achieve the required accuracy. It is a big challenge to estimate the small probabilities via CMC simulation. Otherwise, the results would not be persuasive.

3.4 ISMC Simulation of Overtopping Risks

3.4.1 Framework of ISMC Simulation

The main idea of IS is to make the occurrence of rare events more frequent by carrying out the simulation under a different probability distribution and to estimate the probability of interest via a corresponding likelihood ratio (LR) estimator. According to the proposed CMC simulation approach, the efficient ISMC simulation framework is proposed in this section. Detailed information and the improvement part are shown in Figure 3-3.

It is the same as for the CMC simulation: a standard Gaussian random series is also generated with the same length of a given simulation period at the start of simulation for one time. Each element within the series is generated i.i.d. Then, a transformation has been performed to make the series follow the selected new probability density. Based on the updated random variables, the series of Gaussian random variables or Student's t random variables are generated with the adjustment parameters from inflow hydrograph model. The simulated future inflows are reconstructed as a following with the seasonal cycle added back. Then, the reservoir water elevations are simulated based on the dam-reservoir operation model.

According to the reservoir water elevation series, the overtopping occurrence would finally be counted as a binary variable. The LR estimator is also calculated based on the proposed new variable density. Finally, the frequencies of overtopping occurrence are counted and the probabilities are reached as the simulation outputs.

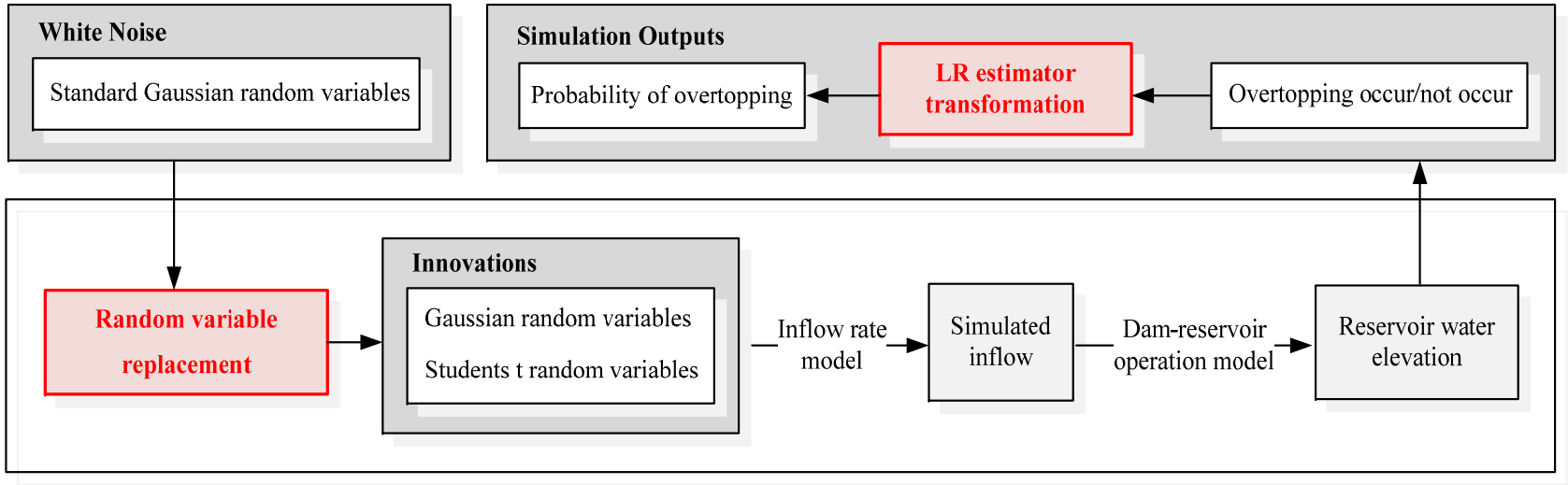

Figure 3-3 Framework of ISMC simulation for overtopping risks estimation

3.4.2 ISMC Overtopping Probability Estimation

In more detail, random series are drawn i.i.d. from the proposed new probability density as a random sample for the *i*th simulation. Equation (3-12) provides a different perspective for showing the stochastic maximum reservoir water elevation, which could be a critical indicator justifying whether overtopping occurs for the dam-reservoir system.

$$\begin{aligned} S(X_i) &= \max\{H_i(t) : t = 0,1,...,n_{IS}\} \\ &= \max\{H_i(1),...,H_i(n_{IS})\} \end{aligned}, \tag{3-12}$$

where X_i stands for the generated random series that follows the selected new probability density for the *i*th simulation, that $X_i = \{X_i(1),....X_i(n_{IS})\}$. $S(\cdot)$ stands for the transformation function from the random series to the maximum reservoir water elevation; $H_i(t)$ stands for the stochastic reservoir water elevation at time *t* for the *i*th simulation; and n_{IS} stands for the length of time series for ISMC simulation.

As a result, the mathematical expression of overtopping probability is updated as Equation (3-13) shown below.

$$l = P\left(\max\{H(t)\} \geq h_f\right) = P\left(S(X) \geq h_f\right), \quad t \in \{0,1,...,n_{IS}\} \tag{3-13}$$

where l stands for the overtopping probability of the dam-reservoir system; $P(\cdot)$ stands for the probability function; $H(t)$ stands for the stochastic reservoir water elevation at time *t*; h_f stands for the top of the dam that could not be exceeded; $I_{(\cdot)}$ stands for the indicator function with binary values in [0, 1]; and n_{IS} stands for the length of time series for ISMC simulation.

In order to estimate the overtopping probability of dam-reservoir system through the ISMC simulation, Equation (3-14) is adopted as shown below. Prior to the LR transformation, Equations (3-8) and (3-14) are in a very similar format.

$$\hat{l}_{IS} = E\left(I_{\{S(X)\geq h_f\}}\right) = \frac{1}{N_{IS}}\sum_{j=1}^{N_{IS}} I_{j\{S(X)\geq h_f\}}\,, \tag{3-14}$$

where $\hat{l}_{IS}$ stands for the ISMC simulation estimator of the overtopping probability for dam-reservoir system; $E(\cdot)$ stands for the function of expectation value; h_f stands for the top of dam that could not exceed; $I_{(\cdot)}$ stands for the indicator function with binary values in [0, 1]; *i* stands for the index of simulation iterations; and N_{IS} stands for the iteration of ISMC simulation.

As discussed before, N_{IS} needs to be very large in order to achieve an estimation of *l* within the acceptable confidence intervals. Using IS is a better way to perform the MC simulation, which replaces the probability density function from $f(\cdot)$ to $g(\cdot)$ as a new probability density. Detailed information is presented in Equations (3-15) and (3-16).

$$g(x) = I_{\{S(x)\geq h_f\}} f(x) = 0, \tag{3-15}$$

where $g(\cdot)$ stands for the probability density function of the replaced random variables; $I_{(\cdot)}$ stands for the indicator function with binary values in [0,1]; and $f(\cdot)$ stands for the probability density function of the original random variables.

$$W(x) = \frac{f(x)}{g(x)}, \tag{3-16}$$

where $W(\cdot)$ stands for the LR function for IS; $f(\cdot)$ stands for the probability density function of the original random variables; and $g(\cdot)$ is the IS density, which stands for the probability density function of the replaced random variables.

As a result, the original random variable $\{X(t)\}$ with probability density function of $f(\cdot)$ is replaced by the updated random variable $\{Y(t)\}$ with a probability density function of $g(\cdot)$. Detailed information is shown in Equation (3-17) below.

$$\begin{aligned} l &= \int I_{\{S(X_i)\geq h_f\}} \frac{f(x)}{g(x)} g(x)dx \\ &= E_g\left[I_{\{S(Y)\geq h_f\}} \frac{f(y)}{g(y)} \right] = E_g\left[I_{\{S(Y)\geq h_f\}} W(y) \right] \end{aligned}, \tag{3-17}$$

where l stands for the overtopping probability for dam-reservoir system; $I_{(\cdot)}$ stands for the indicator function with binary values in [0,1]; $W(\cdot)$ stands for the LR function for IS; $f(\cdot)$ stands for the probability density function of the original random variables; $g(\cdot)$ stands for the probability density function of the replaced random variables; and $E_g(\cdot)$ stands for the function of expectation value for ISMC estimation.

Thus, an updated unbiased estimator of l is shown in Equation (3-18) below.

$$\hat{l}_{IS} = \frac{1}{N_{IS}} \sum_{j=1}^{N_{IS}} I_{j\{S(Y)\geq h_f\}} \frac{f(y)}{g(y)} = \frac{1}{N_{IS}} \sum_{j=1}^{N_{IS}} I_{j\{S(Y)\geq h_f\}} W(y), \tag{3-18}$$

where $\hat{l}_{IS}$ stands for the ISMC simulation estimator of the overtopping probability for the dam-reservoir system; N_{IS} stands for the iteration number of ISMC simulation; $I_{(\cdot)}$ stands for the indicator function with binary values in [0,1]; $W(\cdot)$ stands for the

LR function for IS; $f(\cdot)$ stands for the probability density function of the original random variables; and $g(\cdot)$ stands for the probability density function of the replaced random variables.

3.4.3 Selection of IS Density

The fundamental issue in implementing IS simulation is the choice of the biased distribution that encourages the important regions of the input variables. The rewards for a good IS distribution can be significant run-time savings. The penalty for a bad IS distribution can be longer running times than a CMC simulation without IS. As a result, this section intends to discuss the IS density selection specifically towards the overtopping risk estimation. In theory, there exists a change of measure that yields a zero-variance LR estimator. However, in practice such an optimal IS density is hard to be computed since it depends on the underlying variable quantity or quantities being estimated. Here, the detailed density selection process for both a single random variable and multiple random variables are presented.

3.4.3.1 Density selection for single random variable

The alternative IS probability density function (pdf) usually belongs to the same parametric family as the original distribution. According to Chapter 2, the final ARIMA innovations are fitted to the normal and the Student's t distributions. Due to the transformation, the Student's t distribution is also replaced by the normal distribution. Thus, the normal distribution is the targeted IS density that we are focusing on. The following two methods are most widely used in the applications of IS, scaling and shifting, especially for the normal distribution.

Scaling is one of the earliest biasing methods known and has been extensively used in IS practice. It is simple to implement and usually provides conservative simulation gains. Transforming the probability mass into the event region by positive scaling of the random variable with a number greater than unity has the effect of increasing the mean and the variance at the same time of the density function. This results in a heavier tail of the density, leading to an increase in the event probability. As shown in Equation (3-19) below, the simulation density is chosen as the density function of the scaled random variable $a_{sc}x$, where usually $a_{sc} > 1$ for tail probability estimation.

$$g(x) = \frac{1}{a_{sc}} f\left(\frac{x}{a_{sc}}\right), \qquad a_{sc} > 1 \tag{3-19}$$

where $g(\cdot)$ stands for the pdf of the replaced random variables; $f(\cdot)$ stands for the pdf of the original random variables; and a_{sc} stands for the scaling coefficient, where $a_{sc} > 1$. The corresponding LR function is shown in Equation (3-20) below.

$$W(x) = \frac{f(x)}{g(x)} = a_{sc} \frac{f(x)}{f(x/a_{sc})}, \qquad a_{sc} > 1 \tag{3-20}$$

where $W(\cdot)$ stands for the LR function for IS; $f(\cdot)$ stands for the pdf of the original random variables; $g(\cdot)$ stands for the pdf of the replaced random variables; and a_{sc} stands for the scaling coefficient, where $a_{sc} > 1$.

While scaling transfers probability mass into the desired event region, it also pushes mass into the complementary region, which is undesirable in most situations.

As a consequence, if X is a sum of n random variables, the spreading of mass takes place in an n dimension space. The consequence of this is a decreasing IS gain for increasing n, and is called the dimensionality effect of IS.

Another simple and effective biasing technique employs the shifting of the density function and hence the random variable to place much of its probability mass in the rare event region. Shifting does not suffer from a dimensionality effect and has been successfully used in several applications relating to simulation of digital communication systems. It often provides better simulation gains than scaling. In biasing by shifting, the simulation density is given by the following Equation (3-21) below.

$$g(x) = f(x - a_{sh}), \qquad a_{sh} > 0 \tag{3-21}$$

where $g(\cdot)$ stands for the probability density function of the replaced random variables; $f(\cdot)$ stands for the probability density function of the original random variables; and a_{sh} is the amount of shift to be chosen to minimize the variance of the IS estimator. The corresponding LR function is thus shown in Equation (3-22) below.

$$W(x) = \frac{f(x)}{g(x)} = \frac{f(x)}{f(x - a_{sh})}, \qquad a_{sh} > 0 \tag{3-22}$$

where $W(\cdot)$ stands for the LR function for IS; $f(\cdot)$ stands for the pdf of the original random variables; $g(\cdot)$ stands for the pdf of the replaced random variables; and a_{sh} stands for the amount of shift for IS.

From another perspective of LR calculation, the following Equations (3-23) to (3-25) are listed below. The pdf of the original random variables is shown in Equation (3-23).

$$f(x)=\frac{1}{\sqrt{2\pi}\sigma_f}\exp\left[\frac{-(x-\mu_f)^2}{2\sigma_f^2}\right], \qquad -\infty<x<\infty \tag{3-23}$$

where $f(\cdot)$ stands for the probability density function of the original random variables; μ_f stands for the mean of the original random variables; and σ_f stands for the standard deviation of the original random variables.

The updated pdf of IS is shown in Equation (3-24). Since both $f(x)$ and $g(x)$ are the normal pdf, the general formats are very similar in Equations (3-23) and (3-24).

$$g(x)=\frac{1}{\sqrt{2\pi}\sigma_g}\exp\left[\frac{-(x-\mu_g)^2}{2\sigma_g^2}\right], \qquad -\infty<x<\infty \tag{3-24}$$

where $g(\cdot)$ stands for the probability density function of the replaced random variables; μ_g stands for the mean of the replaced random variables; and σ_g stands for the standard deviation of the replaced random variables.

Based on the Equations (3-23) and (3-24), the LR function is derived as shown in Equation (3-25) below.

$$W(x)=\frac{f(x)}{g(x)}=\frac{\sigma_g}{\sigma_f}\exp\left[\frac{(x-\mu_g)^2}{2\sigma_g^2}-\frac{(x-\mu_f)^2}{2\sigma_f^2}\right], \tag{3-25}$$

$$-\infty<x<\infty$$

where $W(\cdot)$ stands for the LR function for IS; $f(\cdot)$ stands for the pdf of the original random variables; $g(\cdot)$ stands for the pdf of the replaced random variables; σ_g stands for the standard deviation of the replaced random variables; σ_f stands for the standard deviation of the original random variables; μ_g stands for the mean of the replaced random variables; and μ_f stands for the mean of the original random variables.

3.4.3.2 Density selection for multiple random variables

Slightly different from the single random variable, the IS density selection for multiple random variables takes place at a joint pdf. In order to avoid the dimensionality effect of IS, both the scaling and shifting techniques are adopted as a combination. To be more specific, since $x_1, x_2, ..., x_{n_{IS}}$ are independent variables from each other, the joint probability distribution of the original random variables is shown in Equation (3-26).

$$f(x_1, x_2, ..., x_{n_{IS}}) = f_1(x_1) f_2(x_2) ... f_{n_{IS}}(x_{n_{IS}}), \quad -\infty < x_1, x_2, ..., x_{n_{IS}} < \infty \tag{3-26}$$

where $f(\cdot)$ stands for the probability density function of the original random variables; n_{IS} stands for the length of time series for ISMC simulation; and $f_i(x_i)$ stands for the individual probability density function of the original random variables where $i \in \{1, 2, ..., n_{IS}\}$.

Similarly, the joint probability distribution of the replaced random variables is shown in Equation (3-27). $x_1, x_2, ..., x_{n_{IS}}$ are independent variables from each other.

$$g(x_1, x_2, ..., x_{n_{IS}}) = g_1(x_1) g_2(x_2) ... g_{n_{IS}}(x_{n_{IS}}), \quad -\infty < x_1, x_2, ..., x_{n_{IS}} < \infty \tag{3-27}$$

where $g(\cdot)$ stands for the probability density function of the replaced random variables; n_{IS} stands for the length of time series for ISMC simulation; and $g_i(x_i)$ stands for the individual probability density function of the replaced random variables where $i \in \{1, 2, ..., n_{IS}\}$.

Based on the Equations (3-26) and (3-27), the LR function is derived in Equation (3-28) shown below.

$$\begin{aligned} W(x_{1,} x_{2,}, ..., x_{n_{IS}}) &= \prod_{i=1}^{n_{IS}} f(x_i) / g(x_i) \\ &= \frac{1/\sigma_f^{n_{IS}}}{1/\sigma_g^{n_{IS}}} \frac{\exp\left\{\sum_{i=1}^{n_{IS}} [-(x_i - \mu_f)^2 / 2\sigma_f^2]\right\}}{\exp\left\{\sum_{i=1}^{n_{IS}} [-(x_i - \mu_g)^2 / 2\sigma_g^2]\right\}} \\ &= \frac{\sigma_g^{n_{IS}}}{\sigma_f^{n_{IS}}} \exp\left\{\frac{1}{2\sigma_g^2} \sum_{i=1}^{n_{IS}} (x_i - \mu_g)^2 - \frac{1}{2\sigma_f^2} \sum_{i=1}^{n_{IS}} (x_i - \mu_f)^2\right\} \end{aligned} \tag{3-28}$$

where $W(\cdot)$ stands for the LR function for IS; $f(\cdot)$ stands for the pdf of the original random variables; $g(\cdot)$ stands for the pdf of the replaced random variables; σ_g stands for the standard deviation of the replaced random variables; σ_f stands for the standard deviation of the original random variables; μ_g stands for the mean of the

replaced random variables; μ_f stands for the mean of the original random variables; and n_{IS} stands for the length of time series for ISMC simulation.

3.4.4 Procedures for ISMC Simulation Application

For the ISMC simulation with normal distributed innovation, the following steps are listed as the major procedures:

Step 1. Set N_t equal to 0;

Step 2. Set $N_t = N_t + 1$, and N_{IS} as the maximum simulation iterations. If $N_t \geq N_{IS}$, iteration stops and jump to Step 10;

Step 3. Generate $\{Z_1, Z_2, ..., Z_{n_{IS}}\}$, which are i.i.d. as the standard white noise from the distribution of $N(0,1)$ with the time scale length of n_{IS};

Step 4. Replace $\{Z_1, Z_2, ..., Z_{n_{IS}}\}$ with $\{Y_1, Y_2, ..., Y_{n_{IS}}\}$, which are i.i.d. as the white noise from the replaced IS based distribution with the time scale length of n_{IS};

Step 5. Transform from the replaced white noise series to the normal distributed innovation $\{X_{P1}, X_{P2}, ..., X_{Pn_{IS}}\}$, which are i.i.d. with the time scale length of n_{IS};

Step 6. Transform from the normal distributed innovation $\{X_{P1}, X_{P2}, ..., X_{Pn_{IS}}\}$ to the simulated inflow rate series $\{I_P(t) : t = 1, 2, ..., n_{IS}\}$ with all identified patterns added in;

Step 7. Transform from the simulated inflow rate series $\{I_P(t) : t = 1, 2, ..., n_{IS}\}$ to the reservoir water elevation $\{H_P(t) : t = 1, 2, ..., n_{IS}\}$ based on the developed dam-reservoir operation model;

Step 8. Compare with the height of dam top and justify whether the overtopping occurs or not;

Step 9. Return to Step 2;

Step 10. Estimate the estimator of overtopping using LR adjustment $\frac{1}{N_{IS}}\sum_{j=1}^{N_{IS}} I_{j\{S(Y)\geq h_f\}} W(y)$;

Step 11. Estimate the simulated overtopping probability.

Slightly different from the above simulation process, the following steps are listed as the major procedures for the ISMC simulation starting with the student's t distributed innovation:

Step 1. Set N_t equal to 0;

Step 2. Set $N_t = N_t + 1$, and N_{IS} as the maximum simulation iterations. If $N_t \geq N_{IS}$, iteration stops and jump to Step 10;

Step 3. Generate $\{Z_1, Z_2, ..., Z_{n_{IS}*k}\}$, which are i.i.d. as the standard white noise from the distribution of $N(0,1)$ with the length of $n_{IS} * k$, where *k* is the degree of freedom that is estimated through the MLE based on the existing observed residuals;

Step 4. Replace $\{Z_1, Z_2, ..., Z_{n_{IS}*k}\}$ with $\{Y_1, Y_2, ..., Y_{n_{IS}*k}\}$, which are i.i.d. as the white noise from the replaced IS based distribution with the time scale length of $n_{IS} * k$;

Step 5. Transform from the replaced white noise series $\{Y_1, Y_2, ..., Y_{n_{IS}*k}\}$ to the student's t distributed innovation $\{X_{st}(t), t = 1, 2, ..., n_{IS}\}$, which are i.i.d. with the time scale length of n_{IS};

Step 6. Transform from the student's t distributed innovation $\{X_{st}(t), t = 1, 2, ..., n_{IS}\}$ to the simulated inflow rate series $\{I_P(t) : t = 1, 2, ..., n_{IS}\}$ with all identified patterns added in;

Step 7. Transform from the simulated inflow rate series $\{I_P(t) : t = 1, 2, ..., n_{IS}\}$ to the reservoir water elevation $\{H_P(t) : t = 1, 2, ..., n_{IS}\}$ based on the developed dam-reservoir operation model;

Step 8. Compare with the height of the dam top and justify whether the overtopping occurs or not;

Step 9. Return to Step 2;

Step 10. Estimate the estimator of overtopping using LR adjustment $\frac{1}{N_{IS}} \sum_{j=1}^{N_{IS}} I_{j\{S(Y) \geq h_f\}} W(y)$;

Step 11. Estimate the simulated overtopping probability.

3.5 Summary

In summary, this chapter presents the simulation methodology of evaluating the overtopping risks of a dam-reservoir system. It starts with the past research of rare-event simulation and the corresponding engineering application. Then, the research gap is presented for the dam-reservoir system simulation. In order to fill the gap, detailed dam-reservoir system simulation is presented to estimate the probability of overtopping risks. Both the CMC simulation framework and the ISMC simulation framework are then proposed in a sequence. Comparisons of the CMC and the IS on the theoretical bases have also been conducted. Based on this chapter, we could have

a good understanding of why and how to estimate the overtopping risks of the dam-reservoir system through simulations from the theoretical perspective.

Chapter 4: Case Study of Little Long Dam-Reservoir System

4.1 Introduction

This chapter proposes a case application of the Little Long dam-reservoir system. The goal of this chapter is to demonstrate that the proposed model in Chapter 2 could effectively address the characteristics of inflow hydrograph and reservoir operations based on historical information. The results from the inflow hydrograph model play as the prerequisites for future inflow simulation, and the simulated inflow results play as the input variables for the reservoir operations model. Final outputs would be the overtopping probabilities that the reservoir water elevation exceeds the dam top through a specified time scale. This chapter starts with the introduction of project background information, and then the inflow hydrograph modeling. Detailed transformation and statistical test results for the inflow modeling are presented. After that, the outflow control and releasing policies are introduced and modeled. Finally, verification and validation have been conducted for both the inflow and the reservoir operation model, which sets the foundation for both the CMC and rare event-based simulations.

4.2 Project Background

The proposed overtopping risk evaluation approach was applied to a dam-reservoir system operated by Ontario Power Generation (OPG) in northeastern Ontario. As an essential part of the Lower Mattagami River Hydroelectric Complex, the Little Long dam creates a forebay and reservoir upstream in the Mattagami River. The flows for

the Mattagami Complex are thus provided from the Adam Creek reservoir. The whole Lower Mattagami River System includes the Adam Creek reservoir and a cascade of four generation stations (Little Long, Smokey Falls, Harmon, and Kipling) along the Mattagami River. As shown in Figure 4-1 below, this study only focuses on the first part, including the reservoir and the Little Long Generating Station dam and sluiceway, and the Adam Creek Control Structure as a system. Since the number of riparian rights in the river flood plain is few and there is no commercial riverine navigation, system operation safety dominates the considerations.

The selected Little Long dam-reservoir system is within a modified continental climatic zone. During the winter, cold polar air masses often produce dry, clear, cold weather, and in the summer months, successions of cyclonic storms sweep the area, and warm humid air masses from the south alternate with cooler drier air from the north. The average mean daily temperatures for January and July stay at approximately -19ºC and 17ºC, respectively. And the annual average mean daily temperature for the region is about 1ºC. On average, the area is frost free from mid-May to early September. For precipitation, the average annual total precipitation is about 86 cm (water equivalent mean). Rainfall accounts for 63% of the total precipitation, with the maximum occurring in the summer months. Snow cover is present for about 160 days per year, reaching a maximum depth on the ground in February (average depth 61 cm).

Figure 4-1 Geographical location of Little Long dam-reservoir system

Hydro units are heavily dependent on precipitation and snow melting. As a consequence, strong seasonal patterns can be identified for the Adam Creek inflow data. Freeze-up usually occurs by late November or early December on the Mattagami River and reservoirs. The inflow volume into the reservoir reduces gradually. By mid-December, ice cover is complete except in the tailraces and rapids, which stay open all winter. The inflows stay small but positive. During peak winter operation, ice hinges form along the shoreline allowing the central ice sheet in each reservoir to move with the changing water elevations without breaking. In late winter, the central ice sheet subsides and, as the inshore ice settles to the substrate, the central floating ice sheet breaks from the inshore ice and can be pushed downstream. The ice breaks and the snow melts quickly during the spring freshet by mid-March. A corresponding large inflow volume usually occurs. Rainfall is heavier and more frequent during the summer as compared to the winter. The inflow rate is consequently larger during the summer.

4.3 Modeling Inflow Rate under Uncertainty

This section shows a specific case demonstrating the applicability of the inflow hydrograph model proposed in Section 2.3. In general, a 50-year time series data of average daily inflow rate for the Mattagami River is collected for analysis. There are 18,394 records available in total ranging from 08/01/1963 to 12/09/2013. For analysis simplification, the daily data ranging from 01/01/1964 to 12/31/2013 is selected with 18,250 values. Individual missing data is made up through the two-dimensional interpolation techniques. For each year, there are 365 days counted and the extra days

of leap year are not taken into consideration. This dataset serves as the foundation for modeling and simulating the stochastic reservoir inflow hydrograph. Detailed data information is plotted in Figure 4-2.

As presented previously, strong seasonal patterns have been shown in the Adam Creek inflow hydrographs. Taking the most recent inflow data of 2011, 2012, and 2013 as examples, the hydrograph with obvious jumps and fluctuations at specific time through each year is shown in Figure 4-2. Here we subjectively divide the annual inflow data into three sections in order to address the characteristics of data in each section more specifically and accurately. As there are 365 days in a year, Section 1 ranges from Day 1 to Day 80, which is the frozen season with very low inflows and small fluctuations. Section 2 ranges from Day 81 to Day 340, which presents a big contrast with Section 1. The biggest jump on the inflows usually occur within this section, with large fluctuations and uncertainties. Section 3 ranges from Day 341 to Day 365, which connects to Section 1 of the next year. As a result, both the inflow values and fluctuated variations are within a certain range between Section 1 and Section 2.

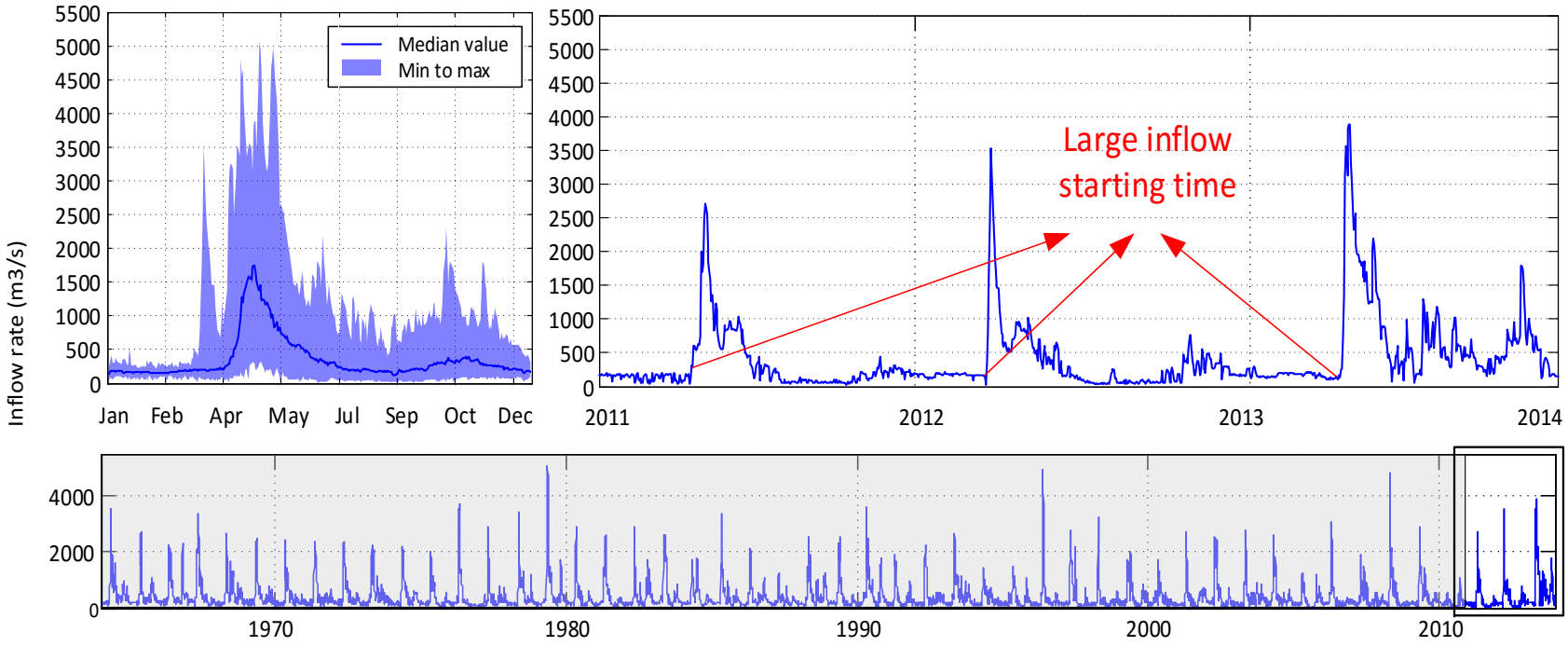

Figure 4-2 Inflow hydrograph of Little Long dam-reservoir system (1964-2013)

4.3.1 Preprocessing of Reservoir Inflow Data

This section is intended to transform the available reservoir inflow time series into the stationary series, which would be fitted to the ARIMA or seasonal ARIMA models. Three steps need to be conducted as a sequence for preprocessing the reservoir inflow data: 1) obtaining the logarithm of data; 2) conducting the Fourier decomposition for the seasonal pattern identification; and 3) testing the inflows residuals and differencing if needed.

In Step 1, the logarithmic transformation is a nonlinear transformation, which compresses the upper end of the distribution and stretches out the lower end. In order to reduce the positive skew of inflow data, the transformation is graphically shown in Figure 4-3 below.

In Step 2, Fourier decomposition, an eight-term Fourier model was fitted to the logarithms of historical inflow data in order to find the annual seasonal cycle. Figure 4-4 below plots the fitting curve. The most recent data ranging from Year 2011 to Year 2013 has been zoomed in. As we can see, two big waves are identified annually in the spring and autumn time, which aligns with the climate characteristics discussed before.

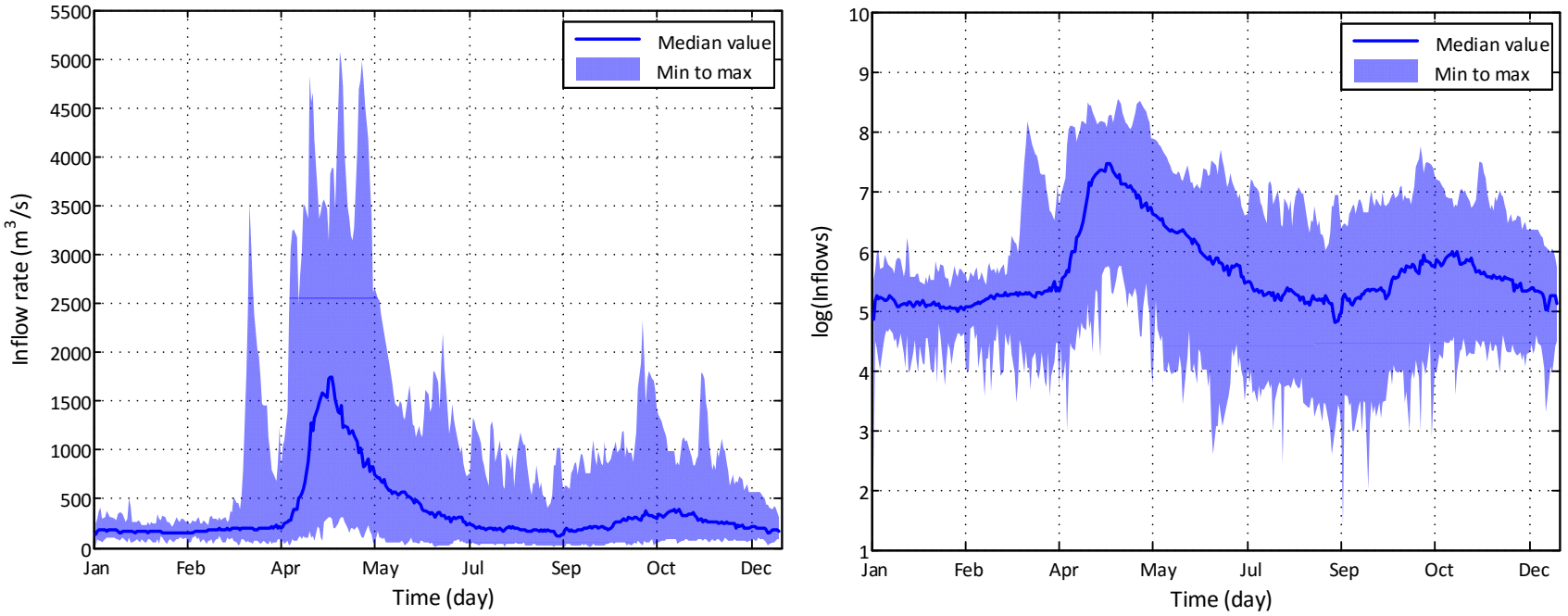

Figure 4-3 Inflow hydrograph and corresponding logarithm

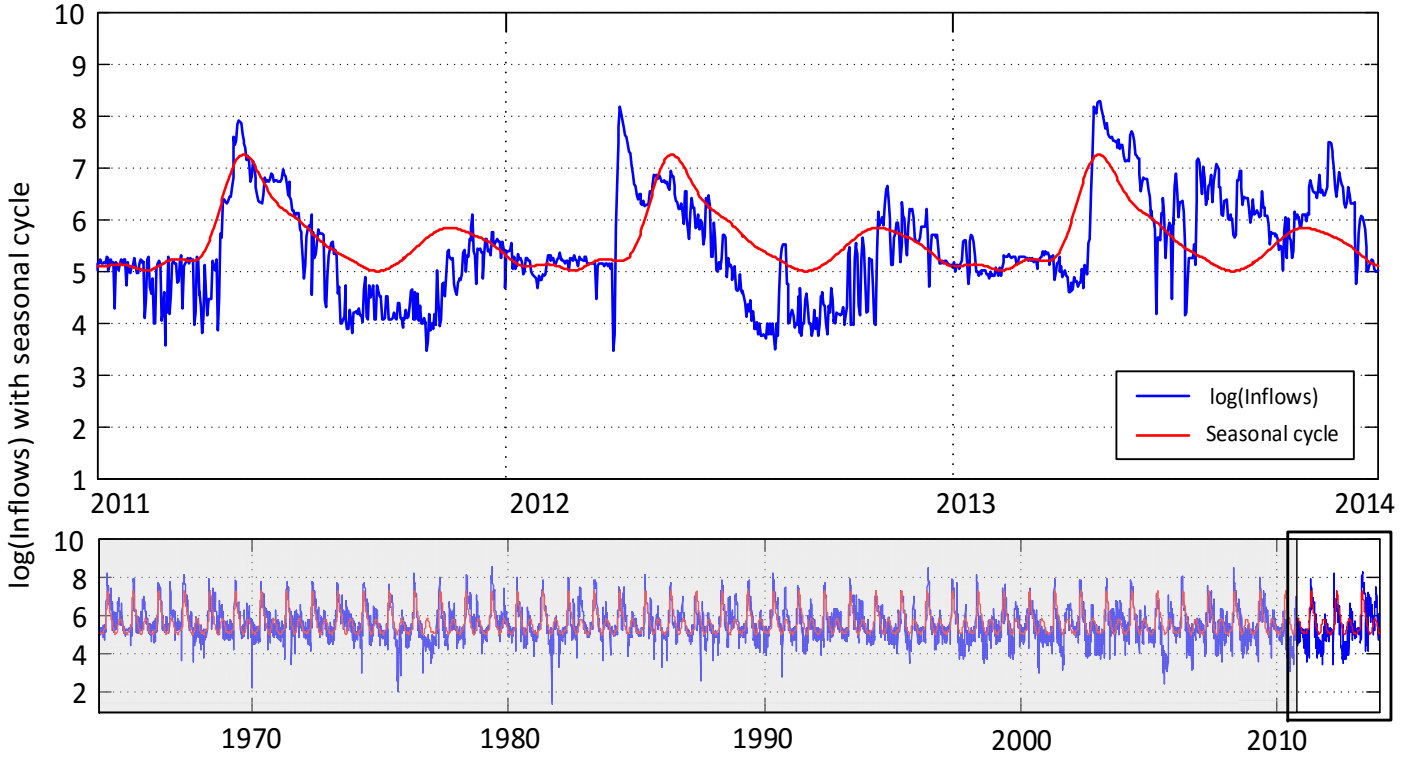

Figure 4-4 Logarithm of inflow hydrograph and fitted eight-term Fourier model

Step 3 calculates the residuals of logarithm inflow minus the value of fitted Fourier decomposition model. A seasonal difference is the difference between an observation and the corresponding observation from the previous year. Time series with trends or seasonality would not be stationary, since the trend and seasonality will affect the value of the time series at different times. In general, a stationary time series will have no predictable patterns in the long-term. As a result, differencing and the seasonal differencing have been conducted to make the time series stationary. As shown in Figure 4-5 below, the differencing and seasonal differencing transformation has been conducted for the residual series as the outputs of Step 2. Lags are picked at 1 and 365.

4.3.2 Fitting ARIMA and Seasonal ARIMA Models

After preprocessing the inflow time series, the original data has been transformed to the series of noise data with the mean values fluctuating around zero. Stationarity is another characteristic for the preprocessed data series. Variance for the dataset at certain time point is relatively balanced below and beyond zero. Simply speaking, the stationary time series looks the same going forward or backward in time. In this section, the ARIMA or seasonal ARIMA model is used to decompose the series into filtered series and noises. Three sections are divided in order to address the different characteristics of the preprocessed inflow series more specifically. Section 1 stands for the preprocessed series from Day 1 to Day 80. Section 2 stands for the preprocessed series from Day 81 to Day 340, and Section 3 stands for the preprocessed series from Day 341 to Day 365.

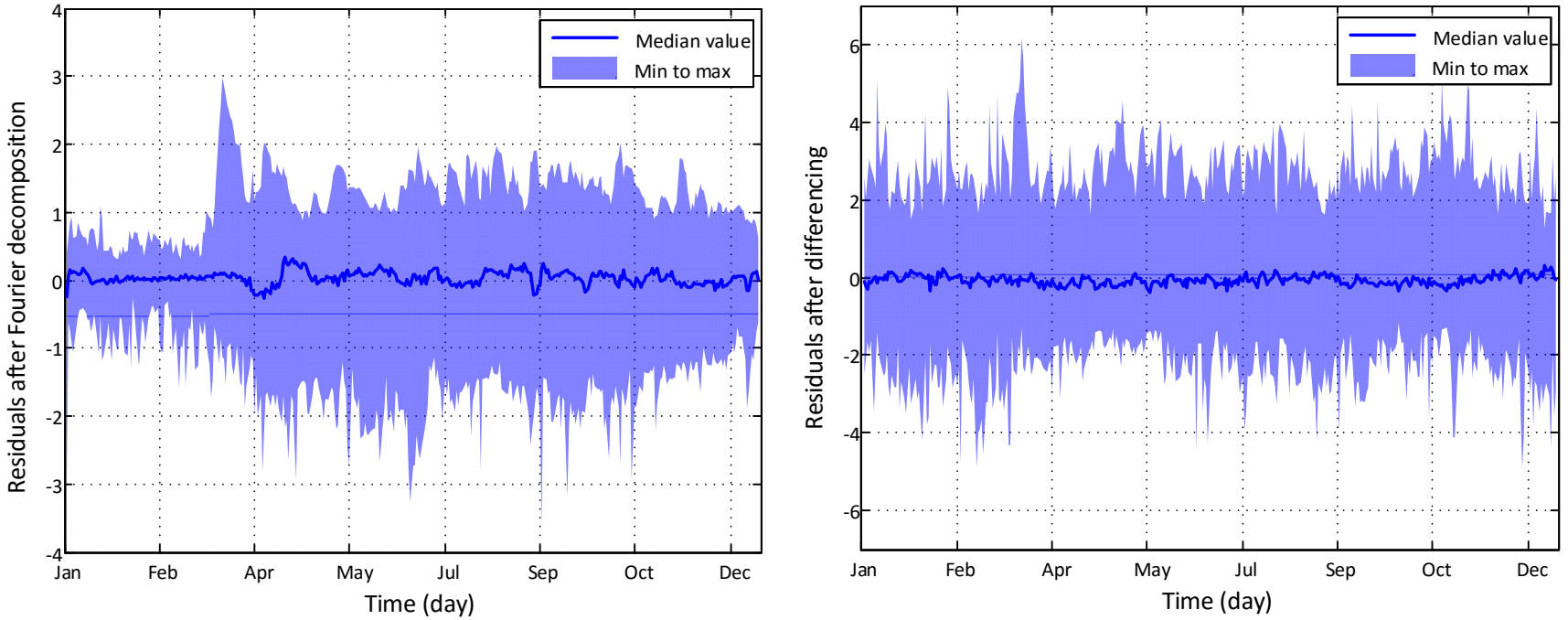

Figure 4-5 Residuals of fitted Fourier model and variance adjustment

As shown in Table 4-1 below, the ADF tests show that no unit root exists in all section data. Since the p-values are smaller or equal than the specified 0.01, we need to reject the original hypothesis of nonstationary. The alternative hypothesis of stationary is confirmed for all section data. The KPSS tests also confirm the stationary nature of the checking time series for all section data. The p-values are larger than the specified 0.01. The null hypothesis of stationary could not be rejected. The BP and LB tests compute the LB

test statistic for examining the null hypothesis of independence in a given time series. The actual p-values are very small, and the null hypothesis of independence has to be rejected.

Table 4-1 Pattern testing results before fitting to ARIMA model

Tests	Section 1 data	Section 2 data	Section 3 data
ADF	Dickey-Fuller = -17.5098, Lag order = 15, p-value = 0.01	Dickey-Fuller = -26.0397, Lag order = 23, p-value = 0.01	Dickey-Fuller = -9.6848, Lag order = 10, p-value = 0.01
KPSS	KPSS Level = 0.1465, Truncation lag parameter = 14, p-value = 0.1	KPSS Level = 0.0352, Truncation lag parameter = 26, p-value = 0.1	KPSS Level = 0.0824, Truncation lag parameter = 8, p-value = 0.1
LB	X-squared = 684.238, df = 1, p-value < 2.2e-16	X-squared = 7370.652, df = 1, p-value < 2.2e-16	X-squared = 227.9802, df = 1, p-value < 2.2e-16

The next step in model fitting is to determine the order of ARIMA model parameters, including both the AR and MA terms. Auto Correlation Function (ACF) and Partial Auto Correlation Function (PACF) are adopted as the major tool for determination. Figures 4-6, 4-7, and 4-8 below are shown as the ACF and PACF of the residuals for different sections of data after preprocessing. Since the lag-1 autocorrelations for all section of data stay beyond zero, a higher order of differencing would be needed. This indication is aligned with the LB test results. An additional interesting part shows in the PACF of Figures 4-6, 4-7, and 4-8. A

periodical spike at every 7 lags with deterioration through the time. As a result, an additional differencing at lag-7 would need to be conducted.

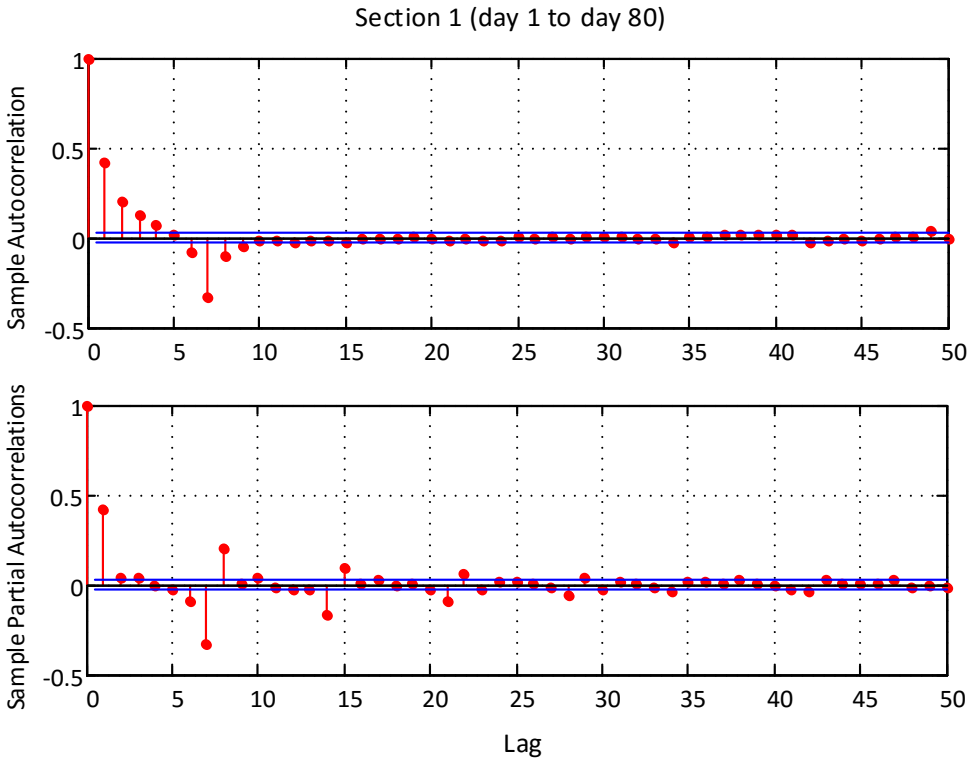

Figure 4-6 ACF and PACF for preprocessed inflows from Day 1 to 80

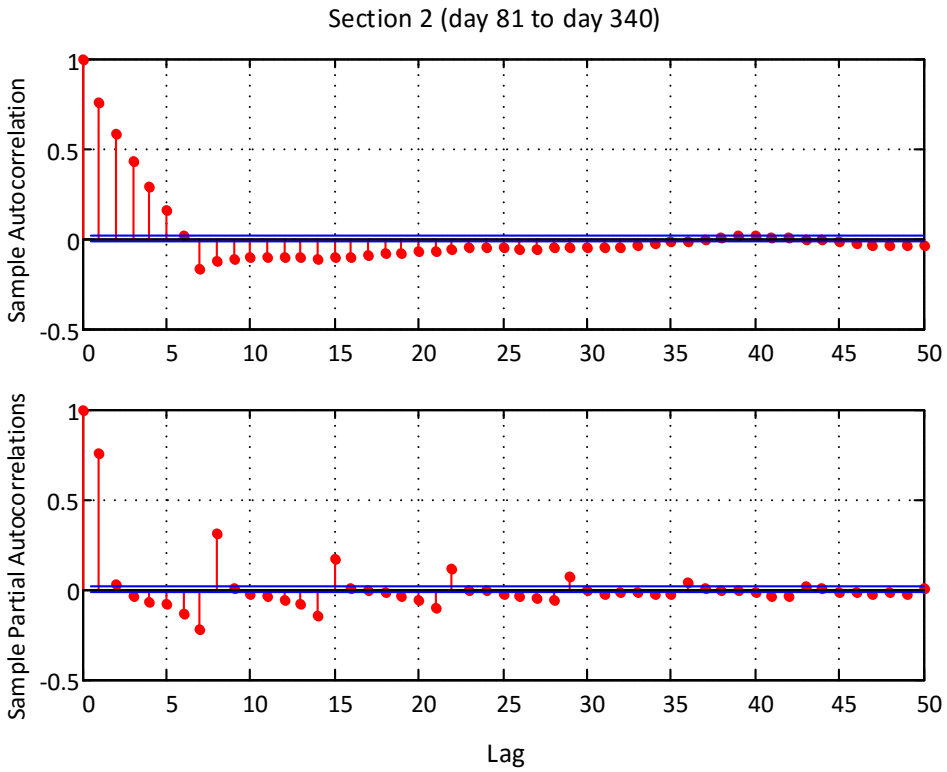

Figure 4-7 ACF and PACF for preprocessed inflows from Day 81 to 340

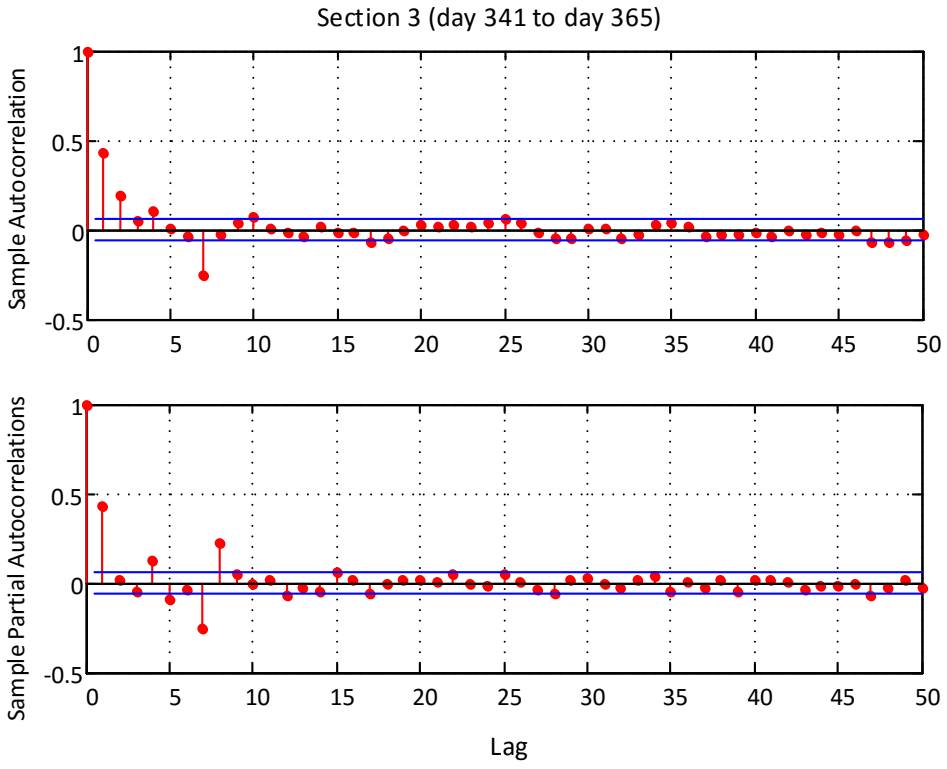

Figure 4-8 ACF and PACF for preprocessed inflows from Day 341 to 365

AICc is Akaike's Information Criterion (AIC) with a correction for finite sample sizes. To obtain an automatic ARIMA model, a variation of the Hyndman-Khandakar algorithm has been used. The unit root tests, minimization of AICc and MLE are all involved. To be more specific, the ARIMA model starts with a first guess. The number of differences, *d*, for ARIMA (*p*,*d*,*q*) model are determined by using repeated KPSS tests. The values of *p* and *q* are then chosen by minimizing the AICc after differencing the data *d* times. Rather than considering every possible combination of *p* and *q*, the algorithm uses a stepwise search to traverse the model space based on the initial guess. Variations of *p* and *q* on the current model are considered by ±1. Finally, the best model with the smallest AICc is selected. If $d = 0$, then the constant *c* is included. If $d \geq 1$, then the constant c is set to be zero.

In order to confirm the adequacy of the selected models, the ACF and PACF diagnostic correlograms as well as the LB test are adopted to verify that the independence of residuals. According to the searching results, ARIMA(2,0,3) model with two AR terms and three MA terms would be a best-fit choice for the Section 1 data. Similarly, ARIMA(3,0,2) would be the best-fit model for both Section 2 and Section 3 data. As shown in the following Tables 4-2, 4-3, and 4-4, the best-fit ARIMA models are presented below, where the estimated parameters providing all of the AR and MA terms that are statistically significant at the 10% level.

Table 4-2 ARIMA(2,0,3) model fitting for Section 1 data

Parameter	Value	Standard error	T statistic
Constant	0.0002923	0.01224	0.02389
AR{1}	1.2114	0.02392	50.6506
AR{2}	-0.7244	0.02135	-33.9255
MA{1}	-0.8754	0.02512	-34.8404

MA{2}	0.4412	0.02074	21.2773
MA{3}	0.3146	0.01465	21.4767
Variance	0.7726	0.01193	64.7738

Note: AIC=10332; BIC=10370; AICc=10332

Table 4-3 ARIMA(3,0,2) model fitting for Section 2 data

Parameter	Value	Standard error	T statistic
Constant	-0.0001977	0.003978	-0.04971
AR{1}	1.8462	0.007657	241.125
AR{2}	-1.5618	0.01231	-126.844
AR{3}	0.5497	0.007458	73.7128
MA{1}	-1.2222	0.004858	-251.602
MA{2}	0.9344	0.004641	201.353
Variance	0.3927	0.003009	130.516

Note: AIC=24813; BIC=24857; AICc=24813

Table 4-4 ARIMA(3,0,2) model fitting for Section 3 data

Parameter	Value	Standard error	T statistic
Constant	-0.003942	0.08410	-0.04687
AR{1}	-1.1133	0.05795	-19.2123
AR{2}	-0.03731	0.04299	-0.8679
AR{3}	0.2143	0.03409	6.2876
MA{1}	1.6121	0.04989	32.3157
MA{2}	0.7665	0.04804	15.9543
Variance	0.7503	0.02279	32.9231

Note: AIC=3201; BIC=3232; AICc=3201

4.3.3 Fitting Innovations of ARIMA and Seasonal ARIMA Models

After fitting to the ARIMA and seasonal ARIMA models, statistical patterns have been released for checking the innovations. The following Table 4-5 shows the updated results of the time series stationary and pattern tests. The ADF tests show that no unit-root exists in all section data and the original hypothesis of nonstationary would be rejected. The actual p-values are smaller than the printed p-values. The alternative hypothesis of stationary is confirmed for all section data. The KPSS tests

also confirm the stationary nature of the checking time series for all section data. The actual p-values are greater than the printed p-values. The null hypothesis of stationary could not be rejected. Different from previous tests, the residual series pass the LB test with a p-value greater than specified. The null hypothesis of independence could not be rejected.

Table 4-5 Pattern testing results after fitting to ARIMA model

Tests	Section 1 data	Section 2 data	Section 3 data
ADF	Dickey-Fuller = -17.5068, Lag order = 15, p-value = 0.01	Dickey-Fuller = -29.571, Lag order = 23, p-value = 0.01	Dickey-Fuller = -10.3517, Lag order = 10, p-value = 0.01
KPSS	KPSS Level = 0.1379, Truncation lag parameter = 14, p-value = 0.1	KPSS Level = 0.0283, Truncation lag parameter = 26, p-value = 0.1	KPSS Level = 0.076, Truncation lag parameter = 8, p-value = 0.1
LB	X-squared = 1.9156, df = 1, p-value = 0.1663	X-squared = 0.032, df = 1, p-value = 0.8581	X-squared = 0.1259, df = 1, p-value = 0.7227

To confirm the independence of ARIMA model innovations, ACF and PACF are adopted again, as shown in Figures 4-9, 4-10, and 4-11 below. All the trends and periodic components have been removed by fitting to the ARIMA models. Except for the negative spike at lag 7, all sample autocorrelations and partial autocorrelations stayed within a controlled range. Based on the results, we could reasonably deem that the innovations are displayed as the random processes. The proposed ARIMA models have described the major behavior of previous datasets. This also set the foundation for the future simulation practice.

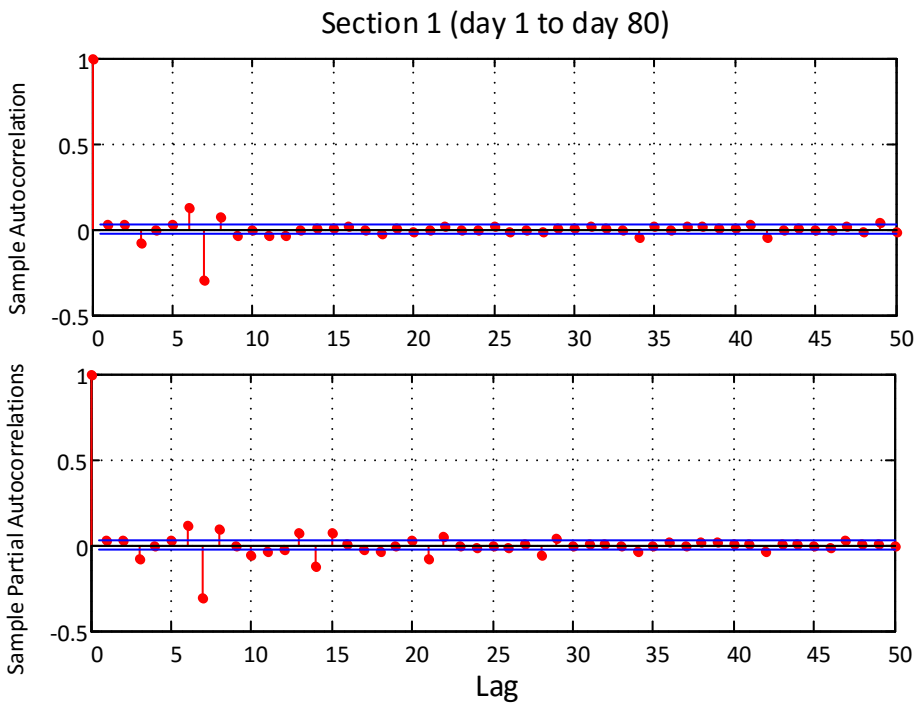

Figure 4-9 ACF and PACF for ARIMA residuals from Day 1 to 80

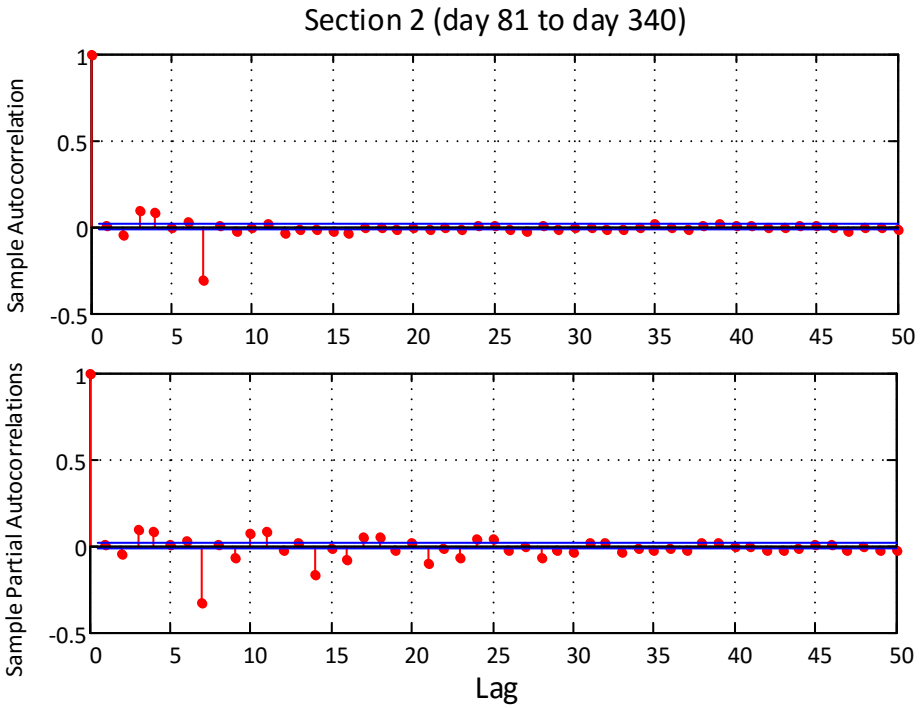

Figure 4-10 ACF and PACF for ARIMA residuals from Day 81 to 340

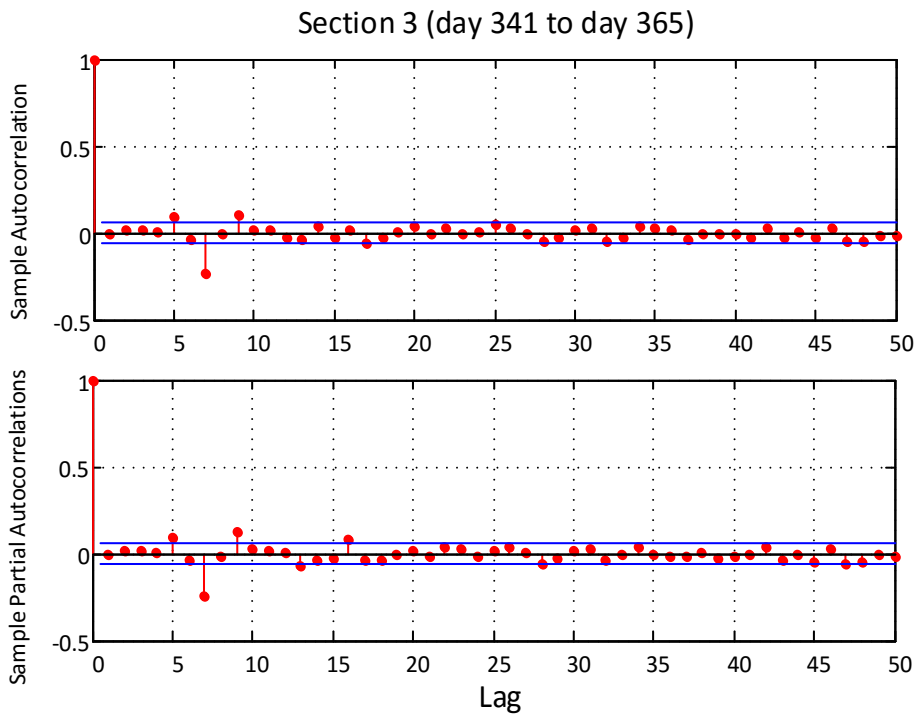

Figure 4-11 ACF and PACF for ARIMA residuals from Day 341 to 365

In order to simulate the ARIMA innovations for a future certain time period, one step has to be taken further so that a well-known distribution needs to be fitted into the simulation model. The histogram and QQ plot have been selected as the tool for doing this fitness. The QQ plot is used for comparing two probability distributions by plotting their quantiles against each other, providing a graphical view of how properties, such as location, scale, and skewness, are similar or different in the two distributions. Histograms and QQ plots have thus been presented in the following Figures 4-12 to 4-17 to check the characteristics of the proposed ARIMA innovations. Among them, Figures 4-12, 4-13, and 4-14 are used for checking the normality, while Figures 4-15, 4-16, and 4-17 are used for checking with the Student's t distribution. As shown below, Figures 4-12, 4-13, and 4-14 are derived from the assumption that

the innovations from the ARIMA time series modeling follow the Gaussian distributions. The curved pattern suggests that the data points follow an approximate linear pattern, although some outliers are shown in the upper right and lower left corners. It represents that more points concentrate on the tails in reality than the proposed normal distributed model. From the conservative thinking of overtopping simulation, the Gaussian distribution could be considered as a simulation model choice. The mean of the points is very close to zero, and the standard deviation is about 0.88.

Similarly, we also use the histograms and QQ plots to check the innovations with the Student's t distributions. Figures 4-15, 4-16, and 4-17 below indicate the departures. The linearity pattern of points suggests that the data could be deemed as the Student's t distribution as well. Outliers are visible in the upper right and lower left corner. Different from the previous fitted Gaussian distribution, fewer points concentrate on the tails in reality than the proposed normal distributed model. There would be the larger annual peak inflows through the simulation than the reality. Therefore, the real innovation distribution could be deemed within the range between the normal distribution fitted results and the Student's t distribution fitted results. Thus in the following discussion, both the normal and Student's t distributed innovations are included.

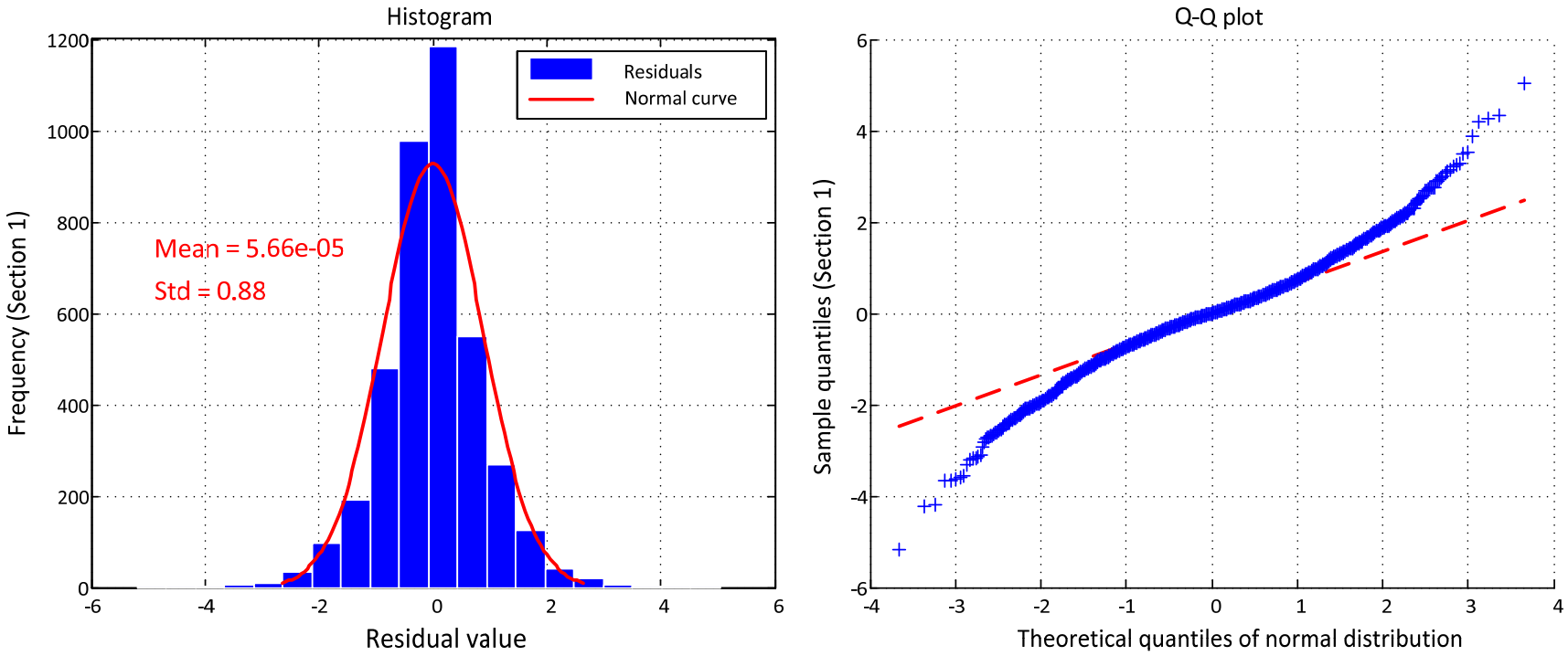

Figure 4-12 Normal histogram fitting of ARIMA residuals and QQ plot from Day 1 to 80

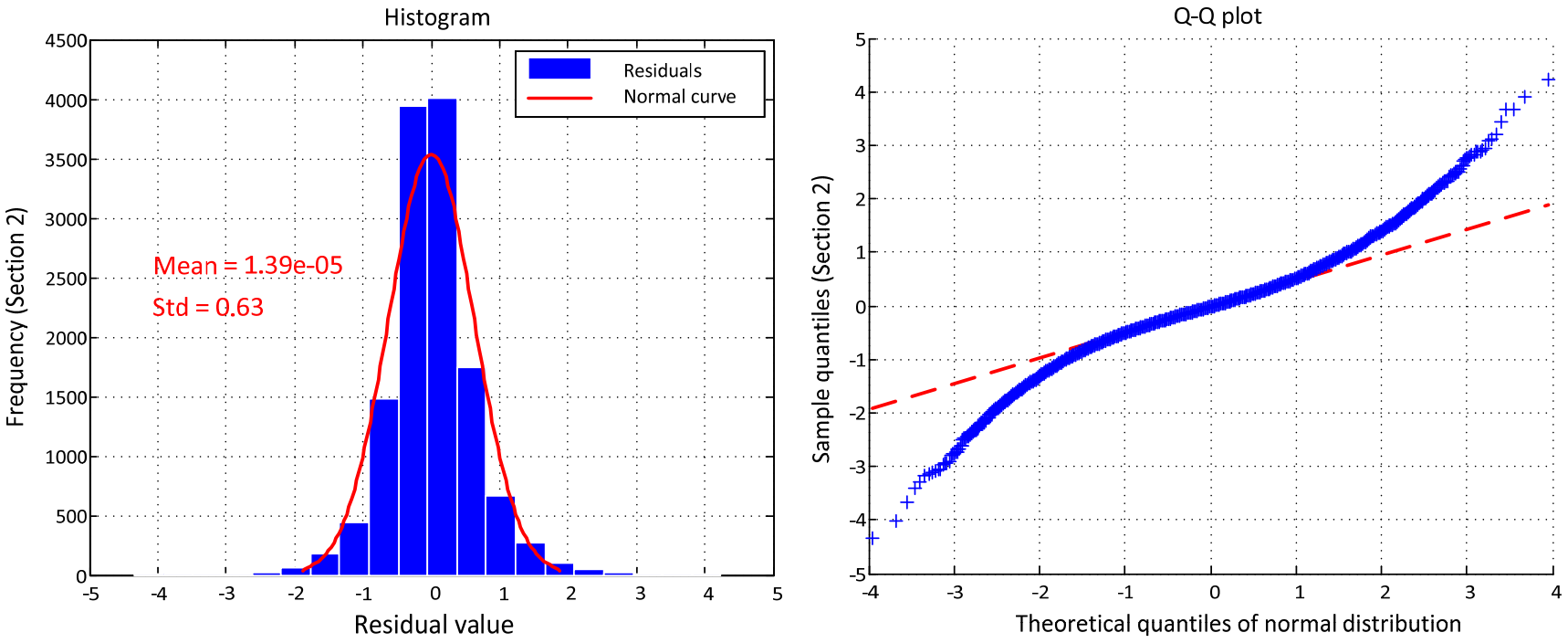

Figure 4-13 Normal histogram fitting of ARIMA residuals and QQ plot from Day 81 to 340

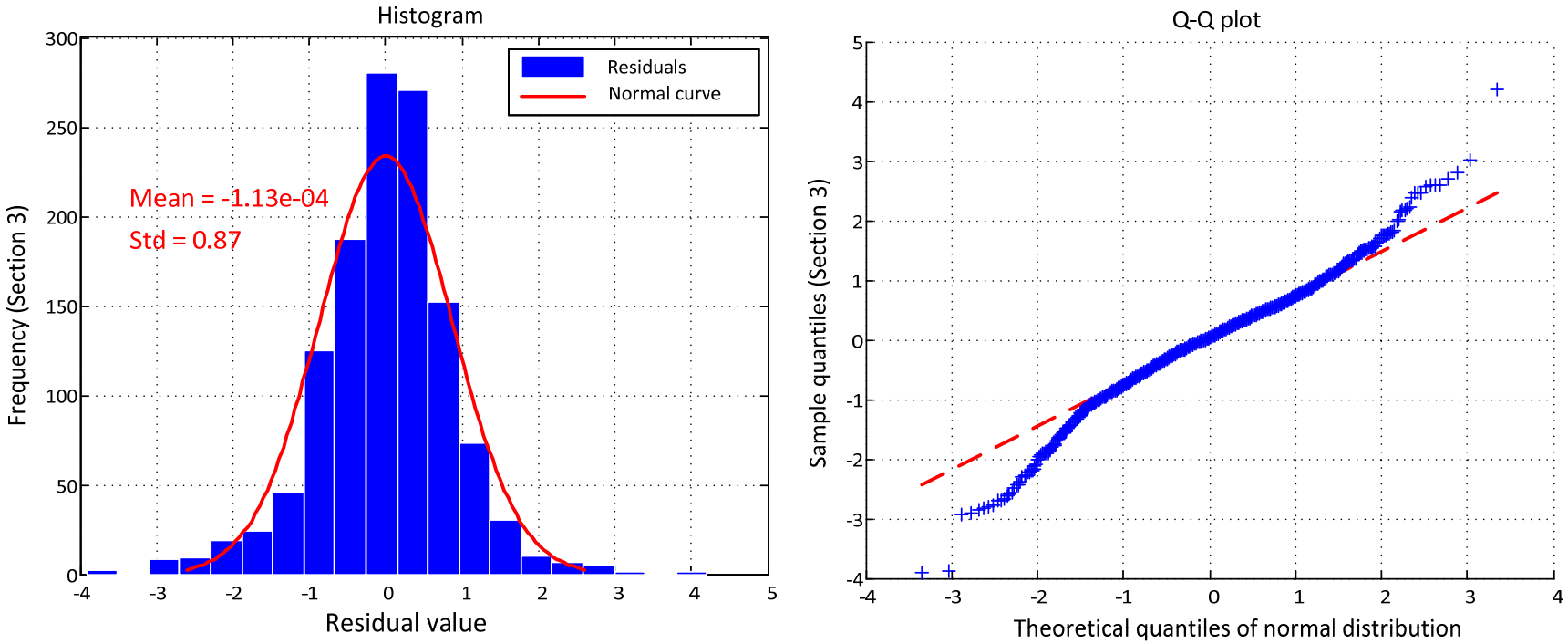

Figure 4-14 Normal histogram fitting of ARIMA residuals and QQ plot from Day 341 to 365

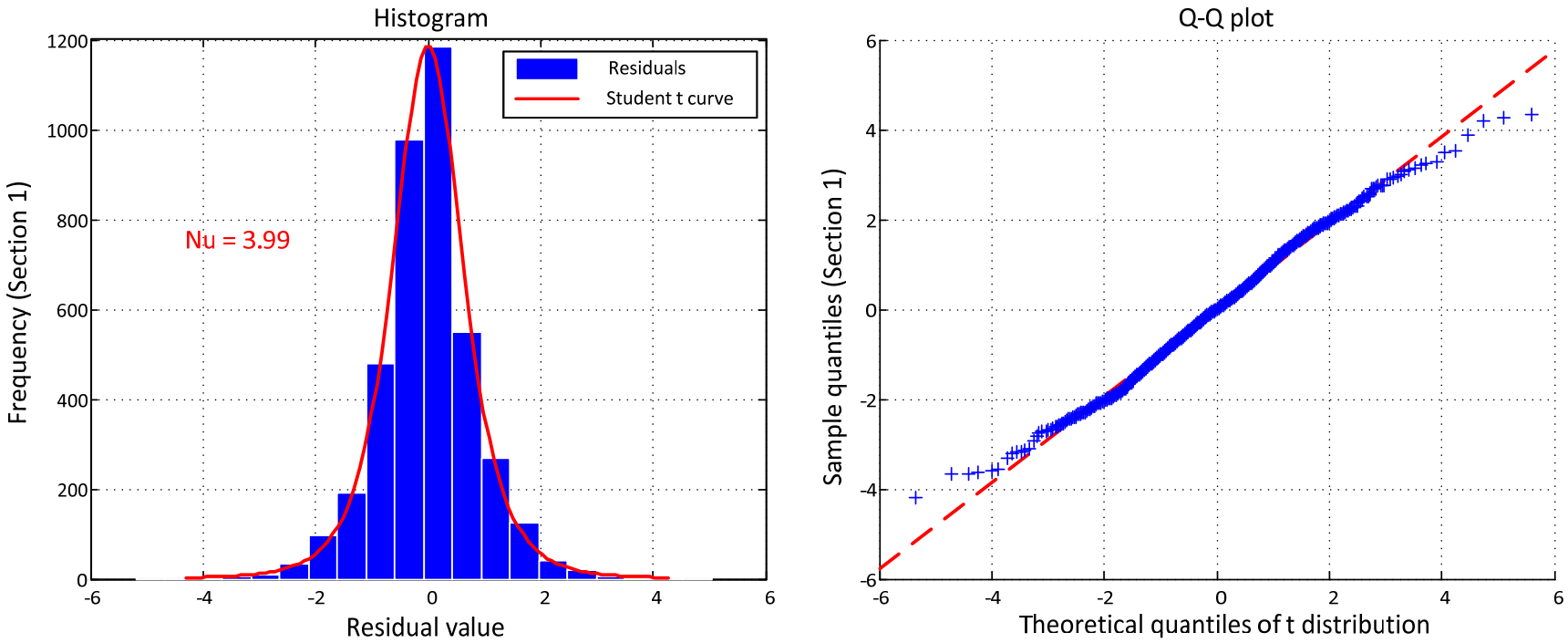

Figure 4-15 Student's t histogram fitting of ARIMA residuals and QQ plot from Day 1 to 80

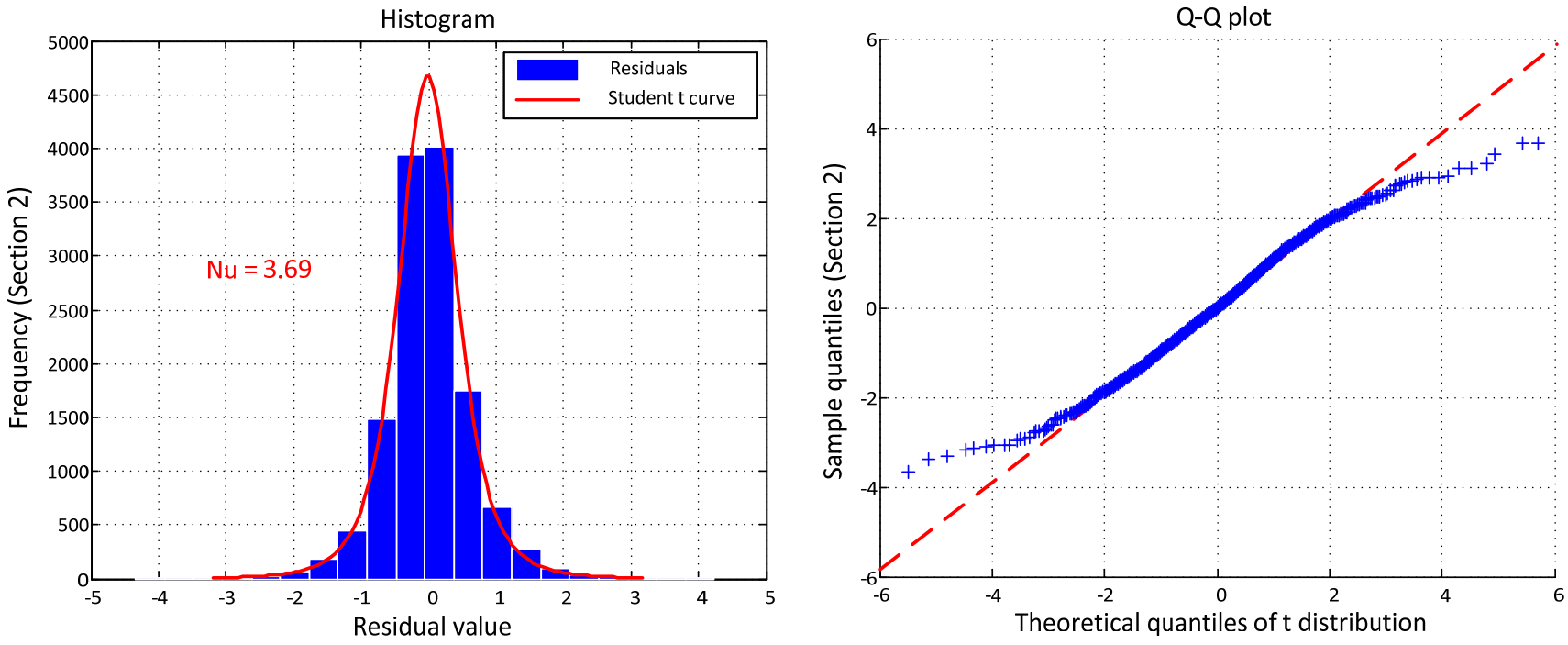

Figure 4-16 Student's t histogram fitting of ARIMA residuals and QQ plot from Day 81 to 340

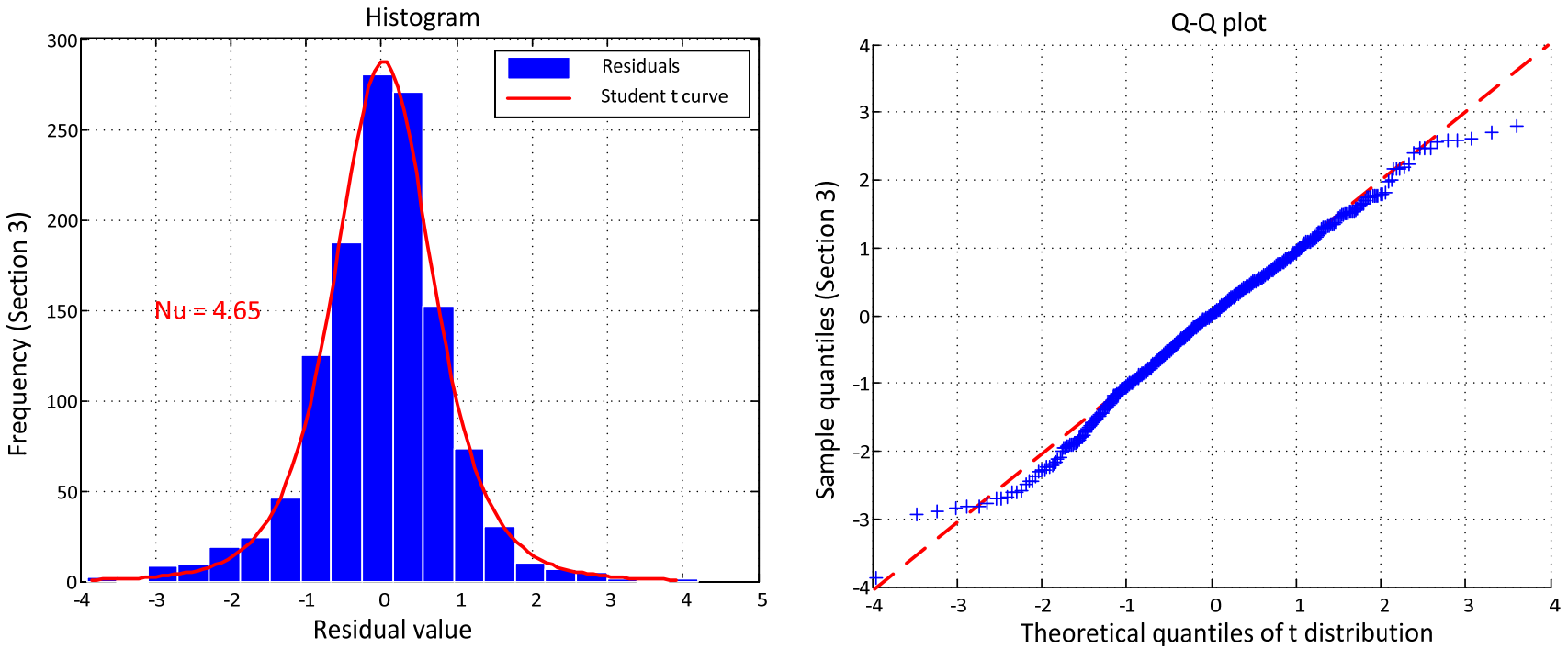

Figure 4-17 Student's t histogram fitting of ARIMA residuals and QQ plot from Day 341 to 360

4.3.4 Model Verification and Validation

Based on the transformed series model, simulations for the innovation can be performed within a specified time scale. Then, the simulated inflow rates can be reconstructed using the reversed transformations conducted in the modeling process. Sample paths from

the CMC simulation with both the innovations of normal distributions and Student's t distributions are displayed in Figures 4-18 and 4-19. In order to show a balanced comparison, the simulated inflows are also presented at the 50 year time scale, the same as the historical inflows on record. As we could observe, the simulated inflows with the Student's t distributed innovations have higher annual peak inflows than the inflows from the normal distributed innovations. As a consequence, the overtopping probability estimation based on the two different distributions would be varied. Overtopping risks of the simulated inflows with the Student's t distributed innovations would be higher than the inflows from the normal distributed innovations.

In order to validate the simulated inflows, two indicators have been selected for the verification comparison: 1) the maximum annual inflow rates, and 2) the time points of the maximum annual inflow rates. Both the results from the normal distributed and the Student's t distributed innovations are presented respectively. To be more specific, Figures 4-20 and 4-21 below demonstrate the results that derived from the simulation with the normal distributed model and the actual data. The linearity patterns in both Figures 4-20 and 4-21 demonstrated a reasonable simulation match. There are three outliers in Figure 4-21 on the upper right corner. The reason might be either the spring peak inflows that did not occur or some omitting occurred in the inflow recording. Thus, these three abnormal points could not be taken into consideration.

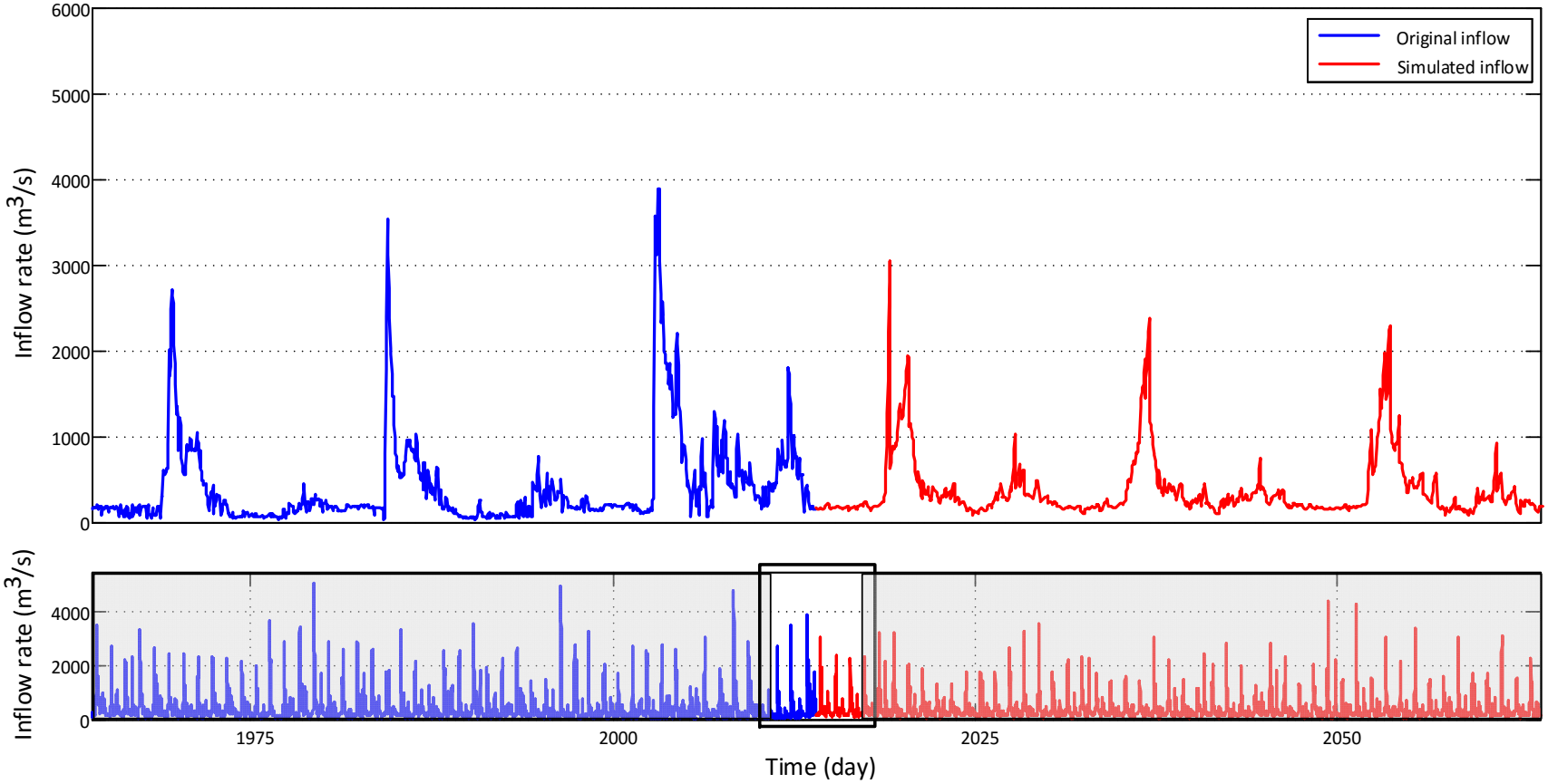

Figure 4-18 Sample paths of historical and simulated inflow hydrograph based on normal innovation

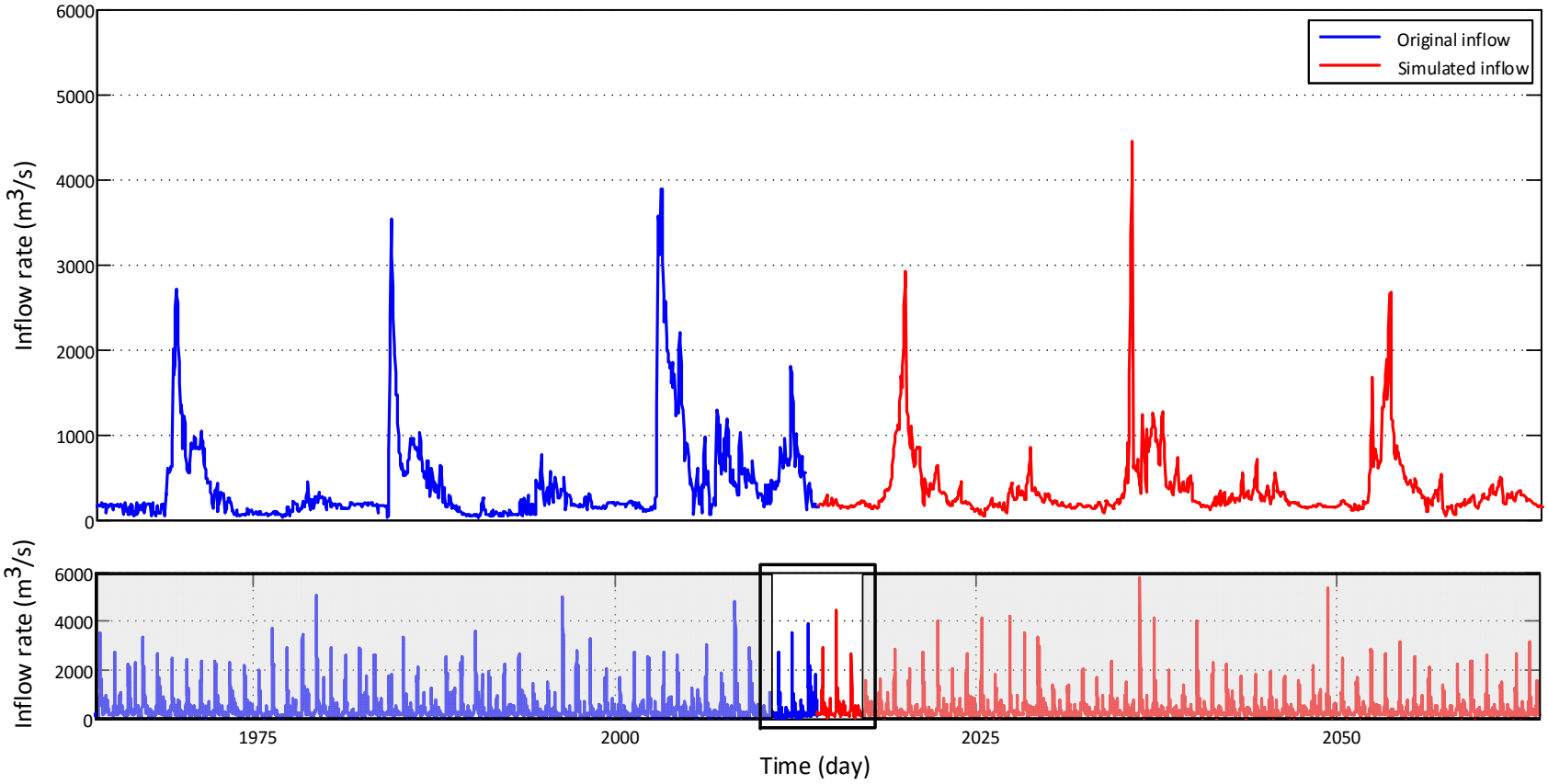

Figure 4-19 Sample paths of historical and simulated inflow hydrograph based on Student's t innovation

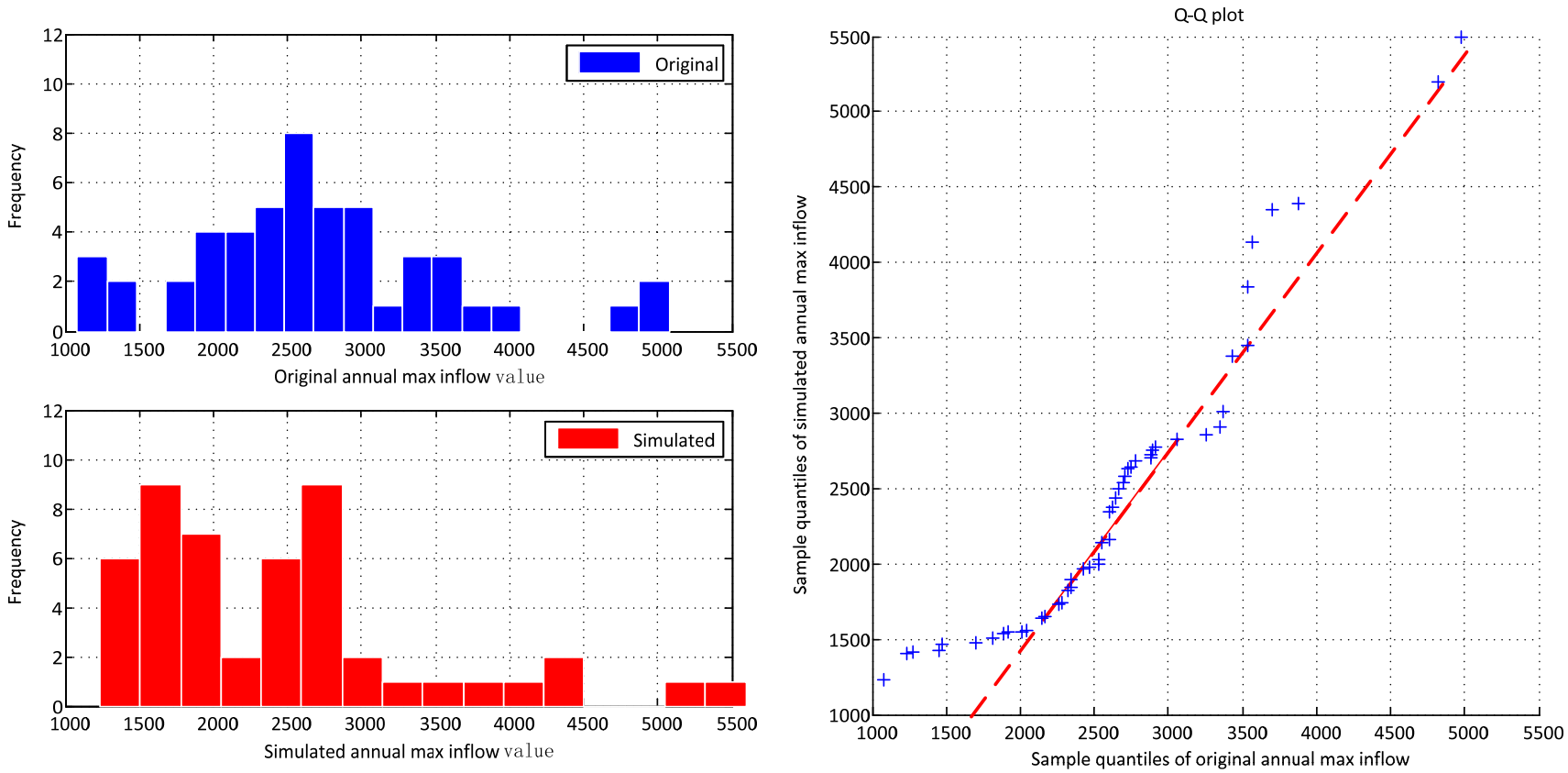

Figure 4-20 Comparison of historical and simulated annual max inflow based on nomal innovation

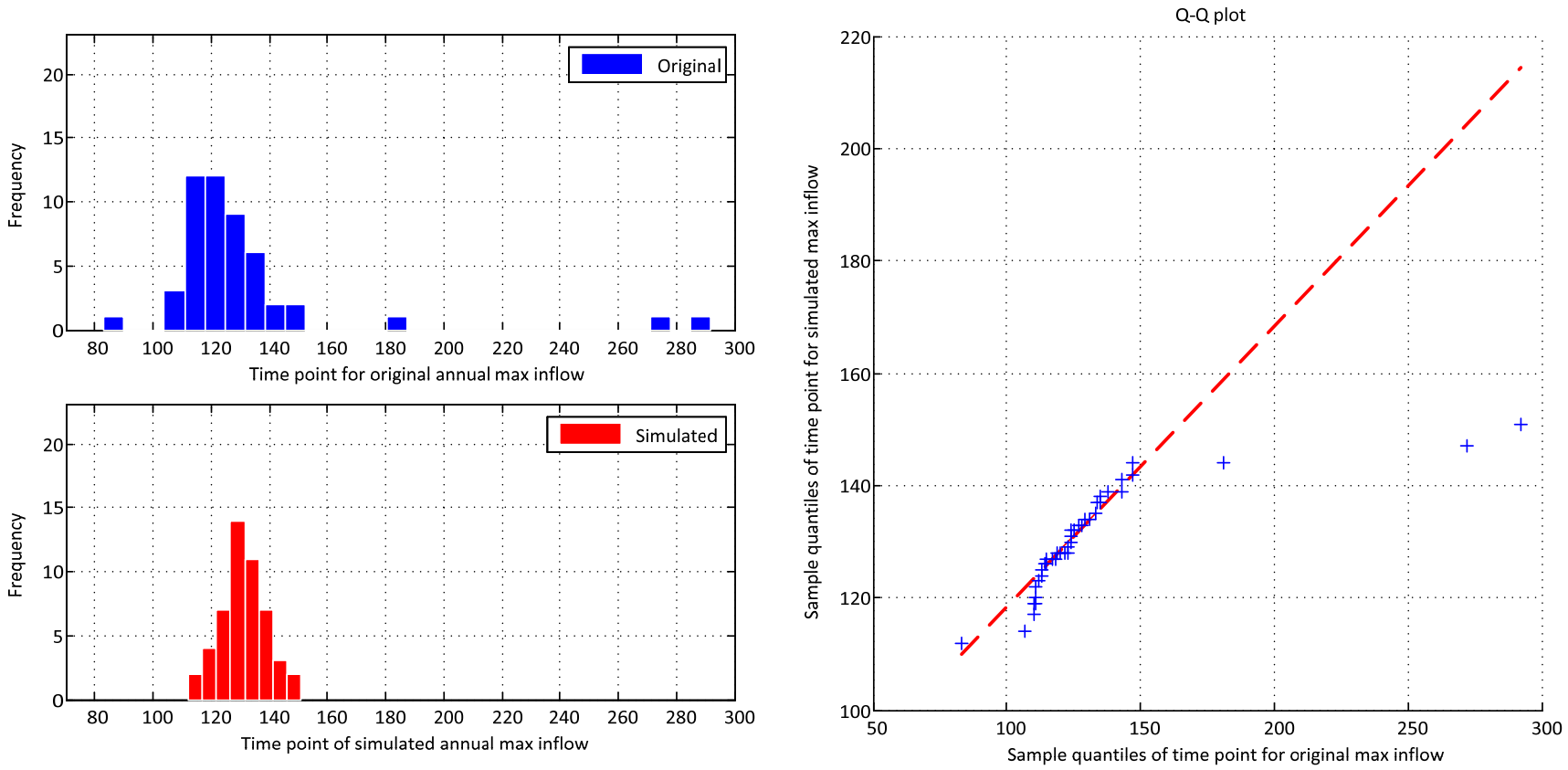

Figure 4-21 Comparison of historical and simulated annual max inflow timelines based on nomal innovation

Similar to the previous normal distribution, Figures 4-22 and 4-23 below demonstrate the results derived from the Student's t distributed innovations. The linearity patterns in Figures 4-22 and 4-23 demonstrated a reasonable simulation good match. There are three outliers in Figure 4-22, the same as Figure 4-20. The reason could be either the regular annual peak inflows did not occur or some omitting occurred in the inflow recording process. Thus, these three abnormal points were not taken into consideration.

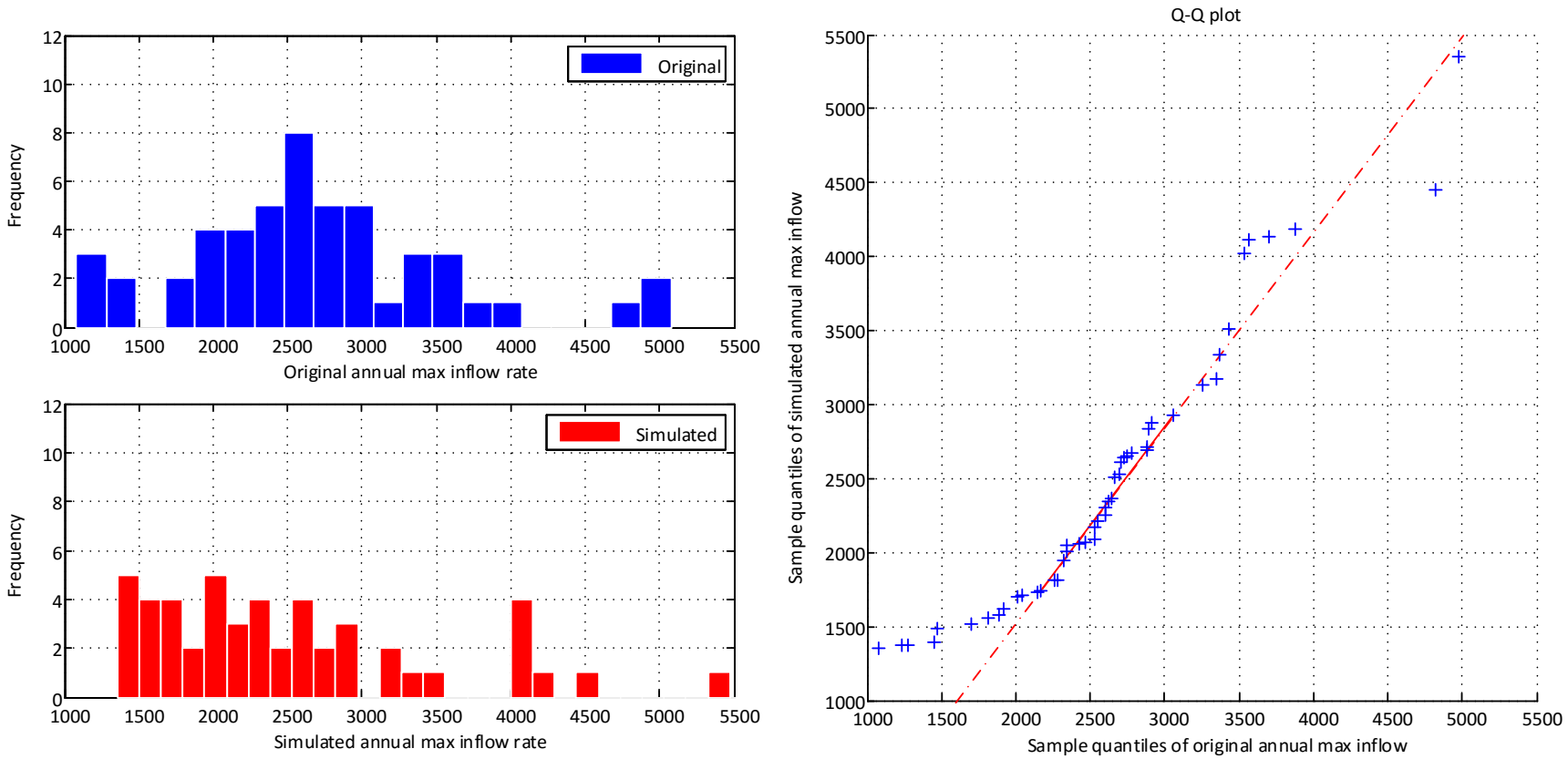

Figure 4-22 Comparison of historical and simulated annual max inflow based on student's t innovation

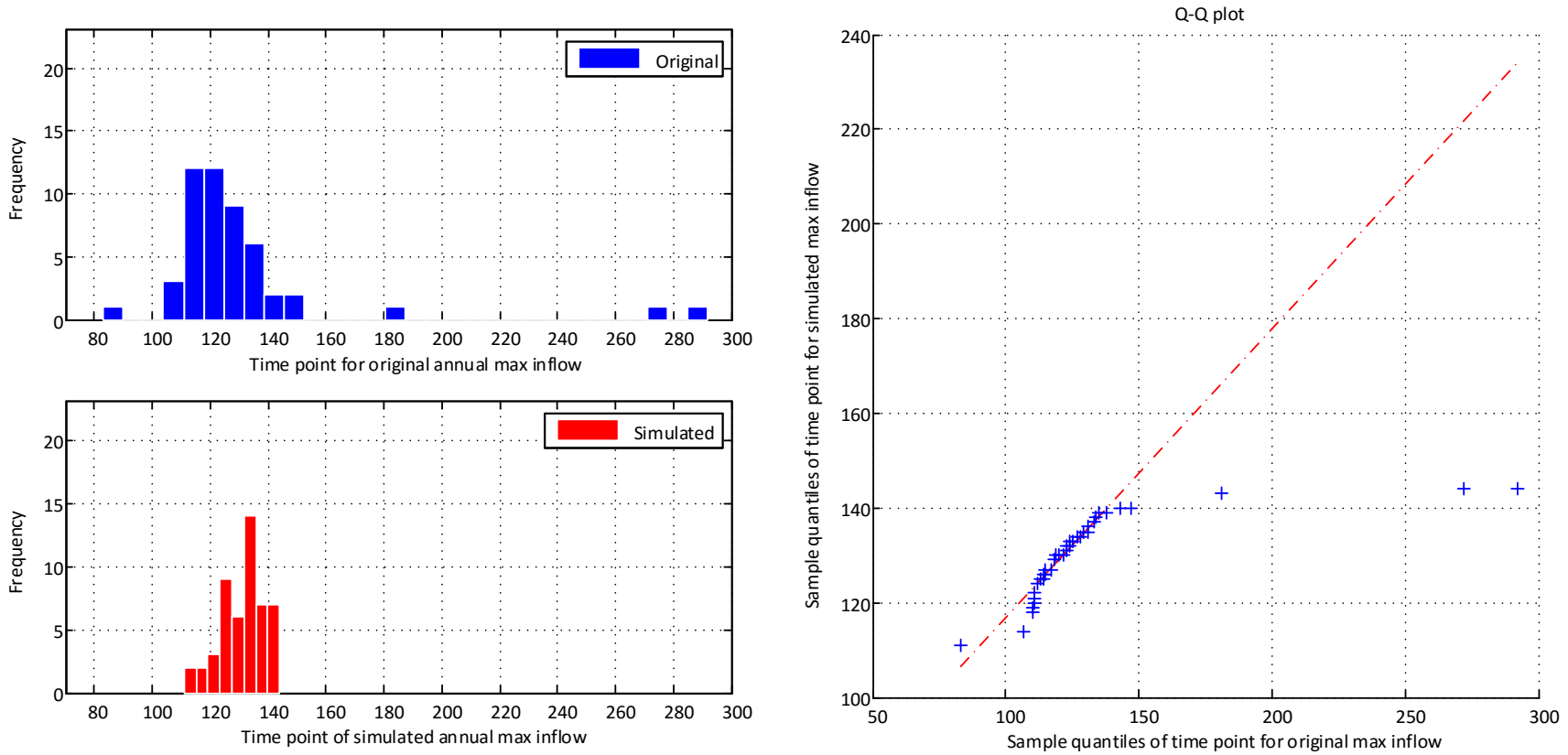

Figure 4-23 Comparison of historical and simulated annual max inflow timelines based on student's t innovation

4.4 Modeling Operation Process of Dam-Reservoir System

4.4.1 Outflows Control and Releasing Policy

The Adam Creek Diversion bypasses the Mattagami River plants from above Little Long Generation Station to below Kipling Generation Station and is the primary floodwater route. Dam safety response water levels have been established in accordance with the requirements of Dam Safety Emergency Preparedness and Response Plan standards to guide operators in case of hydraulic emergency. Water elevations in the Little Long reservoir vary slightly from season to season, usually with the maximum water elevations in the spring and fall, and the minimum in the summer and late winter. During daily peaking operations the water elevation in Little Long reservoir fluctuates within the range of ± 0.15 m. In most situations, the water elevation is within the operating headwater level, ranging from 195.10m to 198.12m. Shown as the green area in Figure 4-24, no additional operation is needed for the dam-reservoir system. The yellow area of energy reserve, ranging from 194.77m to 195.10m, is only used if a system energy emergency occurs. In common cases, all discharge flows are stopped before this 195.10m limit approaches. Another yellow area of potential failure developing from 198.12m to 199.00m stands for the flood allowance, which is only used to hold water in extreme conditions to reduce downstream flooding. At that time, the sluice gates open and start to release extra water beyond the capacity of water elevation 198.12m. The orange area, ranging from 199.00m to 199.30m, stands for the final buffer before overtopping events occur. All of the sluice gates open and the maximum water releasing capacity has been reached.

The dangerous headwater level is the imminent dam failure range (>199.30m) shown as the red area. We think that overtopping would definitely occur if the water elevation exceeds 199.30m.

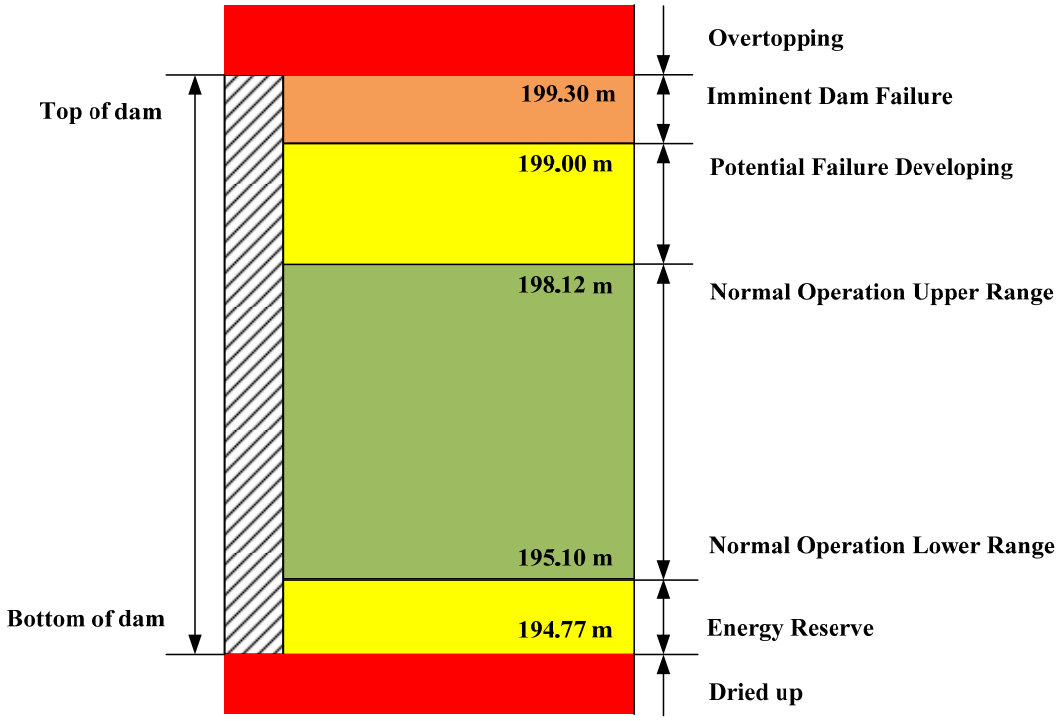

Figure 4-24 Water elevation boundaries for Little Long dam-reservoir system

The storage capacity of a reservoir is the most important characteristic. The available storage capacity of a reservoir depends upon the topography of the site and the height of dam. To determine the available storage capacity of the Little Long Dam-reservoir system, engineering surveys have been conducted to represent the physical characteristics, such as storage volume, surface area, outlet capacity, and elevation tables. The volume of storage to be allocated to each of the reservoir storage levels must also be specified. For accurate determination of the capacity, a topographic survey of the reservoir area is usually conducted, and a contour map of

the area is prepared. The storage capacity and the water spread area at different elevations can be determined from the contour map. In the Little Long case, the basic physical relationship of elevation-storage for the reservoir is displayed in Figure 4-25. The curve indicates that the elevation-storage relation is not linear. For the normal water elevation ranging from 195.10m to 198.12m, the storage capacity is reached in 1,874 m^3/s-days. For energy reserves ranging from 194.77m to 195.10m, the storage capacity is 142 m^3/s-days. Thus for the absolute operational water elevation ranging from 194.77m to 198.12m, the storage capacity is 2,016 m^3/s-days.

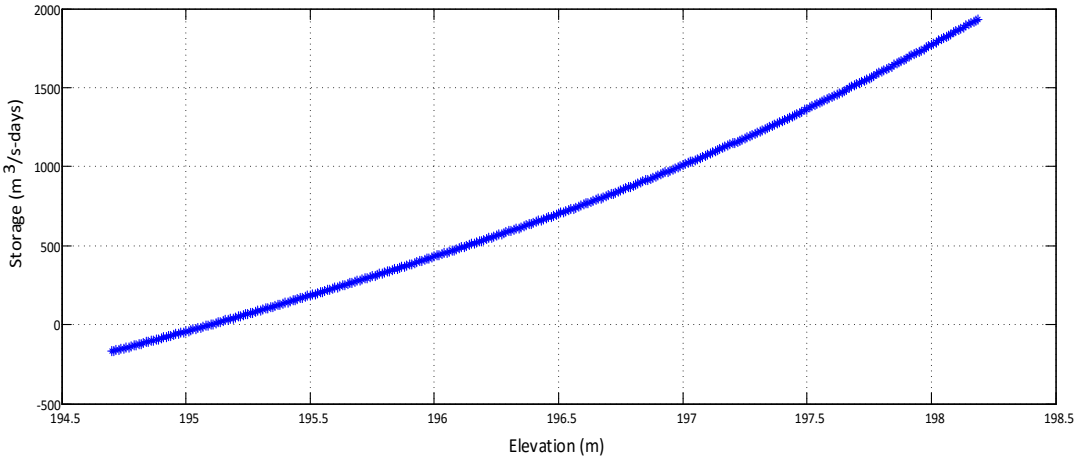

Figure 4-25 Elevation-storage curve for Little Long dam-reservoir system

The spillway flows, controlled by the sluice gates, provide adequate discharge capacity in case of the extreme inflow events occurring. In this specific system, both the Little Long Generating Station and the Adam Creek Control Structure have the reservoir water discharge capabilities. For the Little Long Generating Station, there are 2 units of the turbine which play the role of major resources producing power, and 2 sluice gates that help release extra water. Water is drawn from the Little Long forebay to the generating station via a submerged intake. For the Adam Creek Control

Structure, there are 8 sluice gates that all hold the same discharge capacity as the two in Little Long Generating Station. As a result, there are a total of ten sluices with gates. Six sluices are remotely controlled, and four sluices are locally controlled by the operator agents at the gate. Two to four hours may be required for the operators to reach the site.

At the maximum operating elevation of 198.12m, the discharge rate of one sluice gate could reach 608.80m^3/s. Consequently, the two sluices open into the Lower Mattagami River system with maximum capacity of 1217.60m^3/s, and the eight sluices open into the Adam Creek Bypass with a maximum capacity of 4870.40m^3/s. The maximum sluices outflow could reach 6,088.00 m^3/s at a reservoir water elevation of 198.12m. There are also two turbine outflows totaling 584.10m^3/s at reservoir water elevation of 198.12m. At the start of freshet, the Little Long forebay should be filled to an elevation not exceeding 198.12m. After achieving that elevation, any inflow greater than the amount of water required for two-unit operation (583 m^3/s) should be spilled down to Adams Creek. Thus, the maximum total discharge capacity could reach 6,672.10m^3/s for the whole dam-reservoir system. According to Figure 4-26, both the best and maximum outflow values vary based on different water head levels.

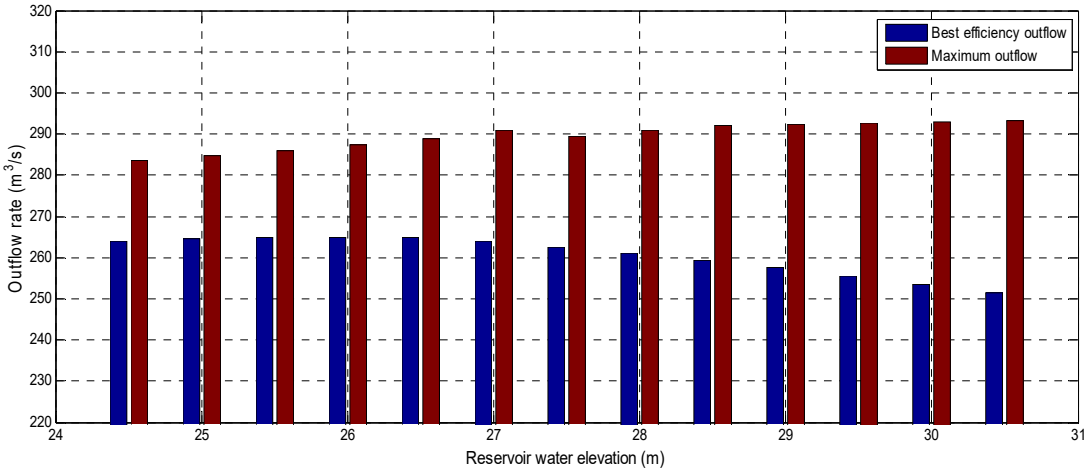

Figure 4-26 Elevation-discharge capacity curve for Little Long control structure

4.4.2 Modeling Dam-Reservoir Operation Process

The problem facing the overtopping risks analysis is to conceptualize a system model for the operation of the dams, generating stations, spillways, and other components, and then to employ the model through stochastic simulation to investigate protocols for safe system operation. Both the inflow rate and water elevation are important to govern the tradeoff between the discharge control and the water conservation. In order to represent the outflow control process in a mathematical way, two important values are presented in Equations (4-1) and (4-2).

$$S_A(t) = I(t) + \eta[H(t) - h_u] \tag{4-1}$$

$$S_B(t) = I(t) + \eta[H(t) - h_l], \tag{4-2}$$

where $S_A(t)$ and $S_B(t)$ stand for two stochastic water storage values used for outflows control; $I(t)$ stands for the inflow rate at time t; η is the reservoir shape coefficient, which reflects the water storage capacity of the reservoir; h_u = 198.12m

standing for the upper limit of water elevation for the normal reservoir operation; and $h_l =$ 195.10m standing for the lower limit of water elevation for the normal reservoir operation. Because $h_u > h_l$, we could reasonably conclude that $S_A(t) < S_B(t)$.

Here we simplified the outflow discharge control process and make it easier to quantify. Based on Equations (4-1) and (4-2), the mathematical expression of outflow discharge control process is shown in Equations (4-3) and (4-4).

$$O(t) = \max(\min(\max(\min(S_A(t), O_{\max}), O_{best}), S_B(t)), 0) \quad (4\text{-}3)$$

$$O(t) = (((S_A(t) \wedge O_{\max}) \vee O_{best}) \wedge S_B(t)) \vee 0, \quad (4\text{-}4)$$

where $S_A(t)$ and $S_B(t)$ stand for two stochastic water storage values used for outflows control; $\vee$ stands for the maximum function among values; and $\wedge$ stands for the minimum function among values. $O_{best} \approx 529\,\text{m}^3/\text{s}$ and $O_{\max} \approx 6671$ m^3/s. Thus $O_{best} + 6142$ m^3/s $\approx O_{\max}$.

In more details, the discharge rate $O(t)$ based on different values of inflow rate $I(t)$ and water elevation $H(t)$ have several possibilities, including: 1) no discharge, where $O(t) = 0$; 2) $O(t) = S_B(t)$ as shown in Eq.(4-2); 3) best efficient turbine flows, $O(t) = O_{best}$; 4) $O(t) = S_A(t)$ as shown in Eq.(4-1); and 5) maximum turbine flows plus 10 sluice capacity, where $O(t) = O_{\max}$. As Table 4-6 shown below, the two critical water storage values $S_A(t)$ and $S_B(t)$ decide the releasing volume of outflows. The simplified operation process of Little Long dam-reservoir is deterministic. But there is still space that the potential stochastic modeling could be incorporated in.

Table 4-6 Outflow releasing controls under different scenarios

Scenarios	Description	Outflow $O(t)$
$0<O_{best}<O_{\max}<S_A(t)<S_B(t)$	Extreme large water volume and inflow that excess maximum reservoir discharge capacity	$O_{\max}$
$0<O_{best}<S_A(t)<O_{\max}<S_B(t)$	Large water volume and inflow but within maximum reservoir discharge capacity	$S_A(t)$
$0<O_{best}<S_A(t)<S_B(t)<O_{\max}$	Large water volume and inflow but within maximum reservoir discharge capacity	$S_A(t)$
$0<S_A(t)<O_{best}<S_B(t)<O_{\max}$	Medium water storage and inflow	O_{best}
$S_A(t)<0<O_{best}<S_B(t)<O_{\max}$	Medium water storage and inflow	O_{best}
$S_A(t)<0<S_B(t)<O_{best}<O_{\max}$	Small water storage and inflow	$S_B(t)$
$S_A(t)<S_B(t)<0<O_{best}<O_{\max}$	Extreme small water storage or none inflow	0

Including all the above logical information, a Simulink model has been built in order to demonstrate the general dam-reservoir system operation process in Figure 4-27. Under the normal conditions, outflows from the Little Long reservoir go through the generating stations. The best efficiency flow capacity, which generates the highest electrical output per unit of water, for the appropriate number of hours matches daily average outflow to inflow and storage. When the inflows are less than the capacities of generating stations, there is no spill to Adam Creek and the local inflows and water elevations in the Mattagami River are low. During periods of high inflow, such as the spring runoff, the spillway at Adam Creek will be operated in conjunction with the Little Long generating station to pass the full Mattagami River flow. The duration and magnitude of the spill down Adam Creek will be less than the existing capacity.

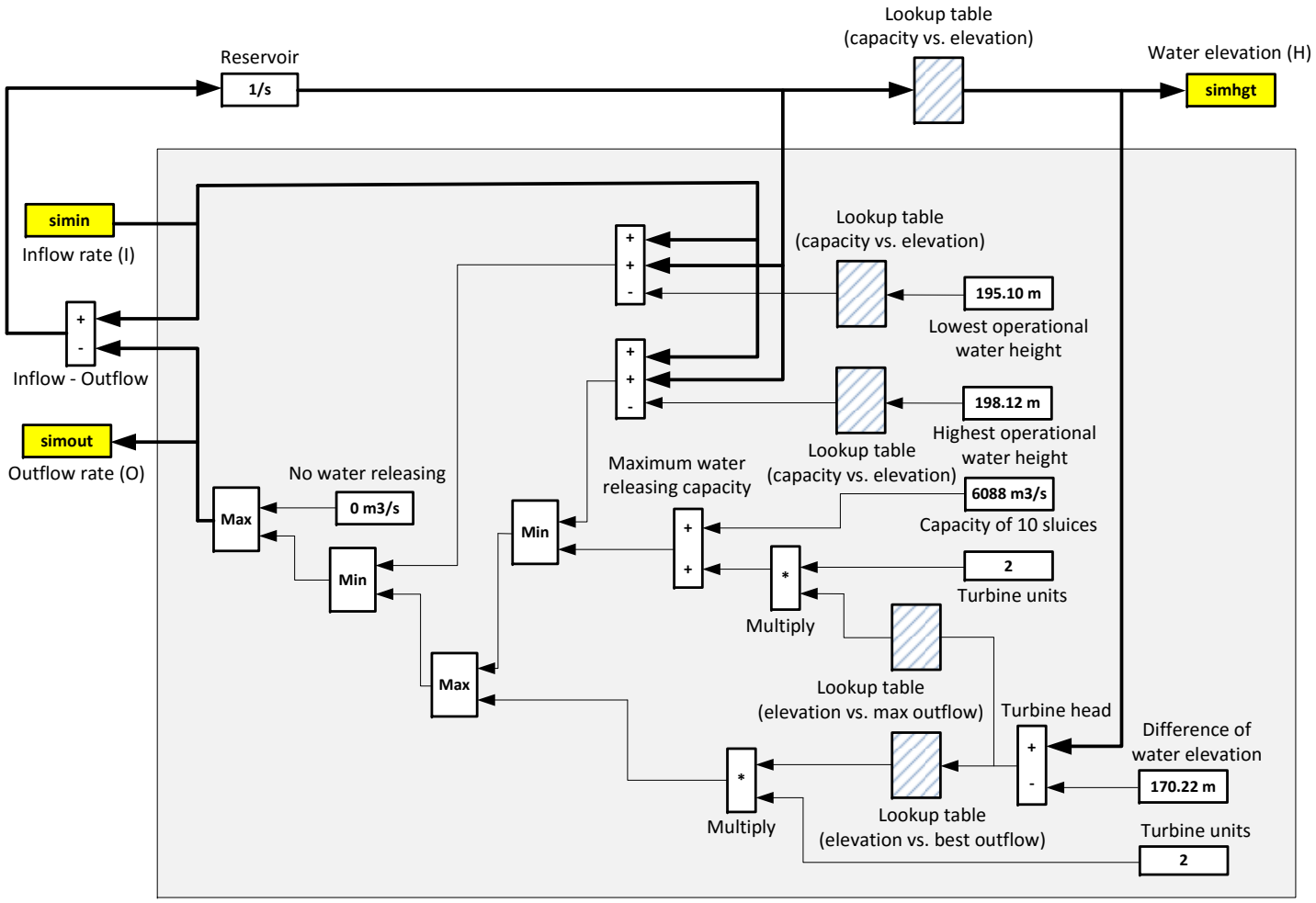

Figure 4-27 Simulink framework of Little Long dam-reservoir system operation

4.4.3 Model Validation

In order to validate the proposed dam-reservoir system operation model, the calculated outflow rates and water elevations are compared with the historical records. Setting the historical inflow rates of the past 50 years (1964-2013) as inputs to the Matlab/Simulink model, the corresponding outflow rates and reservoir water elevation are presented in Figure 4-28 below. The timeline unit is a day. As we observe, the maximum of daily average inflow rates never exceed 6000 m^3/s in historical record. Thus, the assumed extreme precipitation has never been reached and the overtopping events have never occurred. The Little Long dam-reservoir system stays safe, which is aligned with the reality of actual operation practice. Therefore, the dam-reservoir system operation model is demonstrated to be valid.

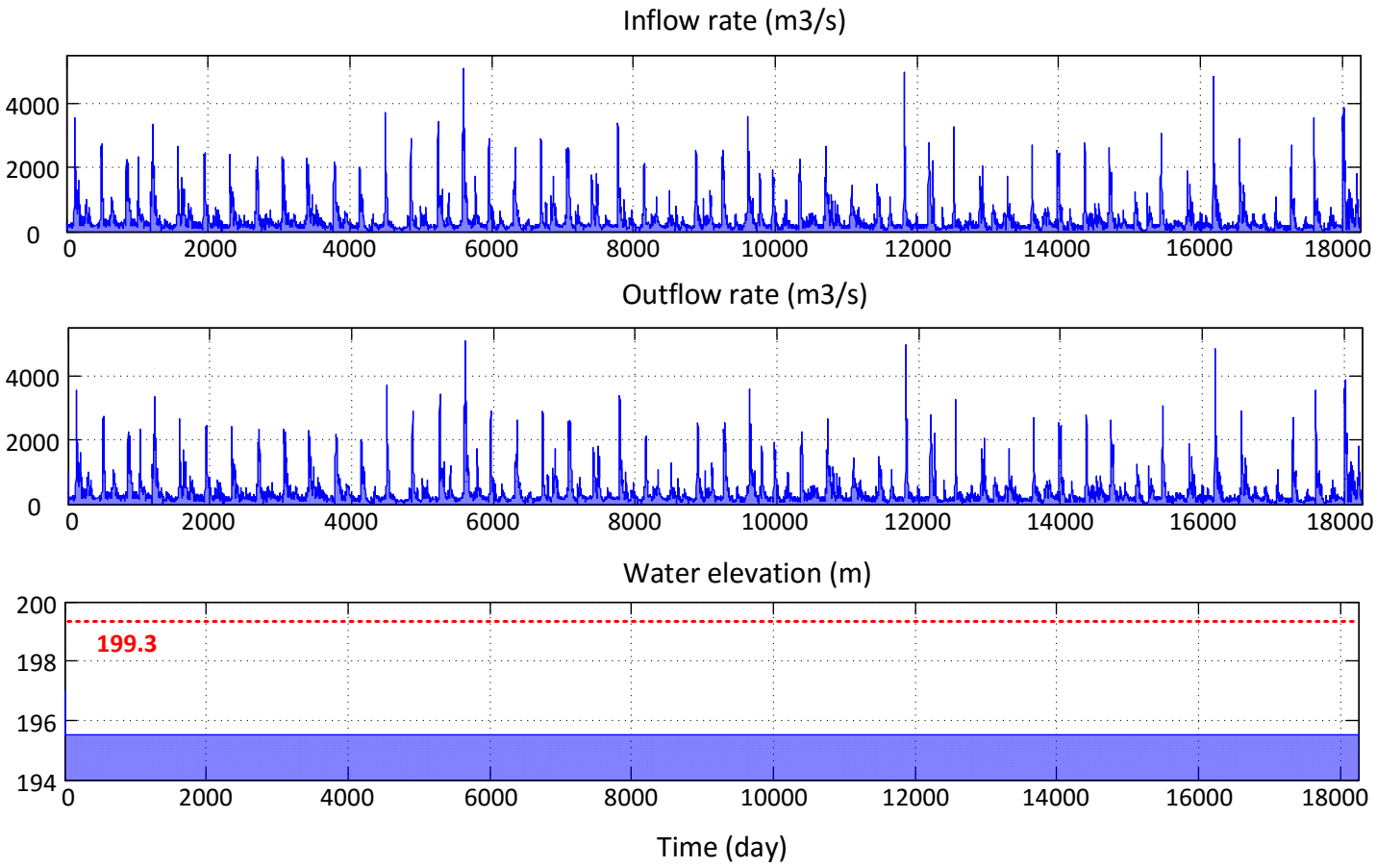

Figure 4-28 Historical inflows and corresponding outflows and water elevation

4.4.4 Model Testing

In order to test the extreme situations, four pseudo inflows are set as the testing inputs for the proposed Simulink model. The inflow rate, and the corresponding outflows and water elevations are demonstrated in Figures 4-29 and 4-30 below. All of the four inflow inputs share the same daily peak inflow rate at $7000m^3/s$, and daily lowest inflow rate at $6000m^3/s$. Only the variation frequencies differentiate.

Based on the above water elevations presented, we could reasonably conclude that different variations of the inflow inputs would result in the different overtopping risks, even when the peak inflow rates stay the same. It would be incomplete to consider only the peak inflows or inflow volume within a certain period of time to address the overtopping risks of dam-reservoir system. In order to evaluate the overtopping risks of the dam-reservoir system accurately, the whole inflow modeling and reservoir operation process needs to be taken into consideration, rather than a certain time period or a specific part of the system.

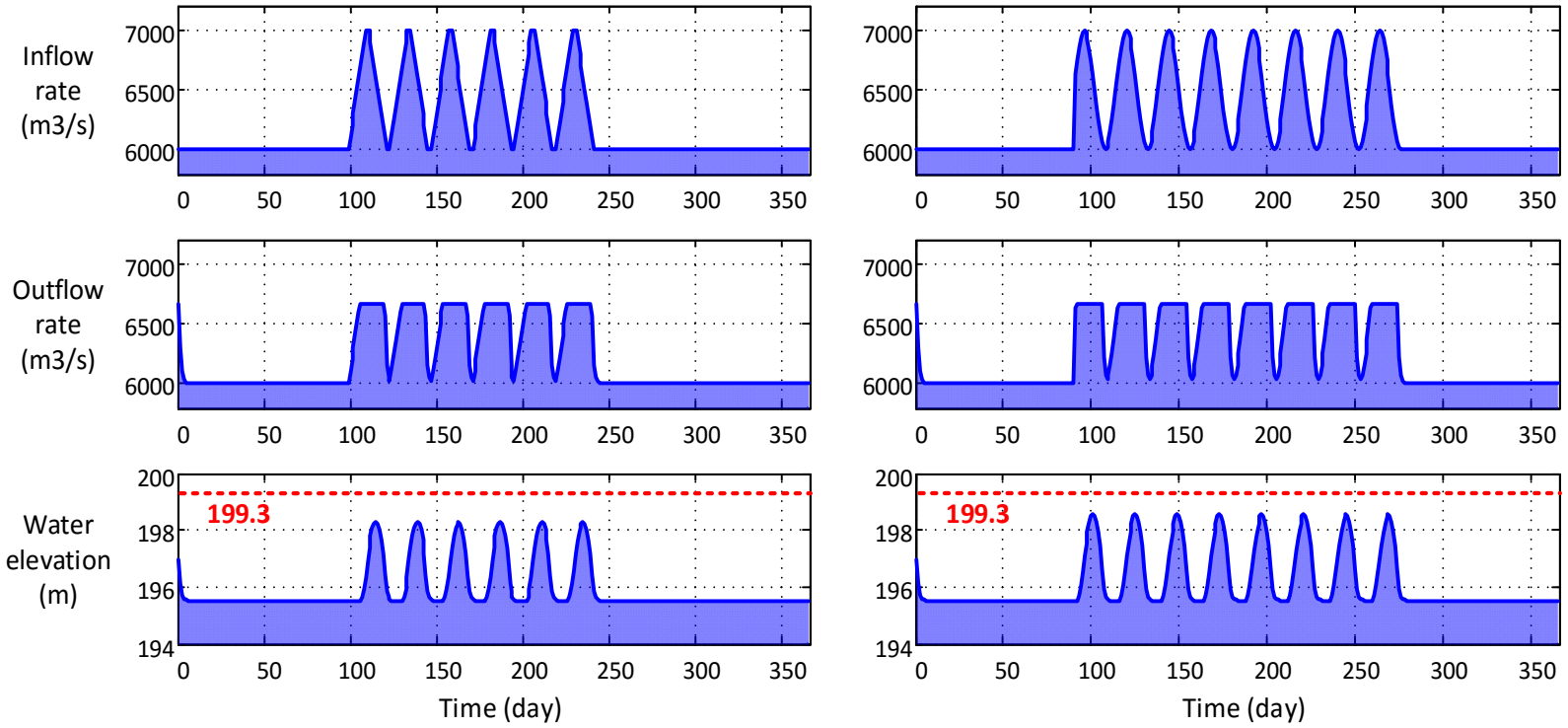

Figure 4-29 Pseudo inflow testing with corresponding outflows and reservoir water elevation (no overtopping)

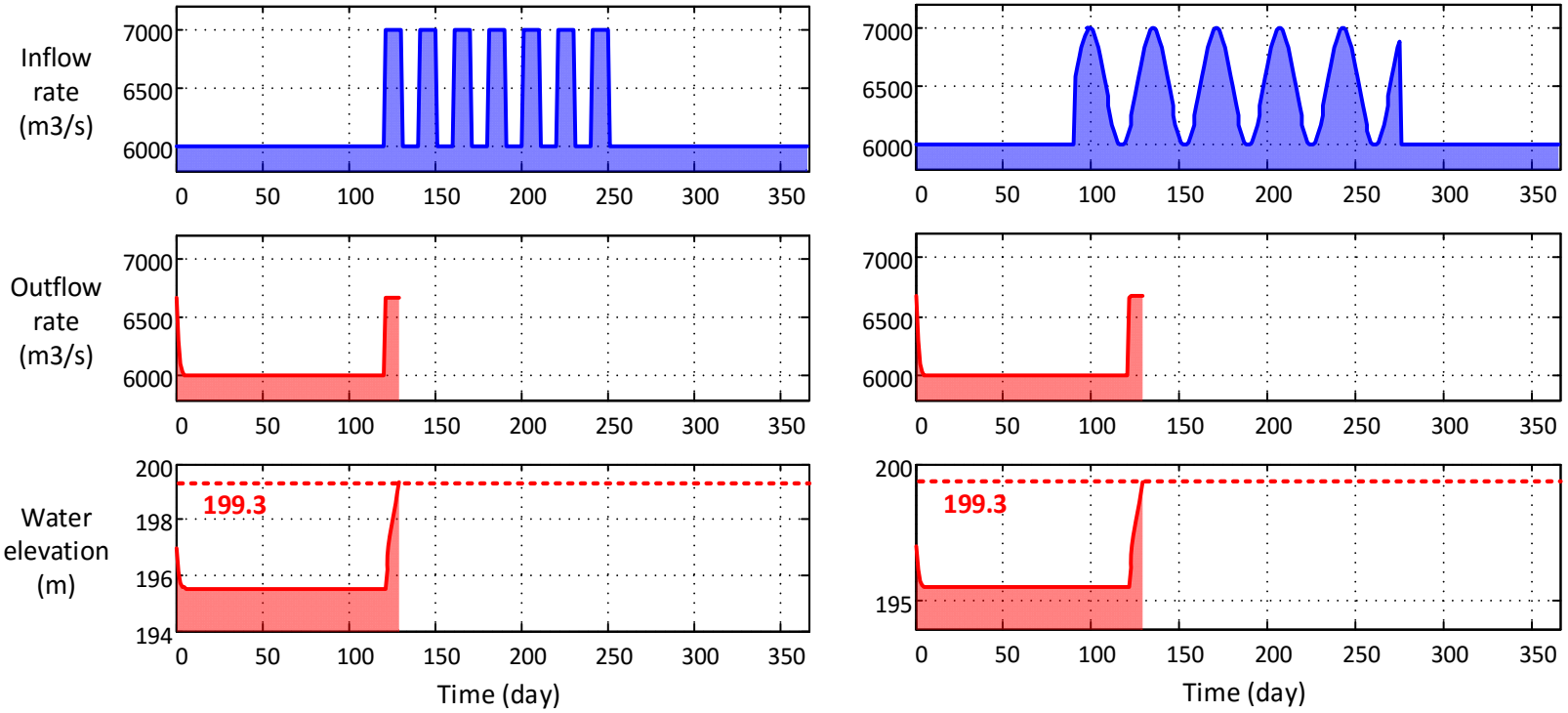

Figure 4-30 Pseudo inflow testing with corresponding outflows and reservoir water elevation (overtopping)

4.5 Summary

In summary, this chapter demonstrates the whole modeling and simulation process using the specific case of Little Long dam-reservoir system in northeastern Ontario, Canada. It starts with the project background introduction. Since the selected Little Long dam-reservoir system is within a modified continental climatic zone, strong seasonal patterns have been shown in the inflow data. As a consequence, the seasonal ARIMA model has been constructed and used for inflow simulation with uncertainty. Sample paths of the simulated inflows have also been tested in order to validate the model. After that, operation of the dam-reservoir system has been modeled as a sequence. The final model testing indicates that different variations of the inflow inputs would result in the different thresholds of overtopping risks, even when the peak and bottom values staying the same. In order to evaluate the overtopping risks of dam-reservoir system accurately, the whole inflow modeling and reservoir operation process needs to be considered.

Chapter 5: Overtopping Risks Evaluation of Little Long Dam-Reservoir

5.1 Introduction

This chapter serves as the case application of Chapter 3 and follows Chapter 4 as the demonstration of the simulation results. Based on the theoretical model developed, estimation of the overtopping risks for the Little Long dam-reservoir system has been conducted and the corresponding computational performance has been tracked. This chapter starts with the introduction of simulation implementation, including two perspectives: 1) the simulation platform; and 2) the probability density selection for importance sampling. Then, the simulation results are presented including the overtopping probability estimation by both the normal distributed innovations and the student's t distributed innovations. Results for both the CMC simulation and ISMC simulation are presented with comparison, and the computational performance measurement are tracked in the meanwhile.

5.2 Simulation Implementation

5.2.1 Simulation Platform

MC simulation has been performed in order to yield the overtopping probabilities of the discrete-time reservoir operation model. Due to computational resource limitations, the simulation is implemented on a personal ThinkPad X1 laptop, which might take longer to reach the results as compared with running the same program on a server of higher capacity. Taking advantages of the longer time intervals, priorities

of the importance sampling based simulation could be shown more obviously. Detailed system configuration information is displayed in Table 5-1.

Table 5-1 System configuration for simulation implemention

Configuration	Setting
Operation system	Windows 8.1
Processor	Intel(R) Core(TM) i5-4200U CPU @ 1.60GHz 2.30GHz
Installed memory (RAM)	8.00 GB (7.90 GB usable)
System type	64-bit Operating System, x64-based processor

R and Matlab/Simulink are major programming languages that are being adopted for simulation in this research. R is a programming language and software environment for statistical computing and graphics, which is widely used among statisticians and data miners for developing statistical software and data analysis. Here R programming is mainly used for modeling and simulating the inflow hydrographs under uncertainty. The version of R is 3.1.2 (2014-10-31), named "Pumpkin Helmet". Besides the base packages of R, packages of "forecast", "tseries", and "R.matlab" are also adopted. Matlab (matrix laboratory) is a multi-paradigm numerical computing environment and fourth-generation programming language, which allows matrix manipulations, plotting of functions and data, implementation of algorithms, and creation of user interfaces. Simulink, developed by MathWorks, is a graphical programming environment for modeling, simulating and analyzing multi-domain dynamic systems. It offers tight integration with the rest of the Matlab environment and can either drive Matlab or be scripted from it. Here Matlab/Simulink is used for modeling and simulating operation process of the dam-reservoir system. Due to the repetitive process, parallel computing is applied to both CMC simulation

and rare event-based MC simulation. The version of Matlab is 8.5.0.197613 (R2015a).

5.2.2 Likelihood Ratios Based on Different Conditions

The fundamental issue in implementing IS simulation is the choice of the biased distribution that encourages the important regions of the input variables. Here we take both the normal distributed and the Student's t distributed residuals into consideration. As presented before, the Student's t distributed residuals are finally transformed into normal distributed variables. In order to find the optimal pdf for IS, a detailed analysis on the mean, the standard variation, and the corresponding LR are discussed below.

The nature of normal distribution depends on two factors - the mean and the standard deviations. The mean of the distribution determines the location of the center for the distribution, and the standard deviation determines the height and width for the distribution. Thus, the aim of finding appropriate probability density function has been transferred to find proper values for the mean and the standard deviations. In order to demonstrate the different influences of mean and standard deviation on the likelihood ratio function, Figures 5-1 to 5-9 are shown below. The seed values for random generators are controlled to make sure of the replication possibility of the simulation process. Initial seeds 1, 6 and 1000 are chosen as three separate streams of random variates in the following discussion as well as the simulation results. The seed numbers 1, 6, and 1000 are selected randomly.

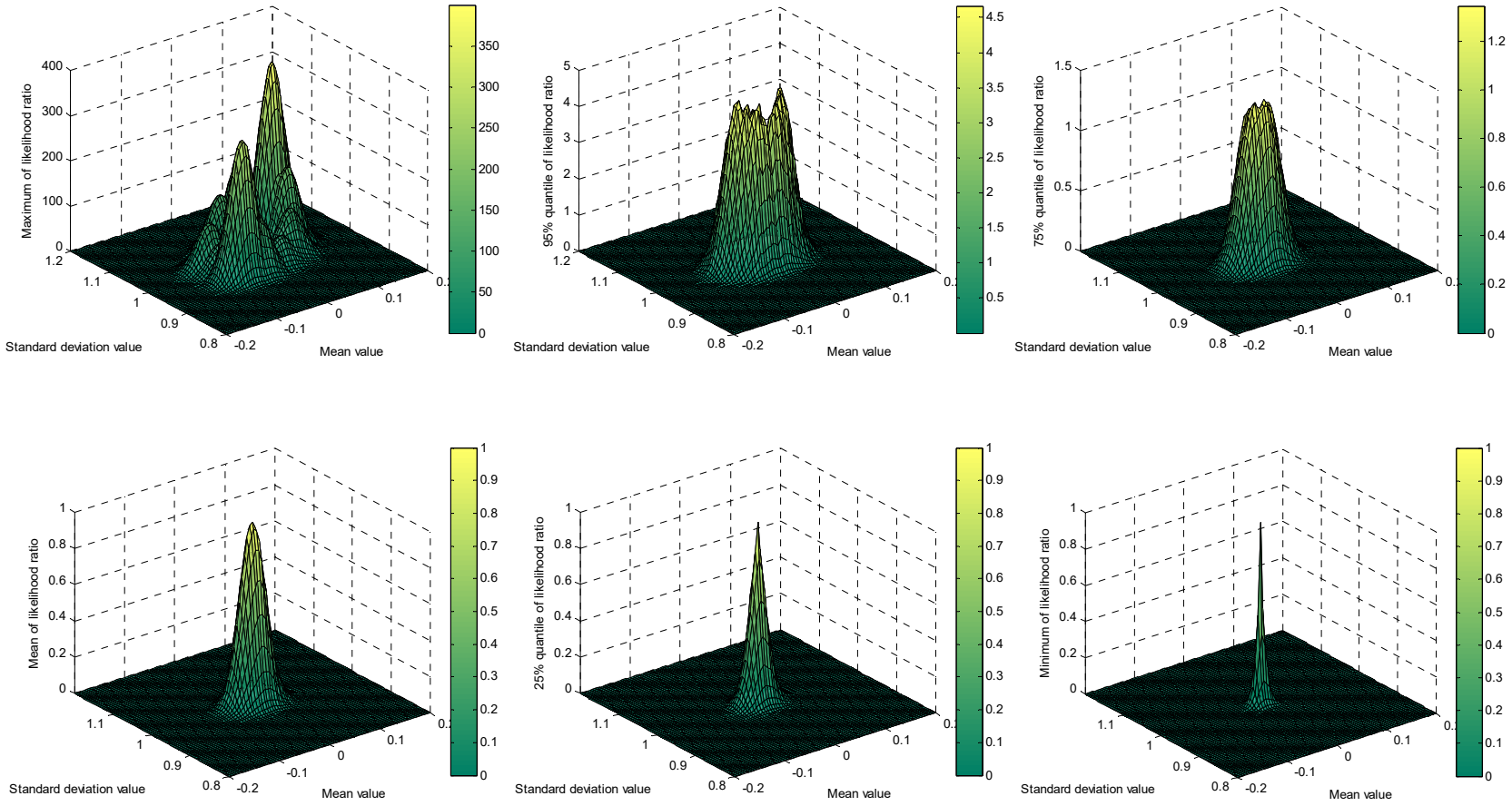

Figure 5-1 Likelihood ratio distributions for normal distributed innovation
(Seed = 1, time period = 5 years, iteration = 1000 times)

Taking seed = 1, simulation period = 5 years, and iteration = 1000 times as an example, Figure 5-1 above presents the LR values derived from different means and standard deviations for each quantile respectively. According to Figure 5-1, the LR values stay as non-zero only within a certain range approaching mean = 0 and standard deviation = 1. The maximum quantile of LR values spread more widely with peak deviated from the center, while the minimum quantile of LR values concentrate in the center as symmetric to both the mean and the standard deviation. In order to demonstrate the presented observations, simulation iterations have been increased from 1000 to 10,000. As shown in Figure 5-2 below, status of seed =1 and time period = 5 years stays the same as Figure 5-1. The observations on the quantiles of LR values stay similar as Figure 5-1.

Remaining seed = 1 and iteration = 1000 times, the values of LR function for time period = 100 years are presented in Figure 5-3. As shown below, the range of LR values as non-zero becomes narrower as compared to Figures 5-1 and 5-2. This means that there is less choice on the mean and standard deviations for the importance sampling density selection.

Different simulation seeds provide slightly different likelihood ratios on the same mean and standard deviation values. In order to show the differences in a more obvious way, the 2D graphs in Figures 5-4 to 5-6, instead of 3D graphs, are adopted. For the maximum values of the likelihood ratio shown below, two peaks are presented for both the fixed mean and standard deviation values, slightly departed from the center point of mean = 0 and standard deviation = 1.

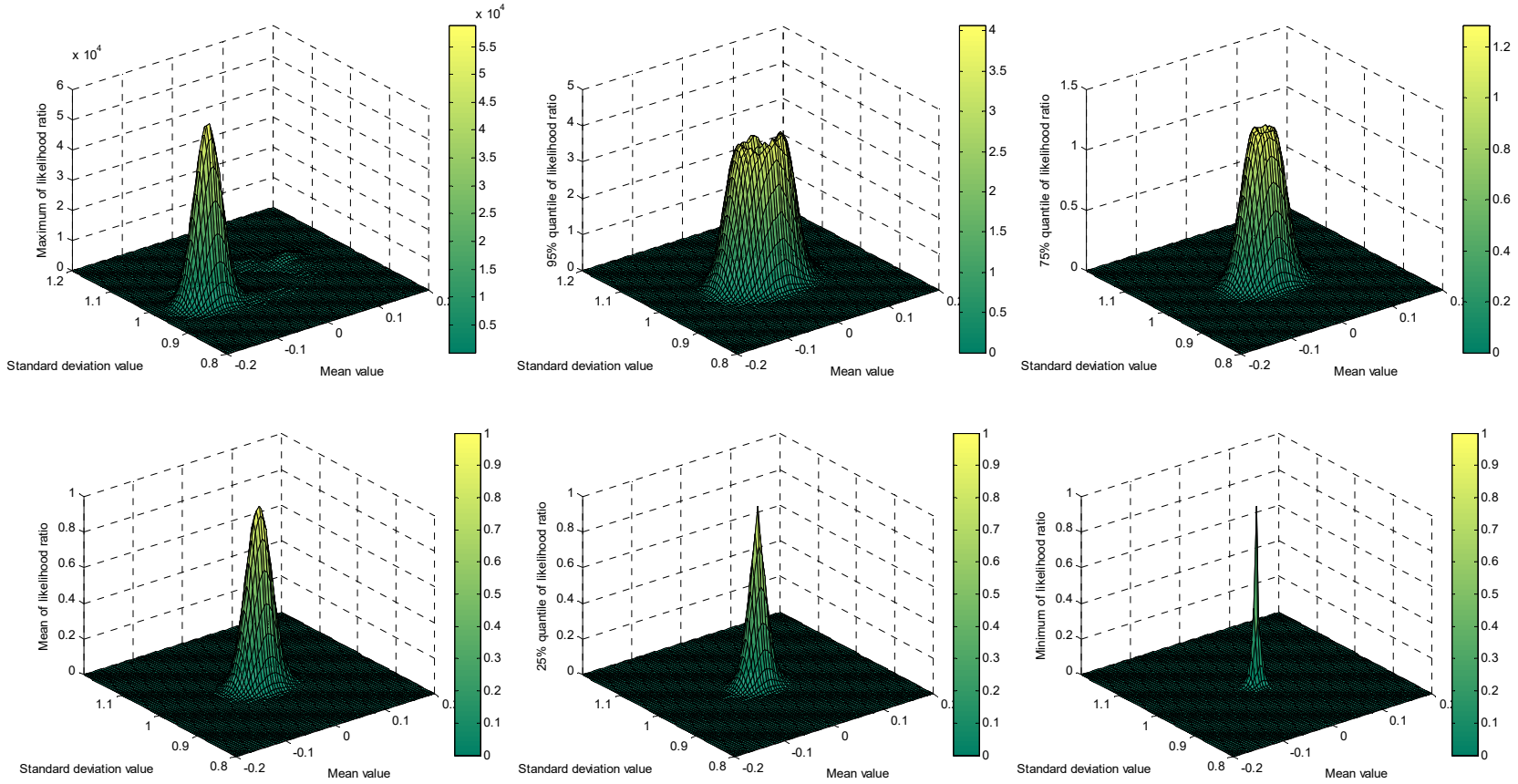

Figure 5-2 Likelihood ratio distributions for normal distributed innovation
(Seed = 1, time period = 5 years, iteration = 10000 times)

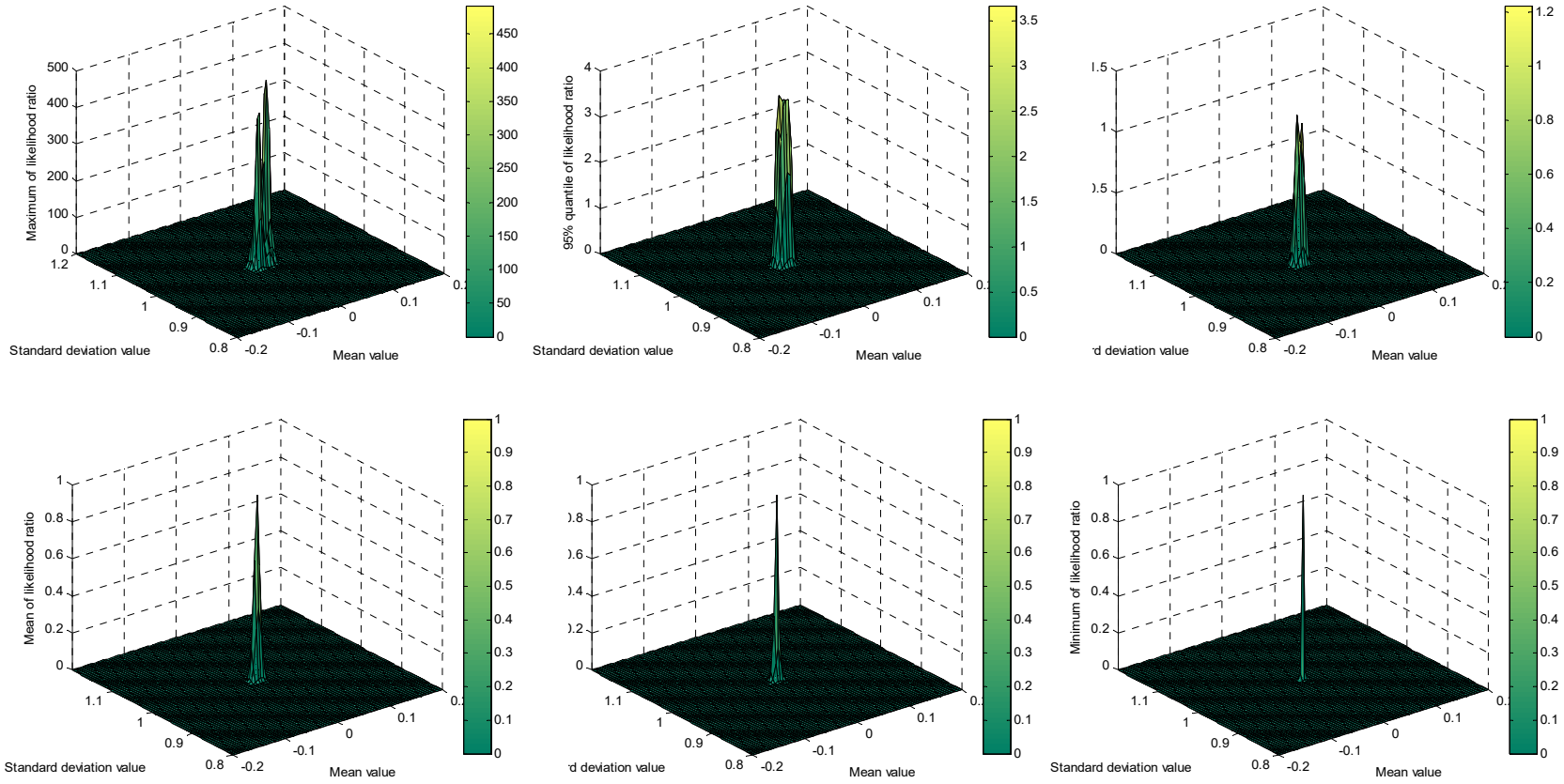

Figure 5-3 Likelihood ratio distributions for normal distributed innovation
(Seed = 1, time period = 100 years, iteration = 1000 times)

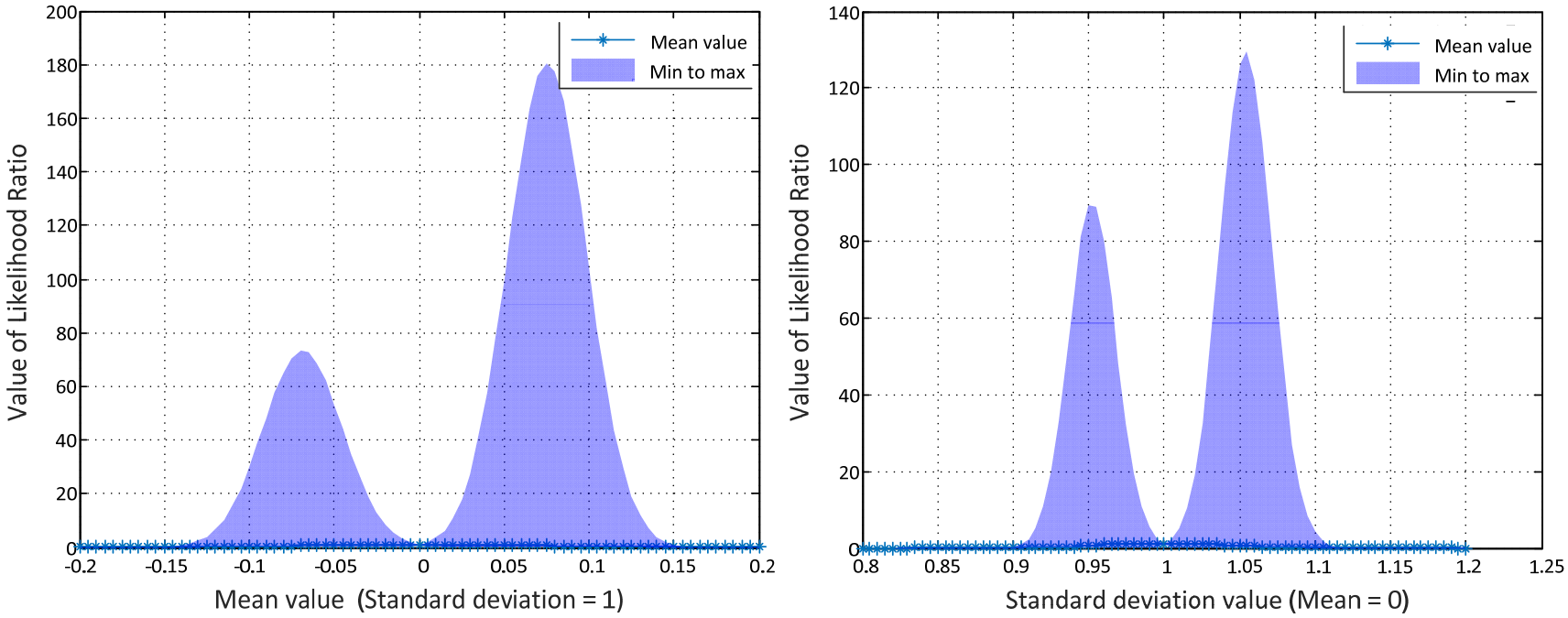

Figure 5-4 Likelihood ratio distributions for normal distributed innovation
(Seed = 1, time period = 5 years, iteration = 1000 times)

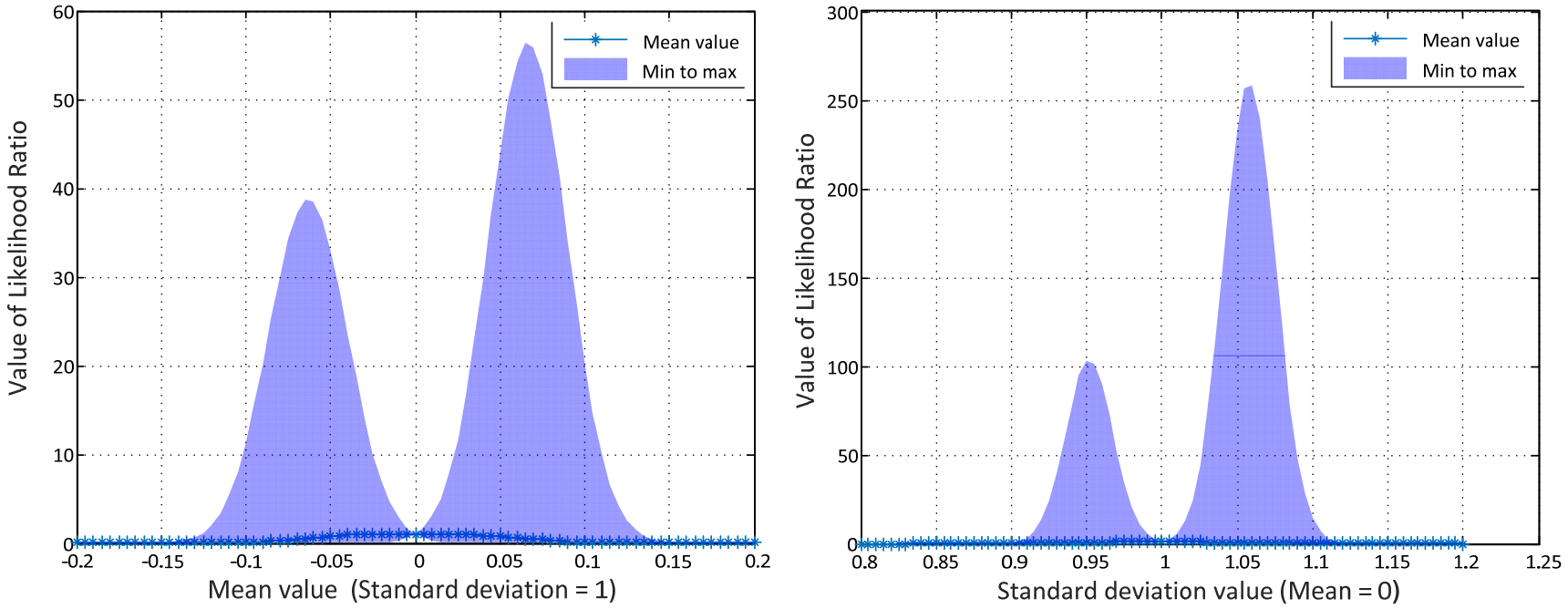

Figure 5-5 Likelihood ratio distributions for normal distributed innovation
(Seed = 6, time period = 5 years, iteration = 1000 times)

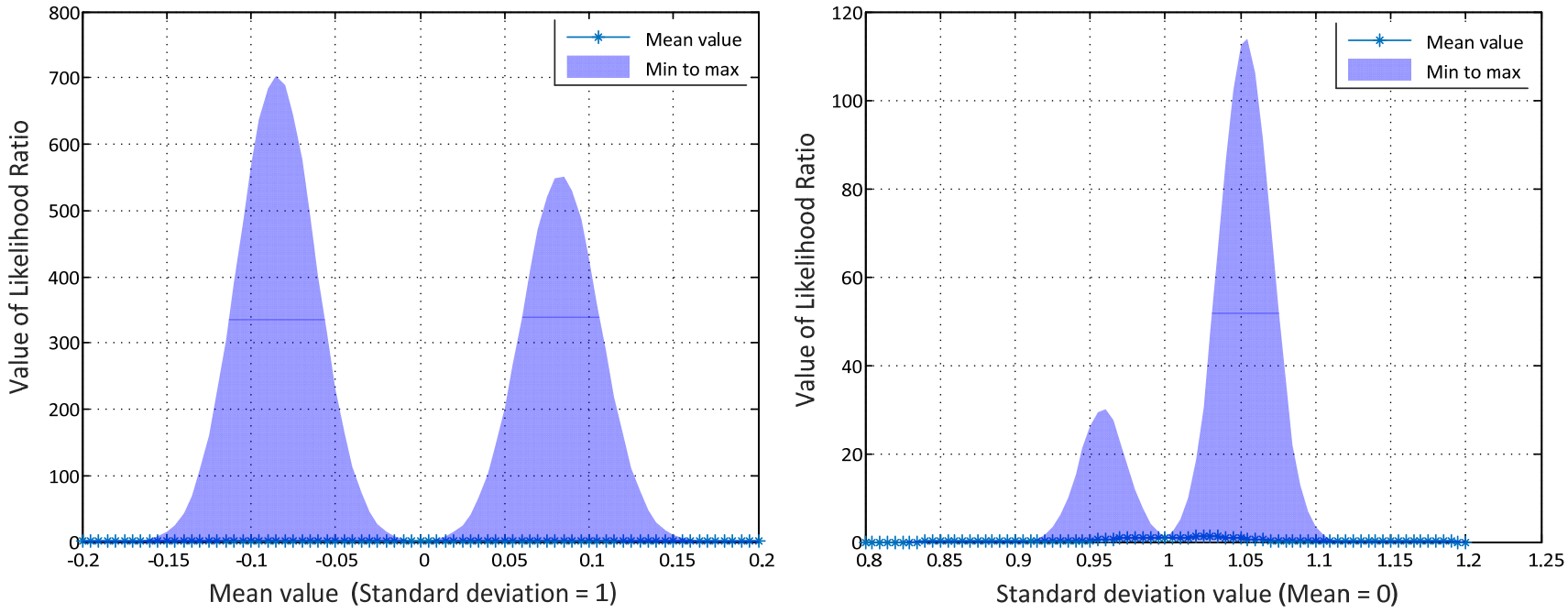

Figure 5-6 Likelihood ratio distributions for normal distributed innovation
(Seed = 1000, time period = 5 years, iteration = 1000 times)

The LRs based on the student's t distributed innovations are presented in Figures 5-7 to 5-9 with the same length of time but different simulation seeds of 1, 6, and 1000 respectively. The ranges of LR values as non-zero show to be narrower as compared with the LR values based on the normal distributed innovations. Similar logic has also been demonstrated in Figure 5-2, which is mainly

due to the more random variables involved. In this case, we transfer the student's t distributed random variables into multiple normal distributed random variables within the simulation process.

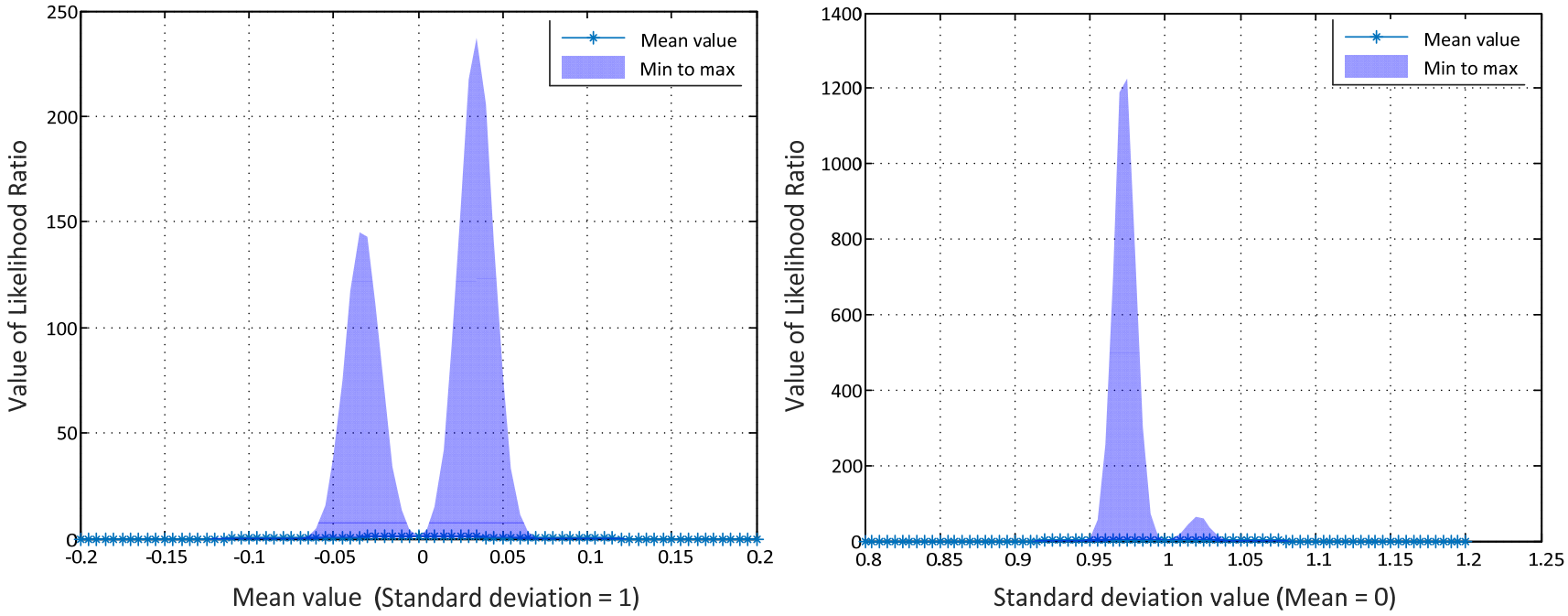

Figure 5-7 Likelihood ratio distributions for student's t distribution innovation
(Seed = 1, time period = 5 years, iteration = 1000 times)

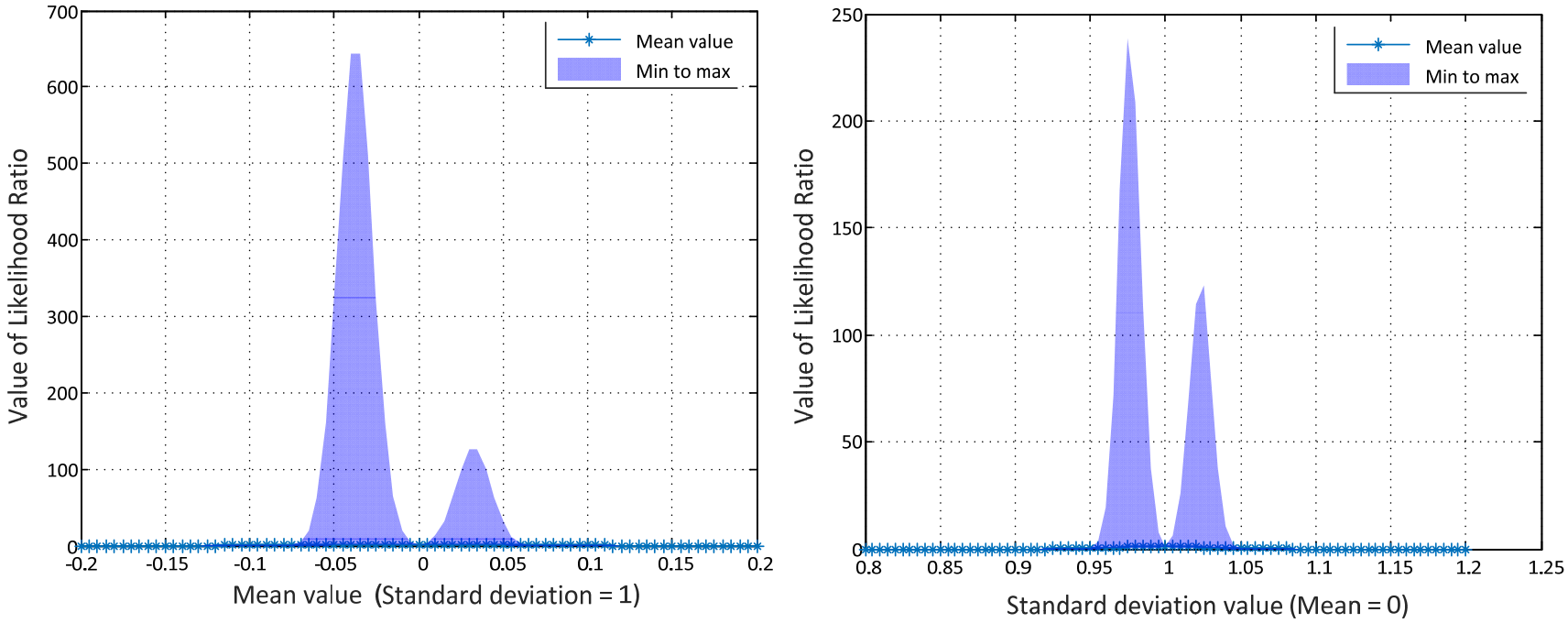

Figure 5-8 Likelihood ratio distributions for student's t distribution innovation
(Seed = 6, time period = 5 years, iteration = 1000 times)

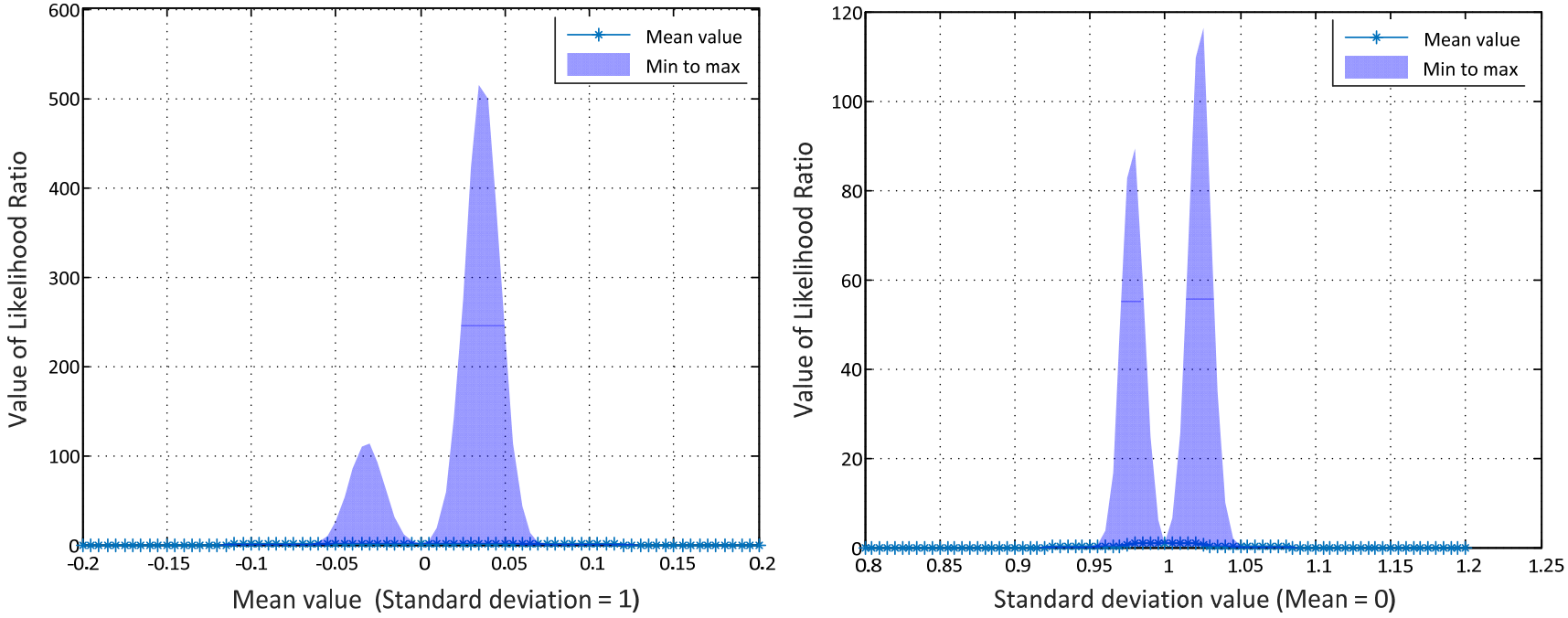

Figure 5-9 Likelihood ratio distributions for student's t distribution innovation
(Seed = 1000, time period = 5 years, iteration = 1000 times)

5.2.3 Importance Sampling Density Selection

Appropriate importance sampling density could not only significantly save computational resources, but also provide a more accurate simulation-based estimation at the same time. As we identified in the previous section, the LR values stay as non-zero only within a certain range centered at mean = 0 and standard deviation = 1. In order to find the appropriate density for the ISMC simulation, discrete points spread in the grid are selected within the domain, and an enumeration method is adopted in this search. Since the intention is to sample extreme regions of the dynamic systems which are unlikely to visit through CMC simulation, scaling and shifting would both be considered to the positive direction in order to minimize the dimensionality effect of IS. As a consequence, the following map is shown in Figure 5-10 below. Searching starts from the inner circle and expanding to the outer one. Each points in Figure 5-10 represents a new pdf choice for ISMC. The proposed approach does not necessarily lead to the optimal zero-variance estimator, but yields significant variance reduction.

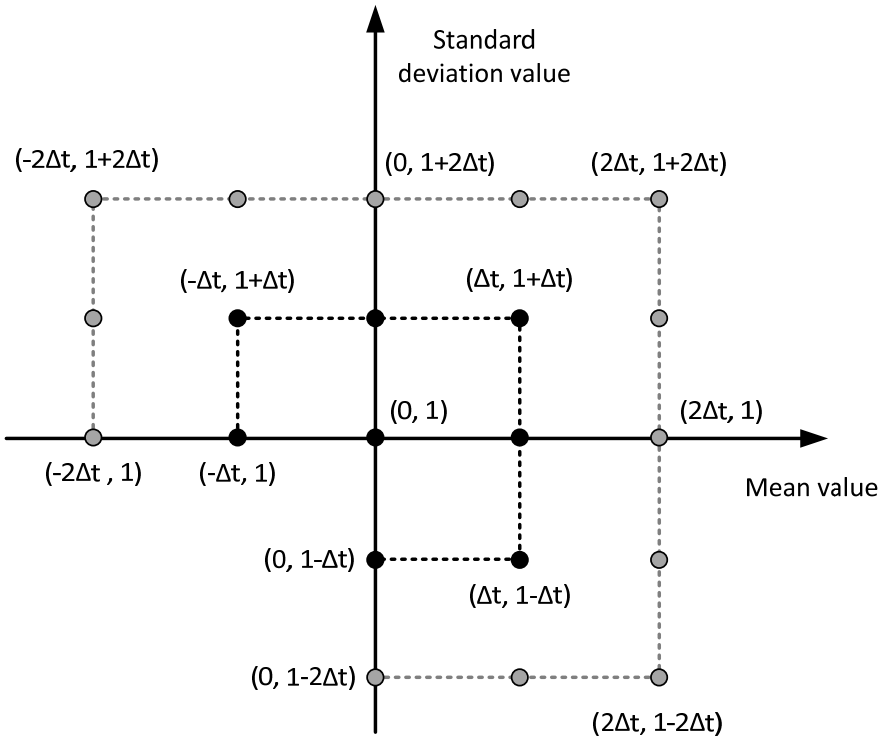

Figure 5-10 Selection of importance sampling density parameters

Here Δt stands for a small change in the values of mean and standard deviation that could be defined based on the simulation accuracy. Since the new density is intended to sample "special" regions of the dynamic space of systems selectively, which are unlikely to visit through CMC simulation, we could reasonably believe that either the mean or the standard deviation value needs to move to the positive direction. As shown in Figure 5-10, the search starts from the inner circle, where 7 points exist, and then continues to the outer circle, where 13 points exist. The length of Δt is chosen as varied on the simulation time scales. For instance, Δt for the 5 year time scale estimation is bigger than Δt for the 100 year time scale estimation. Final simulation results in the following section demonstrate that

appropriate Δt could effectively help to find the appropriate IS density to increase the simulation accuracy.

5.3 Simulation Results of Overtopping Risks

Simulation results with comparison are shown for the innovation fittings, normal and student's t distributions, which are reasonably assumed as the lower and upper bounds of the overtopping probabilities estimation. In order to present this in a more organized way, Table 5-2 below is adopted as an index table to group the results. The estimated probabilities based on the normal random innovations, are very small. As a consequence, the variances for both the CMC and the ISMC simulation are approaching zero. Due to the limited 1,000 times simulation, there are no significant differences to demonstrate the computational priority of the ISMC simulation. As a result, no tables are displayed in the variance estimation grid in Table 5-2. To the contrary, since there are many overtopping occurrences through the ISMC simulation, it is hard to show and compare the simulated occasions of overtopping in the limited table spaces. Thus, there is no table displayed in the grid of "Simulated occasions of overtopping" in Table 5-2 to show the simulated occasions of overtopping.

Table 5-2 Table index of CMC and ISMC simulation results

Assessing variables	Normal random innovation	Student's t random innovation
Overtopping probability	Tables 5-3, 5-5, 5-7	Tables 5-9, 5-11, 5-13
Variance estimation	-	Tables 5-10, 5-12, 5-14
Simulated occasions of overtopping	Tables 5-4, 5-6, 5-8	-

5.3.1 Risk Estimation Based on Normal Distributed Innovation

The same initial seeds, 1, 6, and 1000, are adopted as three separate random variate streams to make the comparison of the results. Both the overtopping probability estimation and the corresponding simulation occasions of overtopping are presented respectively for each seed. Taking seed = 1 for example, Tables 5-3 and 5-4 are shown below with both the CMC and the ISMC simulation results for the 5, 10, 20, 50, and 100 year time scales. Since the simulation has only been run 1,000 times, probabilities for the CMC simulation are cut to three decimal places. As the results below show, the ISMC simulation provides a very close probability estimation as the CMC simulation shows.

Table 5-3 Overtopping probability estimation based on normal innovation (seed = 1)

Simulation	5 year	10 year	20 year	50 year	100 year
CMC	0	0	0.0020	0.0030	0.0070
ISMC	0	0	0.0015	0.0046	0.0067

Note: Normal random innovation; seed = 1; simulation iteration = 1,000 times; $\Delta t = 0.005$

The ISMC simulations are based on the adjusted random variables through the same process as the CMC simulation. Then, the final results are derived through the outputs multiplying the LRs. If there is no overtopping occasion in the ISMC simulation, the probability value for the ISMC simulation would equal to zero. Each number shown in Table 5-4 below stands for an index of an independent simulation. In total, 1,000 times simulation having been conducted.

As we could see, there is no overtopping occurrence in the 5 year and 10 year time scales, thus the overtopping probabilities for the ISMC simulation in the 5 and 10 year scales are zero. For stream seed = 1, there is no difference in the simulation

occasions for the CMC and ISMC simulations. The same situation is also found when the seed = 1000. The major reason is due to the small shift and scaling adjusted on the new IS random variables.

Table 5-4 Simulated overtopping occasions based on normal innovation (seed = 1)

Time scale	CMC	ISMC
5 year	None	None
10 year	None	None
20 year	58, 761	58, 761
50 year	138, 774, 954	138, 774, 954
100 year	89, 306, 541, 589, 668, 986, 987	89, 306, 541, 589, 668, 986, 987

Note: Normal random innovation; seed = 1; simulation iteration = 1,000 times; $\Delta t = 0.005$

For seed = 6, similar outputs are shown in Tables 5-5 and 5-6 below. Two specialties are shown in the seed = 6 stream. In Table 5-5, the overtopping probability for the CMC simulation in the 10 year time scale is larger than the 20 year time scale. The reason is mainly due to the adopted random generator. Different random innovation series are generated without overlapping for the 10 and 20 year time scale. Thus two overtopping occasions occur in the 10 year time scale and only one overtopping occasion occurs in the 20 year time scales. The reversed probability values also prove the inaccuracy of the CMC simulation.

Table 5-5 Overtopping probability estimation based on normal innovation (seed = 6)

Simulation	5 year	10 year	20 year	50 year	100 year
CMC	0	0.0020	0.0010	0.0040	0.0060
ISMC	0	0.0015	0.0016	0.0033	0.0088

Note: Normal random innovation; seed = 6; simulation iteration = 1,000 times; $\Delta t = 0.005$

The other difference comparing to the innovation series based on the stream of seed =1 is that there are more overtopping occurrences in the ISMC simulation. In the section of 50-year time length, Occasion 123 is newly added for ISMC. In the section

of 100-year time length, Occasions 172, 267, and 699 are newly added for ISMC. Detailed information is shown in Table 5-6. Consequently, the IS random series result in more effective values within the cutoff region.

Table 5-6 Simulated overtopping occasions based on normal innovation (seed = 6)

Time scale	CMC	ISMC
5 year	None	None
10 year	79, 446	79, 446
20 year	223	223
50 year	585, 749, 759, 842	123, 585, 749, 759, 842
100 year	96, 385, 471, 498, 500, 798	96, 172, 267, 385, 471, 498, 500, 699, 798

Note: Normal random innovation; seed = 6; simulation iteration = 1,000 times; $\Delta t = 0.005$

Tables 5-7 and 5-8 below demonstrate the simulation results of seed = 1000. Similar to the results of seed = 1, there is no difference on the simulation occasions for the CMC and ISMC simulations.

Table 5-7 Overtopping probability estimation based on normal innovation (seed = 1000)

Simulation	5 year	10 year	20 year	50 year	100 year
CMC	0	0.0020	0	0.0030	0.0060
ISMC	0	0.0017	0	0.0047	0.0089

Note: Normal random innovation; seed = 1000; simulation iteration = 1,000 times; $\Delta t = 0.005$

Table 5-8 Simulated overtopping occasions based on normal innovation (seed = 1000)

Time scale	CMC	ISMC
5 year	None	None
10 year	280, 970	280, 970
20 year	None	None
50 year	32, 90, 899	32, 90, 899
100 year	183, 311, 369, 394, 786, 909	183, 311, 369, 394, 786, 909

Note: Normal random innovation; seed = 1000; simulation iteration = 1,000 times; $\Delta t = 0.005$

5.3.2 Risk Estimation Based on Student's t Distributed Innovation

Graphically for the same symmetric dataset, the fitted student's t distribution has a heavier tail than the fitted normal distribution. It means that there are more data points with both the extreme large and the extreme small points for the student's t distribution than the normal distribution. As a result, the innovation series based on the student's distribution provides a much bigger value of the overtopping probability. Compared to the previous section, Tables 5-9 to 5-14 in this section demonstrate the results. Tables 5-9, 5-11, and 5-13 present the overtopping probability estimation for both the CMC and the ISMC simulation, while Tables 5-10, 5-12, and 5-14 present the corresponding standard deviation of the estimated overtopping probabilities.

Table 5-9 Overtopping probability estimation based on student's t innovation (seed = 1)

Simulation	5 year	10 year	20 year	50 year	100 year
CMC	0.1630	0.2940	0.5210	0.8100	0.9690
ISMC	0.1608	0.2882	0.5222	0.7950	0.9637

Note: Student's t random innovation; seed = 1; simulation iteration = 1,000 times; $\Delta t_5 = 0.005$ standing for Δt in 5 year time scale; $\Delta t_{10} = 0.005$, $\Delta t_{20} = 0.004$, $\Delta t_{50} = 0.002$; and $\Delta t_{100} = 0.001$

According to Table 5-9, the final estimation of the overtopping probability from both the CMC and ISMC simulation are similar. Since only the 1000 times simulation has been run, the probability estimations for the CMC simulation are cut to three decimal places. Compared to the estimation from the previous Table 5-3, the estimation in Table 5-9 is much larger due to the tail characteristic of the Student's t distribution. The probability estimation for the 100 year time scale is approaching to 1, which demonstrates as the upper-bound probability of a risky situation.

Table 5-10 Standard deviation of overtopping probability estimation based on student's t innovation (seed = 1)

Simulation	5 year	10 year	20 year	50 year	100 year
CMC	0.5519	1.2176	1.1782	1.2049	0.8632
ISMC	0.3696	0.4558	0.4998	0.3925	0.1734

Note: Student's t random innovation; seed = 1; simulation iteration = 1,000 times; $\Delta t_5 = 0.005$ standing for Δt in 5 year time scale; $\Delta t_{10} = 0.005$, $\Delta t_{20} = 0.004$, $\Delta t_{50} = 0.002$; and $\Delta t_{100} = 0.001$

Although the estimation of overtopping probability from both the CMC and ISMC simulation are proved to be similar, a significant decrease on the standard deviation of the overtopping probability estimation has been shown for the ISMC simulation according to Table 5-10. This effect is more obvious than the results derived from the normal distributed innovation. The reason is because the Student's t distributed residuals have much fatter tail distributions which directly lead to more frequent high inflow occurrences. Correspondly, the effect is more obvious than the results derived from the normal distributed residuals. Compared to the results in Table 5-10, the role that IS played to improve the accuracy of risk estimation has been demonstrated.

Besides the results from the simulation stream seed = 1, the results derived from the other two streams, seed = 6 or 1000, are close to each other as well, as shown in the following Tables 5-11 to 5-14. Therefore, we could reasonably conclude that the ISMC simulation would help to reduce the variance and, at the same time, give a more accurate estimation.

Table 5-11 Overtopping probability estimation based on Student's t innovation (seed = 6)

Simulation	5 year	10 year	20 year	50 year	100 year
CMC	0.1590	0.2760	0.5010	0.8210	0.9690
ISMC	0.1536	0.2659	0.4870	0.8368	0.9509

Note: Student's t random innovation; seed = 6; simulation iteration = 1,000 times; $\Delta t_5 = 0.005$ standing for Δt in 5 year time scale; $\Delta t_{10} = 0.005$, $\Delta t_{20} = 0.004$, $\Delta t_{50} = 0.002$; and $\Delta t_{100} = 0.001$

Table 5-12 Standard deviation of overtopping probability estimation based on Student's t innovation (seed = 6)

Simulation	5 year	10 year	20 year	50 year	100 year
CMC	0.5017	1.1526	1.0515	1.1226	0.8718
ISMC	0.3659	0.4472	0.5002	0.3835	0.1734

Note: Student's t random innovation; seed = 6; simulation iteration = 1,000 times; $\Delta t_5 = 0.005$ standing for Δt in 5 year time scale; $\Delta t_{10} = 0.005$, $\Delta t_{20} = 0.004$, $\Delta t_{50} = 0.002$; and $\Delta t_{100} = 0.001$

Table 5-13 Overtopping probability estimation based on Student's t innovation (seed = 1000)

Simulation	5 year	10 year	20 year	50 year	100 year
CMC	0.1620	0.2820	0.5070	0.8350	0.9710
ISMC	0.1620	0.2756	0.4705	0.8132	0.9712

Note: Student's t random innovation; seed = 1000; simulation iteration = 1,000 times; $\Delta t_5 = 0.005$ standing for Δt in 5 year time scale; $\Delta t_{10} = 0.005$, $\Delta t_{20} = 0.004$, $\Delta t_{50} = 0.002$; and $\Delta t_{100} = 0.001$

Table 5-14 Standard deviation of overtopping probability estimation based on Student's t innovation (seed = 1000)

Simulation	5 year	10 year	20 year	50 year	100 year
CMC	0.4244	0.8259	0.9466	1.1518	0.4615
ISMC	0.3686	0.4502	0.5002	0.3714	0.1679

Note: Student's t random innovation; seed = 1000; simulation iteration = 1,000 times; $\Delta t_5 = 0.005$ standing for Δt in 5 year time scale; $\Delta t_{10} = 0.005$, $\Delta t_{20} = 0.004$, $\Delta t_{50} = 0.002$; and $\Delta t_{100} = 0.001$

5.3.3 Convergence Comparison and Discussion

In mathematics, convergence means the process of some functions and sequences approaching a limit under certain conditions. In probability theory, the average of results obtained from a large number of trials should be close to the expected value, and will tend to become closer as more trials are performed. This conclusion is known as the law of large numbers. Due to the law of large numbers, stable long-term results for the averages of some random events are guaranteed. Tailored to the Little Long dam-reservoir system, the overtopping probability estimation through simulation displays the convergence feature as the iterations increase. Due to the limitation of computational resources, the 5 year time scale is selected as the scope to show the convergence results. Figure 5-11 below shows the final results for both the normal and the student's t distributed innovations. Simulation seeds are selected randomly, and the simulation iterations are selected from 500 to 8000 with 100 as the interval. For each curve with fluctuation, 76 points are plotted as shown below.

According to Figure 5-11, the convergence diagrams of different simulation realizations are presented above. There are two obvious indications which could be concluded there. The first one is that high fluctuations are displayed when the simulation realizations stay small, and then gradually converge to a certain value as the realizations increase. The other one is that the ISMC simulation holds less fluctuation ranges all through the different simulation realizations. The final probability estimation result for the overtopping event based on the normal distributed innovation converges to 0.6×10^{-3}, and the final result based on the student's t distributed innovation converges to 0.165 or so.

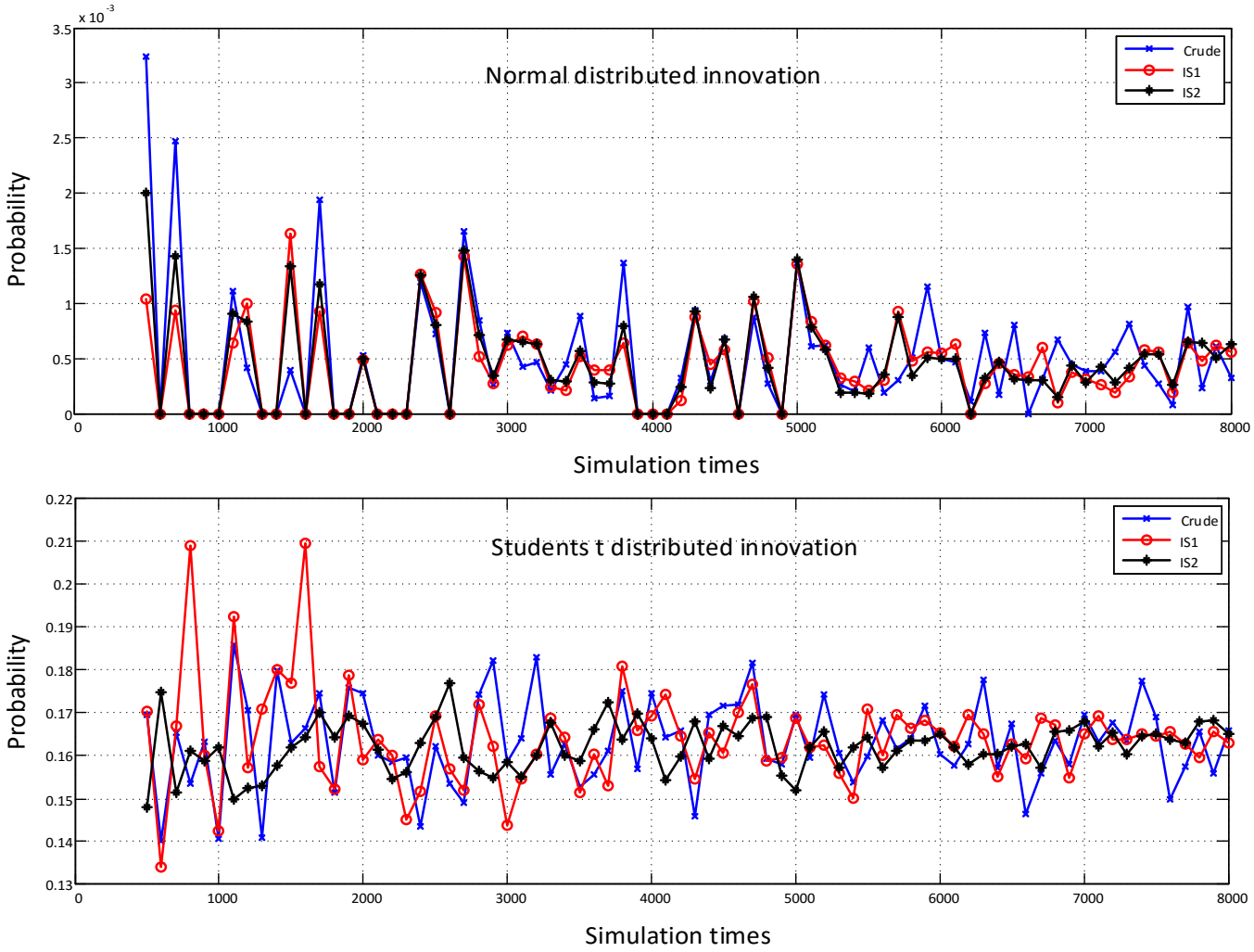

Figure 5-11 Convergence comparison of sampling strategies (time period = 5 years)

5.4 Performance Measurement of Simulation Program

Computer performance is a measure of how long it takes to perform a task, or how many tasks can be performed in a given time period. In order to demonstrate the performance improvement of the ISMC simulation, further quantitative measurement is conducted in this section. There are two measures that are commonly used to evaluate the goodness of importance sampling scheme. The first one is the ratio of variance obtained by CMC and ISMC simulation, σ_C^2/σ_{IS}^2. Since the estimator variances are not analytically possible when their mean is intractable, this has to be computed empirically. The second one is the ratio of the number of realizations required by each scheme, given the same output variance, N_C/N_{IS}. This indicator could be interpreted as the speed-up factor by which the importance sampling estimator achieves the same precision as the MC estimator.

5.4.1 Ratio of Variance by CMC and ISMC Simulation

The ratio of variance for the overtopping probability estimation are listed respectively for the three simulation streams, seeds = 1, 6, and 1000. For the 1,000 times simulation without fixing the seed, Tables 5-15 and 5-16 below present the results for both normal random innovation and the student's t random innovation. For Table 5-15, the results σ_C^2/σ_{IS}^2 are within the range of [0.63, 1.48]. The value of NaN exists mainly because there is no overtopping occurrence within the 1,000 times simulation for both the CMC and the ISMC simulations. Due to the limited occurrence of

overtopping, advantages of the ISMC simulation is not obvious for the normal distributed innovation. Only about a half situations show that σ_C^2 is larger than σ_{IS}^2.

Table 5-15 Ratio of variance for CMC and ISMC simulation based on normal innovation

Simulation stream	5 year	10 year	20 year	50 year	100 year
Seed = 1	NaN	NaN	1.2882	0.8982	0.9698
Seed = 6	NaN	1.2994	0.6307	1.4766	0.8764
Seed = 1000	NaN	1.1316	NaN	0.9271	0.8637

Note: Normal random variable; simulation iteration = 1,000 times, ratio is derived by CMC/ISMC

For Table 5-16, the results σ_C^2/σ_{IS}^2 of 1,000 times simulation are within the range of [1.15, 5.03]. Compared to the results presented in Table 5-15, the results σ_C^2/σ_{IS}^2 from the student's t distributed innovation in Table 5-16 demonstrated the advantages of the ISMC simulation in variance reduction. Also as the simulation time scale expanded, the ratio σ_C^2/σ_{IS}^2 increases and the effect of variance reduction becomes more obvious.

Table 5-16 Ratio of variance for CMC and ISMC simulation based on Student's t innovation

Simulation stream	5 year	10 year	20 year	50 year	100 year
Seed = 1	1.4932	2.6713	2.3573	3.0698	4.9781
Seed = 6	1.3711	2.5774	2.1021	2.9272	5.0277
Seed = 1000	1.1514	1.8345	1.8924	3.1012	2.7487

Note: Student's t random variable; simulation iteration = 1,000 times; ratio is derived by CMC/ISMC

5.4.2 Ratio of Realization Times by CMC and ISMC Simulation

In order to enhance the ISMC simulation advantages, the ratios of realization times that achieves the same precision, N_C/N_{IS}, are presented in Table 5-17 below.

Beyond the previous indicator σ_C^2/σ_{IS}^2 , this one could be interpreted as a speed-up factor by which the IS-based estimator achieves the similar variance as the CMC estimator does. The results showing below ranges in [1.27, 3.67], which demonstrates a prominent improvement that ISMC simulations achieve on computational times saving. As we could see, the ratio of realization times gives the most significant difference of performance at the length of 20-year time period, with an increase before and a decrease thereafter. Trade-offs between the time lengths and the convergence rate might be the reason for the explanation.

Table 5-17 Ratio of realization times for CMC and ISMC simulation

Simulation stream	5 year	10 year	20 year	50 year	100 year
Normal	1.91	2.30	3.67	1.92	1.27
Student's t	1.89	2.36	3.33	1.78	1.50

Note: Ratio is derived by CMC/ISMC

5.4.3 Elapsed Time Measurement

Followed by the ratio of realization times, it is also useful to measure the total elapsed time savings due to the use of the ISMC simulation approach. In order to demonstrate the significant computational time reduction that ISMC simulation achieves, the following Tables 5-18 and 5-19 present the total elapsed time cost below. As in the previous performance measurement, the time measurements here are based on the non-fixing seed simulation. The elapsed time cost of normal distributed innovation is shown in Table 5-18. Taking the 20 year time length as an example, the ISMC simulation could reduce to 10+ minutes from the CMC simulation of 30+ minutes.

An average savings of 21% is achieved in the total elapsed time for the normal distributed innovation.

Table 5-18 Total elapsed time of simulation based on normal innovation

Simulation	5 year	10 year	20 year	50 year	100 year
CMC	765.77	916.88	1897.06	1491.29	1108.11
ISMC	585.45	892.95	665.50	1368.36	1047.35

Note: Unit is represented by second; ratio is derived by CMC/ISMC

As with the results in Table 5-18, an average savings of 18.3% is achieved in the total elapsed time based on the student's t distributed innovation. Detailed information is shown in Table 5-19 below.

Table 5-19 Total elapsed time of simulation based on Student's t innovation

Simulation	5 year	10 year	20 year	50 year	100 year
CMC	1082.38	1174.13	1130.20	1227.51	929.55
ISMC	742.09	1129.35	1011.55	1044.67	641.49

Note: Unit is represented by second; ratio is derived by CMC/ISMC

5.5 Summary

In summary, this chapter serves as a case application of Chapter 3 and follows Chapter 4 as the demonstration of the simulation results. Based on the theoretical model developed, an estimation of the overtopping risks for the Little Long dam-reservoir system has been conducted. This chapter starts with the introduction of simulation implementation, including two perspectives: 1) the simulation platform; and 2) the optimal importance sampling density selection. Then, the results are presented including both the CMC simulation and the ISMC simulation with comparison. Also, the results are separately discussed by the normal distributed innovations and the student's t distributed innovations. The corresponding

computational performance measurement is also tracked in order to demonstrate the priority of ISMC simulation. The results show that the ISMC simulation could effectively provide a better estimation of accuracy and, at the same time reduce the computational resources.

Chapter 6: Conclusions and Future Work

6.1 Summary

Although overtopping could result in significant consequences, such events are observed very rare in reality. Estimation of those small probabilities using conventional simulation requires huge computational resources, both time and space, to the reach satisfied results. Otherwise, the estimation would not converge to an acceptable range. Computational expense has served as one of the prohibitive reasons that the simulation technique has not been widely applied to dam-reservoir system operation. In order to expedite computation speed, save simulation cost, and increase the estimation accuracy, this study has presented an efficient importance sampling-based simulation approach to estimate the overtopping risks of dam-reservoir systems.

The study starts with the dam-reservoir system performance model. Literature reviews on the critical factors leading to overtopping risks of dam-reservoir systems have been conducted. Natural inflow uncertainties and outflow control disturbances serve as the direct causes. Thus, the reservoir inflow hydrograph model and the dam-reservoir system operation model are proposed as a sequence. Based on the model, simulation could be run in order to predict the potential overtopping probabilities within a certain time period. Then, the importance sampling based rare event simulation is presented. In more details, both the CMC simulation framework and the ISMC simulation framework are proposed with comparison. In order to prove the theoretical model, the Little Long dam-reservoir case is presented as a follow up.

Results of the overtopping risk estimation for both the CMC and ISMC simulations are shown in the case results chapter. The proposed ISMC approach could not only improve the estimation accuracy in order to reach the satisfied estimation results, but also save the computational resources at the same time.

6.1.1 Contributions

This research addresses the natural stochastic characteristics of the dam-reservoir system, such as the reservoir inflow rate and the system operation process. Two major contributions could be concluded from this study: 1) the industrial contribution to the dam-reservoir system, and 2) the theoretical contribution to the rare event simulation on infrastructure systems.

From the industrial perspective, the final estimation results of overtopping probability would be used as importance indexes to guide the future dam safety investigations and studies. Based on the existing dam-reservoir system design, knowing the corresponding overtopping probability would not only inform the decision maker potential loss risks, but also supplement their knowledge and judgement on necessity of renovation and improvements. The proposed modeling and simulation procedures are also compatible if changing the precipitation settings or the operation rules

From the theoretical perspective, the proposed methodology of ISMC simulation is reasonably robust and proved to improve the overtopping risk estimation. The smaller variance of simulation results and the less computational

elapsed time, expand the application of the Monte Carlo technique on evaluating rare event risks for infrastructures.

6.1.2 Limitations

Overtopping failures of dams, for most cases, are not from a singular causation but through some uncommon combinations of mishaps that are usually difficult or impossible to identify accurately during the design. As a result, limitations of this study could also be sourced from two aspects: 1) the methodology limitation, and 2) the application limitation.

For the methodology limitation, fragility risks are commonly aroused by a chain of component malfunctions plus exterior factors, since the dam-reservoir systems are complicated. The current model proposed in Chapters 2 and 3 might not reflect all the correlations and interactions among the varied factors of the dam-reservoir system with uncertainty. This limitation might constrain the accuracy of the overtopping risk estimation. The actual risks would potentially be higher than the current estimation.

For the application limitation, the computational resource is limited and only 1,000 iterations have been conducted in the ISMC simulation. Results would become more persuasive if the iterations increase to 10,000+ times. The features of convergence would be more obvious, and the variance of the overtopping probability estimation would be reduced more significantly.

6.2 Recommendation of Future Work

Based on the discussions of study contributions and limitations, future efforts could be made through the following two aspects: 1) methodology and 2) computational environment.

From the methodology perspective, broader concerns could be taken into analysis. The reliable performance of dams and their appurtenant systems depends on the interactions of a large number of natural, engineering, and human systems. More information with available data resources, such as temperature, rainfall and snowfall, could be involved, as well as their inner correlations. At the same time, more failure modes of the dam-reservoir system, such as piping, erosion, or cracking, would also be taken into consideration, and be analyzed through the ISMC simulations;

From the computational environmental perspective, computers of higher computational capacity could be taken into consideration in order to increase the simulation iterations. This consideration goes along with the methodology improvements as mutual dependences. High performance computing generally refers to the practice of aggregating computing power in a way that delivers much higher performance than one could get out of a typical desktop computer or workstation. It has been widely applied to solve large problems in science, engineering, or business. There are multiple high performance computing resources available for use by campus researchers, such as supercomputers, at University of Maryland system, or other universities and national labs. Parallel coding and applications are required especially for the repetitive iterations. Future work can be done in order to take use of

those available computation resources and improve the parallel computation algorithms.

Glossary

ACF	Autocorrelation function
ADF	Augmented Dickey–Fuller test
AIC	Akaike's Information Criterion
AICc	Akaike's Information Criterion with correction
AR	Autoregression
ARIMA	Autoregressive integrated moving average
BP	The Box-Pierce test
cdf	Cumulative density function
CMC	Crude Monte Carlo
i.i.d	independent, identically distributed
IS	Importance sampling
ISMC	Importance sampling based Monte Carlo
KPSS	The Kwiatkowski-Phillips-Schmidt-Shin test
LB	The Ljung-Box test
LR	Likelihood ratio
MA	Moving average
MDP	Markov decision process
MLE	Maximum likelihood estimation
OLS	Ordinary Least Squares
PACF	Partial autocorrelation function
pdf	Probability density function
RE	Relative error

Bibliography

1. Afzali, R., Mousavi, S., and Ghaheri, A. (2008). "Reliability-Based Simulation-Optimization Model for Multireservoir Hydropower Systems Operations: Khersan Experience." *Journal of Water Resources Planning and Management*, 134(1), 24–33.

2. Alexopoulos, C., and Shultes, B. C. (2001). "Estimating reliability measures for highly-dependable Markov systems, using balanced likelihood ratios." *IEEE Transactions on Reliability*, 50(3), 265–280.

3. Apel, H., Thieken, A. H., Merz, B., and Blöschl, G. (2006). "A Probabilistic Modelling System for Assessing Flood Risks." *Natural Hazards*, 38(1-2), 79–100.

4. Association of State Dam Safety Officials. (2015). "Dam Failures and Incidents."

5. Au, S. K., and Beck, J. L. (1999). "A new adaptive importance sampling scheme for reliability calculations." *Structural Safety*, 21(2), 135–158.

6. Baecher, G., Brubaker, K., Galloway, G., and Link, L. (2011). *Review and Evaluation of the National Dam Safety Program*. A Report for the Federal Emergency Management Agency, University of Maryland, College Park.

7. Bassamboo, A., Juneja, S., and Zeevi, A. (2008). "Portfolio Credit Risk with Extremal Dependence: Asymptotic Analysis and Efficient Simulation." *Operations Research*, 56(3), 593–606.

8. Bee, M. (2009). "Importance Sampling for Sums of Lognormal Distributions with Applications to Operational Risk." *Communications in Statistics - Simulation and Computation*, 38(5), 939–960.

9. Belmudes, F., Ernst, D., and Wehenkel, L. (2008). "Cross-Entropy Based Rare-Event Simulation for the Identification of Dangerous Events in Power Systems." *Proceedings of the 10th International Conference on Probabilistic Methods Applied to Power Systems, 2008. PMAPS '08*, 1–7.

10. Blanchet, J., and Lam, H. (2014). "Rare-Event Simulation for Many-Server Queues." *Mathematics of Operations Research*, 39(4), 1142–1178.

11. Box, G. E., and Jenkins, G. M. (1976). *Time series analysis: forecasting and control, revised ed*. Holden-Day.

12. Bucklew, J. (2004). *Introduction to Rare Event Simulation*. Springer Science & Business Media.

13. Chan, N. H., and Wong, H. Y. (2015). *Simulation Techniques in Financial Risk Management*. John Wiley & Sons.

14. Chepuri, K., and Homem-de-Mello, T. (2005). “Solving the Vehicle Routing Problem with Stochastic Demands using the Cross-Entropy Method.” *Annals of Operations Research*, 134(1), 153–181.

15. Chiew, F. H. S., Stewardson, M. J., and McMahon, T. A. (1993). “Comparison of six rainfall-runoff modelling approaches.” *Journal of Hydrology*, 147(1–4), 1–36.

16. Clémençon, S., Cousien, A., Felipe, M. D., and Tran, V. C. (2013). “On Computer-Intensive Simulation and Estimation Methods for Rare Event Analysis in Epidemic Models.” *arXiv:1308.5830 [math, stat]*.

17. Cooper, N. G., Eckhardt, R., and Shera, N. (1989). *From Cardinals to Chaos: Reflections on the Life and Legacy of Stanislaw Ulam*. CUP Archive.

18. Curt, C., Peyras, L., and Boissier, D. (2010). “A Knowledge Formalization and Aggregation-Based Method for the Assessment of Dam Performance.” *Computer-Aided Civil and Infrastructure Engineering*, 25(3), 171–184.

19. Dai, H., Zhang, H., and Wang, W. (2012). “A support vector density-based importance sampling for reliability assessment.” *Reliability Engineering & System Safety*, 106, 86–93.

20. Dawson, R., and Hall, J. (2006). “Adaptive importance sampling for risk analysis of complex infrastructure systems.” *Proceedings of the Royal Society of London A: Mathematical, Physical and Engineering Sciences*, 462(2075), 3343–3362.

21. Delatte, N. J. (2008). *Beyond Failure: Forensic Case Studies for Civil Engineers*. American Society of Civil Engineers, Reston, VA.

22. Dewals, B., Erpicum, S., Detrembleur, S., Archambeau, P., and Pirotton, M. (2010). “Failure of dams arranged in series or in complex.” *Natural Hazards*, 56(3), 917–939.

23. Ding, J., and Chen, X. (2013). “Assessing small failure probability by importance splitting method and its application to wind turbine extreme response prediction.” *Engineering Structures*, 54, 180–191.

24. Feinberg, E. A., and Shwartz, A. (2012). *Handbook of Markov Decision Processes: Methods and Applications*. Springer Science & Business Media.

25. Froehlich, D. (2008). “Embankment Dam Breach Parameters and Their Uncertainties.” *Journal of Hydraulic Engineering*, 134(12), 1708–1721.

26. Ganji, A., and Jowkarshorijeh, L. (2011). “Advance first order second moment (AFOSM) method for single reservoir operation reliability analysis: a case study.” *Stochastic Environmental Research and Risk Assessment*, 26(1), 33–42.

27. Gee, D. (2009). “Comparison of Dam Breach Parameter Estimators.” *World Environmental and Water Resources Congress 2009*, American Society of Civil Engineers, 1–10.

28. Glasserman, P., and Li, J. (2005). “Importance Sampling for Portfolio Credit Risk.” *Management Science*, 51(11), 1643–1656.

29. Glynn, P. W., and Iglehart, D. L. (1989). “Importance Sampling for Stochastic Simulations.” *Management Science*, 35(11), 1367–1392.

30. Goodarzi, E., Mirzaei, M., and Ziaei, M. (2012). “Evaluation of dam overtopping risk based on univariate and bivariate flood frequency analyses.” *Canadian Journal of Civil Engineering*, 39(4), 374–387.

31. Grooteman, F. (2008). “Adaptive radial-based importance sampling method for structural reliability.” *Structural Safety*, 30(6), 533–542.

32. Heidelberger, P. (1995). “Fast Simulation of Rare Events in Queueing and Reliability Models.” *ACM Trans. Model. Comput. Simul.*, 5(1), 43–85.

33. Hsu, Y.-C., Tung, Y.-K., and Kuo, J.-T. (2010). “Evaluation of dam overtopping probability induced by flood and wind.” *Stochastic Environmental Research and Risk Assessment*, 25(1), 35–49.

34. Huang, Z., and Shahabuddin, P. (2004). “A Unified Approach for Finite-dimensional, Rare-event Monte Carlo Simulation.” *Proceedings of the 36th Conference on Winter Simulation*, WSC ’04, Winter Simulation Conference, Washington, D.C., 1616–1624.

35. Jacquemart, D., and Morio, J. (2013). “Conflict probability estimation between aircraft with dynamic importance splitting.” *Safety Science*, 51(1), 94–100.

36. Juneja, S., and Shahabuddin, P. (2002). “Simulating Heavy Tailed Processes Using Delayed Hazard Rate Twisting.” *ACM Trans. Model. Comput. Simul.*, 12(2), 94–118.

37. Kahn, H., and Marshall, A. W. (1953). “Methods of Reducing Sample Size in Monte Carlo Computations.” *Journal of the Operations Research Society of America*, 1(5), 263–278.

38. Kalos, M. H., and Whitlock, P. A. (2008). *Monte Carlo Methods*. John Wiley & Sons.

39. Kang, B., Lee, S.-J., Kang, D.-H., and Kim, Y.-O. (2007). “A flood risk projection for Yongdam dam against future climate change.” *Journal of Hydro-environment Research*, 1(2), 118–125.

40. Karamouz, M., Zahraie, B., and Araghinejad, S. (2005). “Decision Support System for Monthly Operation of Hydropower Reservoirs: A Case Study.” *Journal of Computing in Civil Engineering*, 19(2), 194–207.

41. Klein, B., Schumann, A. H., and Pahlow, M. (2011). “Copulas – New Risk Assessment Methodology for Dam Safety.” *Flood Risk Assessment and Management*, A. H. Schumann, ed., Springer Netherlands, 149–185.

42. Kuo, J.-T., Hsu, Y.-C., Tung, Y.-K., Yeh, K.-C., and Wu, J.-D. (2008). "Dam overtopping risk assessment considering inspection program." *Stochastic environmental research and risk assessment*, 22(3), 303–313.

43. Kuo, J.-T., and Sun, Y.-H. (1993). "An intervention model for average 10 day streamflow forecast and synthesis." *Journal of Hydrology*, 151(1), 35–56.

44. Kuo, J., Yen, B., Hsu, Y., and Lin, H. (2007). "Risk Analysis for Dam Overtopping—Feitsui Reservoir as a Case Study." *Journal of Hydraulic Engineering*, 133(8), 955–963.

45. Kuwahara, H., and Mura, I. (2008). "An efficient and exact stochastic simulation method to analyze rare events in biochemical systems." *The Journal of Chemical Physics*, 129(16), 165101.

46. Kwon, H.-H., and Moon, Y.-I. (2006). "Improvement of overtopping risk evaluations using probabilistic concepts for existing dams." *Stochastic Environmental Research and Risk Assessment*, 20(4), 223–237.

47. L'Ecuyer, P., and Tuffin, B. (2009). "Approximating zero-variance importance sampling in a reliability setting." *Annals of Operations Research*, 189(1), 277–297.

48. Liu, J. S. (2008). *Monte Carlo Strategies in Scientific Computing*. Springer Science & Business Media.

49. Li, X.-Z., Xu, L.-Z., and Chen, Y.-G. (2010). "Implicit stochastic optimization with data mining for reservoir system operation." *2010 International Conference on Machine Learning and Cybernetics (ICMLC)*, 2410–2415.

50. Lohani, A. K., Kumar, R., and Singh, R. D. (2012). "Hydrological time series modeling: A comparison between adaptive neuro-fuzzy, neural network and autoregressive techniques." *Journal of Hydrology*, 442–443, 23–35.

51. Morio, J., Pastel, R., and Gland, F. L. (2010). "An overview of importance splitting for rare event simulation." *European Journal of Physics*, 31(5), 1295.

52. Morio, J., Pastel, R., and Le Gland, F. (2013). "Missile target accuracy estimation with importance splitting." *Aerospace Science and Technology*, 25(1), 40–44.

53. Neumann, J. V. (2005). *John Von Neumann: Selected Letters*. American Mathematical Soc.

54. Osti, R., Bhattarai, T. N., and Miyake, K. (2011). "Causes of catastrophic failure of Tam Pokhari moraine dam in the Mt. Everest region." *Natural Hazards*, 58(3), 1209–1223.

55. Perninge, M., Lindskog, F., and Soder, L. (2012). "Importance Sampling of Injected Powers for Electric Power System Security Analysis." *IEEE Transactions on Power Systems*, 27(1), 3–11.

56. Peyras, L., Royet, P., and Boissier, D. (2006). “Dam ageing diagnosis and risk analysis: Development of methods to support expert judgment.” *Canadian Geotechnical Journal*, 43(2), 169–186.

57. Pisaniello, J. D., Burritt, R. L., and Tingey-Holyoak, J. (2011). “Dam safety management for sustainable farming businesses and catchments.” *Agricultural Water Management*, 98(4), 507–516.

58. Pisaniello, J. D., and McKay, J. (2007). “A tool to aid emergency managers and communities in appraising private dam safety and policy.” *Disasters*, 31(2), 176–200.

59. Poulin. (2007). “Importance of Tail Dependence in Bivariate Frequency Analysis.” *Journal of Hydrologic Engineering*, 12(4), 394–403.

60. Roebuck, K. (2012). *Random password generators: High-impact Strategies - What You Need to Know: Definitions, Adoptions, Impact, Benefits, Maturity, Vendors*. Emereo Publishing.

61. Rubino, G., and Tuffin, B. (2009). *Rare Event Simulation using Monte Carlo Methods*. John Wiley & Sons.

62. Shahabuddin, P. (1995). “Rare Event Simulation in Stochastic Models.” *Proceedings of the 27th Conference on Winter Simulation*, WSC ’95, IEEE Computer Society, Washington, DC, USA, 178–185.

63. Smith, P. J., Shafi, M., and Gao, H. (1997). “Quick simulation: a review of importance sampling techniques in communications systems.” *IEEE Journal on Selected Areas in Communications*, 15(4), 597–613.

64. Sun, Y., Chang, H., Miao, Z., and Zhong, D. (2012). “Solution method of overtopping risk model for earth dams.” *Safety Science*, 50(9), 1906–1912.

65. Tsakiris, G., and Spiliotis, M. (2012). “Dam- Breach Hydrograph Modelling: An Innovative Semi- Analytical Approach.” *Water Resources Management*, 27(6), 1751–1762.

66. Valipour, M., Banihabib, M. E., and Behbahani, S. M. R. (2013). “Comparison of the ARMA, ARIMA, and the autoregressive artificial neural network models in forecasting the monthly inflow of Dez dam reservoir.” *Journal of Hydrology*, 476, 433–441.

67. Vedachalam, S., and Riha, S. J. (2014). “Small is beautiful? State of the dams and management implications for the future.” *River Research and Applications*, 30(9), 1195–1205.

68. Walter, C., and Defaux, G. (2015). “Rare event simulation : a point process interpretation with application in probability and quantile estimation.”

69. Wang, S.-P., Chen, A., Liu, C.-W., Chen, C.-H., and Shortle, J. (2011). “Rare-event splitting simulation for analysis of power system blackouts.” *2011 IEEE Power and Energy Society General Meeting*, 1–7.

70. Wang, Z., and Bowles, D. S. (2006). “Dam breach simulations with multiple breach locations under wind and wave actions.” *Advances in Water Resources*, 29(8), 1222–1237.

71. Xu, W., Zhao, J., Zhao, T., and Wang, Z. (2014). “Adaptive Reservoir Operation Model Incorporating Nonstationary Inflow Prediction.” *Journal of Water Resources Planning and Management*, 0(0), 04014099.

72. Xu, Y., and Zhang, L. (2009). “Breaching Parameters for Earth and Rockfill Dams.” *Journal of Geotechnical and Geoenvironmental Engineering*, 135(12), 1957–1970.

73. Zhang, L. M., Xu, Y., and Jia, J. S. (2009). “Analysis of earth dam failures: A database approach.” *Georisk: Assessment and Management of Risk for Engineered Systems and Geohazards*, 3(3), 184–189.